Doctoral Dissertation

Characteristic Modes Analysis for Antenna Parameters Optimization

固有モード解析法を用いた アンテナのパラメータ最適化に関する研究

Supervisor: Prof. Hiroyuki Arai

Submitted in March 2015

Shen Wang

王 珅

Specialization in Electrical and Computer Engineering
Department of Physics, Electrical and Computer Engineering
Graduate School of Engineering
Yokohama National University

ABSTRACT

Antenna is always one of the most remarkable wireless devices. Every wireless communication system need antenna to couple propagating electromagnetic waves from and to the system. The antenna, which is a guide wave – free space wave converter, was firstly established by Hertz in 1886. The wireless system worked at meter wave, used a dipole as transmitting antenna and a loop as receiving antenna. However, the system was only in experimental stage. Decades later, another researcher, Marconi, started normal wireless communication commercial service over Atlantic Ocean. Since then, antenna has been more and more important and is indispensable to our life now.

Nowadays, antennas are designed to have diverse geometries and sizes to be used for diverse applications. However, as we are not able to directly see, hear or touch electromagnetic wave, it is not easy to design an antenna. Moreover, the antenna design means we have to consider how to make the design satisfy appropriate feeding impedance, radiation pattern, polarization, efficiency and sometimes even limited size. The appropriate feeding impedance indicates sufficient small reflections losses due to mismatch at the interface between transmission line and the antenna. Thus, we have to make radiation reactance approximate to zero, and match radiation resistance of the antenna to characteristic impedance of the transmission line. Besides, not only impedance but also other indexes must be considered. Although antenna can be regarded as a kind of high-frequency circuit, the process of the design is obviously more complex than designing other high-frequency circuits.

In modern times, people usually use computer simulation software to calculate and design antennas. These software are based on some ripe numerical analysis method, e.g. Method of Moment (MoM), Finite Element Method (FEM) and Finite-Difference Time-Domain method (FDTD). The software provide intuitionistic graphical interface, and greatly reduce calculation time. As a result, people can arbitrarily change antenna parameters to study antenna characteristics and obtain desired results. The high speed of calculation bring about convenience, but also cause some negative phenomenon. E.g. as the software are not able to provide thorough physical insight of antenna operating mechanism and fundamental design guidance, the people who can design antennas by using the software may not understand more principles of the antenna. It would bring about a severer problem that the procedure of the design may cost more time because of blind parameter adjustments.

Thus, we need an analysis method providing thorough physical insight to explain antenna working mechanism. Theory of characteristic modes, which is based on the MoM, is one of the best choices for this issue. Antenna analysis based on the theory provide a set of characteristic modes which have characteristic currents orthogonal to each other at source area and characteristic fields orthogonal to each other at infinity. This set of characteristic modes are current modes numerically obtained for discretionarily shaped conducting bodies, only relate to structure, size and frequency of the antenna, and provide a physical explanation of the radiation phenomena taking place on the antenna. However, it can obtain and control these modes by setting suitable feeding position, amplitude and phase. According to the theory, the excited modes and their synthetic field result as antenna's resonance and radiation field. This point is the reason why it worth being studied. By calculating and analyzing these characteristic modes in concerned frequency range it may get more information about antenna's working mechanism, which may be difficult or not that clear by using common analysis. Moreover, by adjusting antenna structure or feeding type may control the modes' response, therefore these information can provide guidance for antenna parameters adjustment and optimization.

Study of characteristic modes for the antenna parameters optimization is going to be expounded as following. In chapter 1, we introduce background and our target for this study. In chapter 2, brief overview and the theory of characteristic modes are expounded. Before this,

overview of MoM will be involved as warm-up. A compact composite antenna composed of two orthogonally polarized component antennas is proposed to reduce correlation and realize miniaturization in chapter 3. In Chapter 4, we use the characteristic modes analysis to discuss problem of cross-polarization of a disk loaded monopole antenna which is introduced in Chapter 3. In Chapter 5, at first, a double notched antenna is used as an example to show how to make it radiate both omni-directional and bi-directional radiation patterns by adjusting the associated characteristic modes of the antenna. Then, characteristic modes of an omni-directional four notched array antenna are calculated to identify the relationship between an unexcited mode and antenna radiation pattern.

In Appendix I, the characteristic modes analysis is tried to explain neutralizing phenomenon occurring on two closely adjacent PIFA elements that are connected by a shorted line. While in Appendix II, A 4G cellular antenna designed for eyewear wireless devices is introduced and analyzed by using the theory of characteristic modes to understand the antenna's operational principle and optimized antenna feeding position.

CONTENTS

CHAPTER 1
INTRODUCTION

1.1 Background

Since it was firstly invented and used, antenna has become more and more important and indispensable to our life. As one of the most significant applications, personal mobile communication system has only developed for less than 30 years, and has been evolving from 1st generation to 5th generation during the period. A huge number of base station antennas have been established to form the worldwide cellular networks. At the same time, billions of wireless devices such as smart phones, mobile phones and tablet computers are connecting the internet at every minute. Especially due to the development of smart phones and tablet computers in these years, demand of data communication is rapidly increasing. The situation causes various advanced antennas to satisfy the huge demand.

The *IEEE Standard Definitions of Terms for Antennas*[1] defines the antenna as "a means for radiating or receiving radio waves." [1] In other words, the antennas belong to a kind of convertor to transform current at radio frequency to electromagnetic wave or its opposition. For wireless communication systems, the antenna is one of the most critical components. A

[1] IEEE Transactions on Antennas and Propagation, vols. AP-17, No. 3, May 1969; AP-22, No. 1, January 1974; and AP-31, No. 6, Part II, November 1983.

good design of the antenna can relax system requirements and improve overall system performance. A typical example is TV, for which the overall broadcast reception can be improved by utilizing a high-performance antenna. The antenna serves to a communication system the same purpose that eyes and eyeglasses serve to a human. In addition, to receiving or transmitting energy, an antenna in an advanced wireless system is usually required to optimize or enhance the radiation energy in some directions and suppress it in others. Thus the antenna must also serve as a directional device. Then, it must take various forms to meet the particular need. It may be a piece of conducting wire, an aperture, a patch, an array, a reflector, a lens, etc.

The field of antennas is vigorous and dynamic. Over the last 60 years antenna technology has been always an indispensable partner of communications revolution. Many major advances that occurred during this period are in common use today. However, many more issues and challenges are facing us today, especially since the demands for system performances becomes even greater. Designing a novel and high-performance antenna is a complex process. Originally, as we are not able to directly see, hear or touch electromagnetic wave, it is not an easy process to design an antenna. Moreover, the antenna design means we have to consider how to make the design satisfy appropriate feeding impedance, radiation pattern, polarization, efficiency and sometimes even limited size. The appropriate feeding impedance indicates sufficient small reflections losses due to mismatch at the interface between transmission line and the antenna. Thus, we have to make radiation reactance approximate to zero, and match radiation resistance of the antenna to characteristic impedance of the transmission line. Besides, not only impedance but also other indexes must be considered. Although antenna can be regarded as a kind of high-frequency circuit, the process of the design is obviously more complex than designing other high-frequency circuits.

While in the first half of this century antenna designs may have been considered almost as “cut and try” operations, in these years people usually use computer simulation software to calculate and design antennas. These software are based on some ripe numerical analysis method, such as Method of Moment (MoM), Finite Element Method (FEM), Finite-Difference Time-Domain method (FDTD) and Transmission Line Method (TLM) for low frequency

applications, and Geometrical Theory of Diffraction (GTD) or Physical Theory of Diffraction (PTD) for high frequency applications, etc. These software provide intuitionistic graphical interface, and are able to greatly reduce calculation time. Thus, people can arbitrarily change antenna parameters to study antenna characteristics and obtain desired results. High speed of the calculation bring about convenience, but also cause some negative phenomenon. As the software are not able to provide thorough physical insight of antenna operating mechanism and fundamental design guidance, the people who can design antennas by using the software may not understand more principles of the antenna. Moreover, it would bring about a severer problem that the procedure of the design may cost more time because of the blind parameter adjustments.

Therefore, we need an analysis method providing thorough physical insight to explain antenna working mechanism. Theory of characteristic modes, which is based on the MoM, is one of the best choices for this issue. Antenna analysis based on the theory provide a set of characteristic modes which have characteristic currents orthogonal to each other at source area and characteristic fields orthogonal to each other at infinity. This set of characteristic modes are current modes numerically obtained for discretionarily shaped conducting bodies, only relate to structure, size and frequency of the antenna, and provide a physical explanation of the radiation phenomena taking place on the antenna. However, it can obtain and control these modes by setting suitable feeding position, amplitude and phase. According to the theory, the excited modes and their synthetic field result as antenna's resonance and radiation field. This point is the reason why it worth being studied. By calculating and analyzing these characteristic modes in concerned frequency range it may get more information about antenna's working mechanism, which may be difficult or not that clear by using common analysis. Moreover, by adjusting antenna structure or feeding type may control the modes' response, therefore these information can provide guidance for antenna parameters adjustment and optimization.

1.2 Numerical Methods for Antenna Analysis

Generally as numerical methods, Integral Equation method and high frequency methods such as the Geometrical Theory of Diffraction (GTD), have been used for the analysis of many previously intractable antenna problems in the last three decades.

As its name, the Integral Equation method solves the solution of the antenna problem in form of an integral where unknown is a part of the integrand. The unknown is usually the induced current density. Then, numerical calculations such as the MoM, which will be briefly discussed in Chapter 2, are used to solve the unknown. Once the current density is found, radiation integrals are used to find the fields radiated and other antenna parameters. This method is originally most convenient for wire-type antennas and more efficient for antenna structures that are electrically small [2][3].

When the dimensions of the antenna are too big comparing with concerned frequency wavelength, the Integral Equation method will be not so computationally efficient. However, high-frequency asymptotic methods can be used to analyze this kind of mathematically intractable problems. One such method that has received considerable attention and application over the years is the GTD, which is an extension of geometrical optics (GO), and it overcomes some of the limitations of GO by introducing a diffraction mechanism. Other methods, such as the PTD and Multi-Level Fast Multi-pole Method (MLFMM) are also the high frequency asymptotic methods. These methods will not be discussed in this thesis. However, for example, detailed introduction of the GTD can be found in [3], while some interesting advances and applications are found in [4][5].

Another method, which has received a lot of attention in scattering, is the Finite-Difference Time-Domain (FDTD) method. This method has also been studied and successfully applied to many antenna radiation problems [6]-[9]. Besides, a method named Finite Element Method (FEM) has also been extensively utilized [10]-[13].

Part of the numerical methods for antenna analysis and computational electromagnetics are briefly summarized and compared in following Table 1. 1 and Figure 1. 1.

Table 1. 1

Comparison of part of the numerical methods for antenna analysis

	Most suitable problems	Features of modeling	Problems in computation
MoM	Wire and surface structures	Difficult for interior constructions	Heavy for inhomogeneous mediums, almost only for low frequency problems
FDTD	Complex interior constructions	Easy for inhomogeneous mediums	Heavy and may cause inaccurate for intensive structures such as array antennas
FEM	Effective for interior EM problems	Electrical and physical dimension can be separately defined	Hard for intensive structures. Boundary modeling is necessary
GTD / PTD	Electrically big structures and scatterers	Cannot provide any antenna parameters information	Fast, but only effective for high frequency and far field issues

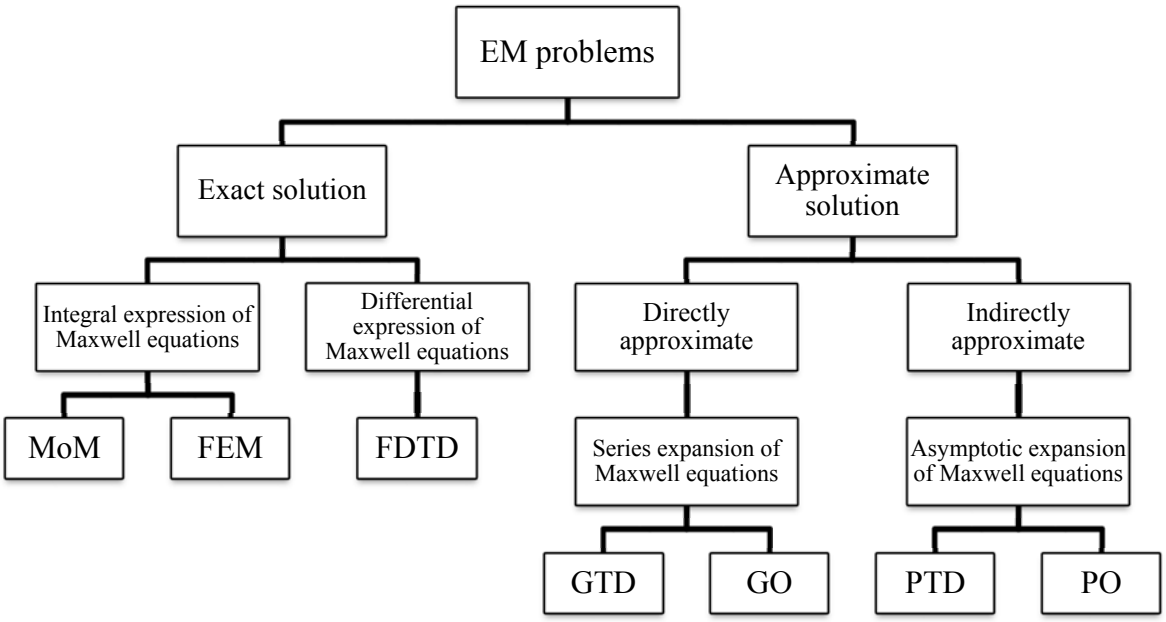

Figure 1. 1 Relation between the numerical methods.

1.3 Brief Overview of Characteristic Modes

As it has been introduced in 1.1, other than the classical numerical methods for antenna analysis, some other analysis method that can provide thorough physical insight to explain antenna working mechanism is meaningful and interesting for both challenge and practicability. The theory of characteristic modes is such a method. The characteristic modes are essentially current modes numerically calculated for discretionarily shaped conducting bodies, and only relate to structure, size and frequency of the antenna. The modes are able to indicate natural resonance of the antenna, and are expected to provide physical explanation of the radiation phenomena taking place on the antenna.

Looking back to its history, the theory of characteristic modes was firstly generalized to analyzing conductors in arbitrary shape by Robert J. Garbacz in 1971 [14], based on the MoM. Then, Roger. F. Harrington and Joseph R. Mautz summarized and improved the theory [15][16]. There is a point significantly noticeable that although the theory of characteristic modes is mainly used for perfectly conducting bodies, it was generalized to calculating dielectric and magnetic bodies by Harrington [17]. The major difference is verified that the characteristic currents in material bodies are volume distributions, while for perfectly conducting bodies they are surface distributions. This point will be mentioned in Chapter 2. By this time, the theory is named classical theory of characteristic modes. In this theory, the characteristic currents are orthogonal to each other over source region, and the characteristic fields are orthogonal to each other only over spherical surface at infinity.

While in 1982, a Japanese researcher, N. Inagaki proposed another generalized theory of characteristic modes [18][19]. Inagaki treated more general case where the region of observation does not necessarily coincide with the source region, resulting in orthogonal properties over more general regions than the body surface and the sphere at infinity. According to the study, the modes are more general than the classical characteristic modes in that they can

be constructed to be orthogonal over any sector of space, as well as orthogonal over the source region. Except when the operator is improperly singular, the completeness and orthogonality properties of the eigensolutions make them attractive for expanding arbitrary fields and sources associated with discrete or continuous radiating or scattering systems. 2 years later, David M. Pozar summarized and discussed the set of the referred weighted Inagaki modes [20][21]. The orthogonality properties of the generalized characteristic modes are considered make them ideally suited for problems in antenna pattern synthesis and optimization, providing advantages such as versatility and computational efficiency over other methods. Pozar used the method to constrain pattern synthesis for a line source and a printed dipole array, and for constrained directivity optimization of a free-space dipole array, as examples. The examples demonstrated the weighted Inagaki modes' good computational efficiency and generality. While in 1990, D. Liu with Garbacz and Pozar proposed another set of generalized characteristic modes which is similar with the Inagaki modes but can reduce computation time [22]. It was confirmed that new eigenvalues have a clear physical meaning, i.e., they relate the power radiated to the net reactive power stored around the obstacle.

1.4 Early Studies on Applications for Reference

Since the theory of characteristic modes was proposed, Harrington and Mautz reported its application for loaded N-port scatterer, scattering sections and radiation pattern synthesis [23]-[25]. In their reports, the mode currents diagonalize the loaded N-port impedance matrix. The mode fields form an orthonormal set on the radiation sphere. Because of these properties, problems of analysis, synthesis and optimization become conceptually simpler. Moreover, if the resonated mode current provides the major contribution to the scattered field, then the reactively loaded object will have a scattering pattern approximately equal to the radiation pattern of the same object excited by the given set of port currents. Various synthesis and

optimization procedures can be used to obtain real port currents whose fields have desirable radiation characteristics.

Originally, the theory was applied to antenna shape synthesis [22][26][27], and control of obstacle scattering by reactive loading [23]-[25], but practically almost fell into disuse later during a long time. Although it has not been found there is any report explains the reason of disuse, the author[2] thinks the computational complexity of the MoM, which is the foundational numerical method of the characteristic modes, is the primary restrict, especially for complex and electrically big antenna structures, through that period.

However, with considerable improvement of computation, the theory was revisited little by little in recent years. As even whole body of a car can be calculated by MoM, a study on vehicle antenna was proposed [28]. This paper reviewed the problems associated with near-vertical-incidence mode of skywave propagation via the ionosphere, and examined the stringent requirements that these place on the antennas. Since unusual problems often require unusual solutions, the method of characteristic modes was used. This determined how the natural distribution of currents, both on the antenna and on the vehicle itself could be used to enhance the radiation towards the zenith.

There is an outstanding paper [29] in that the theory of characteristic modes is briefly and clearly introduced. Design examples of different types of antennas was presented in the paper, with the aim of demonstrating that characteristic modes are really helpful for antenna design and optimization. There are some studies reported the method can be successfully used to widen impedance bandwidth of planar dipole antenna [30], wire antenna [31] and helical spherical antenna [32]. The method is thought suitable for antennas with multiple potential operating modes, such as antennas with multiple resonances or more than one polarizations. These years, some antennas for MIMO systems [33]-[38] or that with UWB property [39][40] have been analyzed by using the theory of characteristic modes. Also, the theory can be finely used for circularly polarized antenna [29][41], because the two orthogonal current modes can be easily observed.

[2] Shen Wang

Most of the related studies are for applications on various antennas, while there is one paper [42] is for a considerable important problem that is how to find and decide feeding position to excited desired mode. As an alternative feeding method, reactive near-field behaviors of the characteristic mode were studied, since they give insights into where the coupled energy can be maximized for a given mode, while reducing the probability of coupling to other modes.

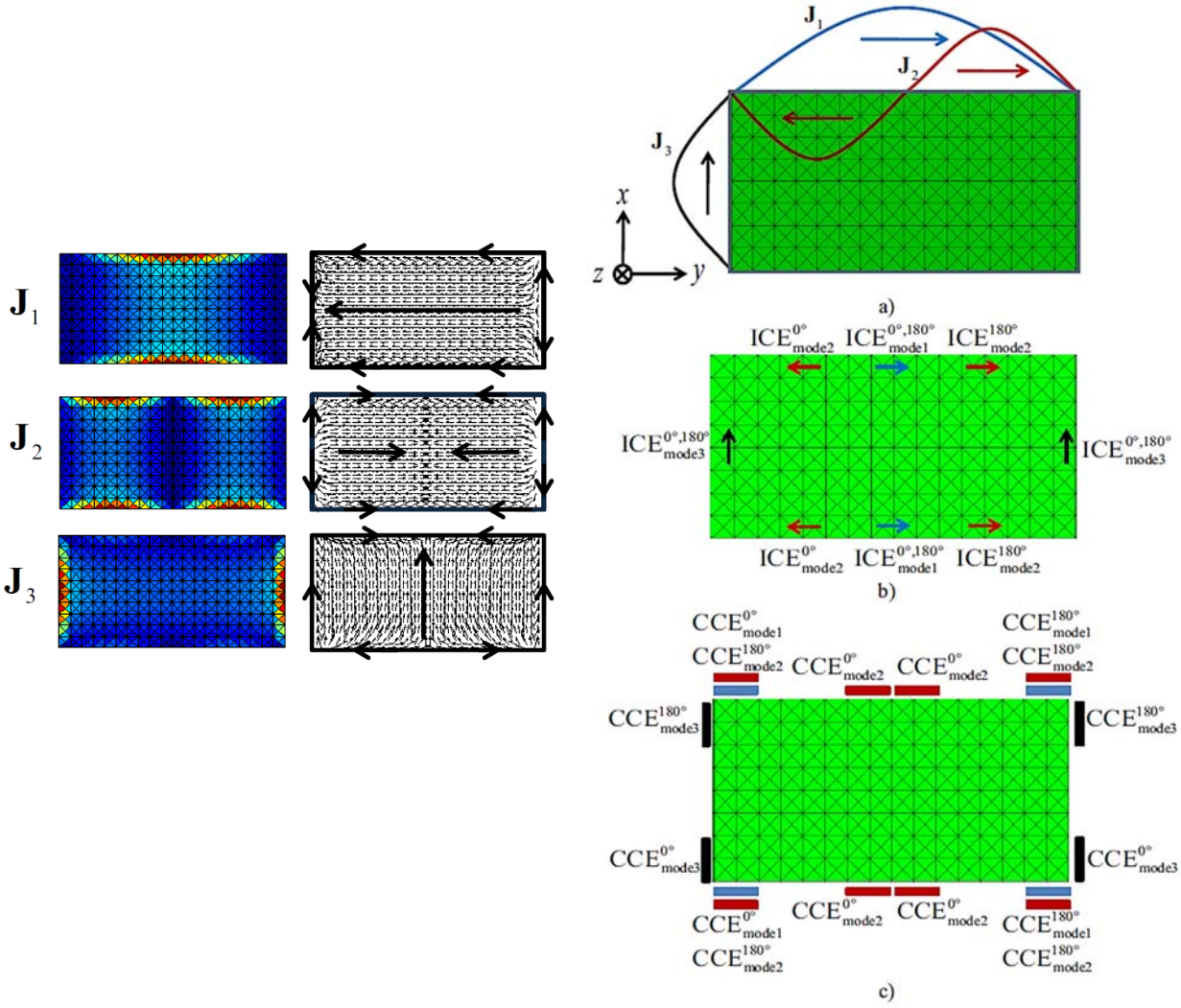

Figure 1. 2 Surface current distribution of the first three characteristic modes of a rectangular PCB (left). Current distribution at edges of the PCB of the first three characteristic modes (right, a), and the optimum location of inductive (right, b) and capacitive (right, c) exciters [42].

Figure 1. 2 shows surface current distribution of the first three characteristic modes of a rectangular PCB as an example in [42]. The specific current distributions of the characteristic modes can be confirmed mainly characterized by the sinusoidal behavior at the edges of the PCB. It illustrates the current distributions of the characteristic modes J1, J2 and J3 at the edges of the major and minor axes (right, a). Also, it shows that each characteristic mode has its maxima and minima of the current distribution at specific positions. In addition, to the current distribution, we can also consider electric near field distribution on the plate. The electric near field and the current distribution will have a phase difference of 90°. I.e. the electric near field distribution will have its minima amplitude at maxima of the current distribution, and vice versa. Therefore, a specific mode can be excited by inductive couplers located at the maxima of the current distribution (right, b), while capacitive couplers should be placed in the minima of the current distribution (right, c). This investigation shows that a desired mode can be excited separately either by inductive or capacitive couplers placed in predefined positions. In addition, the authors of [42] were able to show that inductive couplers offer advantages over capacitive couplers in terms of selective excitation of specific wave modes. More details may be found in [43]-[46].

1.5 Objectives and Contributions of this Thesis

As has been introduced in Section 1. 4, so far, studies of the characteristic modes almost concentrated on discussing antennas resonance characteristics. It is true that frequency response of the modes is directly related to antennas resonance response when specific excitation is decided. This special property of the characteristic modes make itself significantly useful for problems of deeply exploring antennas resonance characteristics. However, reports about relationship between modes response and radiation pattern of the antennas with specific

excitation are seldom seen. It is known that similar with antennas resonance response, radiation pattern of the antenna with specific excitation will perform that of the excited modes. However, to the modes which are unexcited by the specific excitation, it is not very clear how they can impact the antennas radiation pattern.

Moreover, the theory of characteristic modes is used for antenna design so far. There is rarely not any research try to utilize the theory for clarifying physical phenomenon that cannot be clearly explained by utilizing general analysis methods.

The objectives and contributions of this thesis are summarized as follows.

- This thesis devotes to engineering applications of the theory but not the theory itself.
- This thesis contributes to illustrating how to use the characteristic modes to analyze antenna, adjust antenna parameters and help us to effectively realize desired antenna performances.
- This thesis provides a concise refinement of Integral Equation method based on the MoM and the theory of characteristic modes, in Chapter 2.
- As an indoor antenna for MIMO system that is able to reduce mutual correlation between component antennas and meanwhile, keep compact structure and size, a compact composite antenna composed of two orthogonally polarized component antennas is proposed to reduce correlation and realize miniaturization. Besides, a bandwidth and radiation pattern enhanced sample antenna is proposed, in Chapter 3.
- We use the characteristic modes analysis to discuss problem of cross-polarization of a disk loaded monopole antenna which is introduced in Chapter 3. It finds the feeding structure of disk loaded monopole tends to excite those modes have radial current distribution from center area to edge areas of the ground plane; and a ground mode providing absolutely uniform radial current distribution is considered that can reduce the horizontal polarization component radiated by the ground plane. Chapter 4 provides detailed discussion.
- A double notched antenna is used as an example to show how to get both omni-directional and bi-directional radiation patterns by adjusting characteristic modes of the

antenna, in Chapter 5. Considering the issue that it was not very clear that how the unexcited modes of an antenna can impact its radiation pattern, characteristic modes of an omni-directional four notched array antenna are calculated to identify the relationship between an unexcited mode and antenna radiation pattern, also in Chapter 5.

- The characteristic modes analysis is tried to explain neutralizing phenomenon occurring on two closely adjacent PIFA elements that are connected by a shorted line. The characteristic modes are calculated to discuss how the optimized shorted line helps reducing S21 coefficient, in Appendix I.
- A 4G cellular antenna designed for eyewear wireless devices is introduced and analyzed by using the theory of characteristic modes in Appendix II. The analysis of the characteristic modes, which occur on the antenna's ground plane, clearly helped us to understand the antenna's operational principle and optimized antenna feeding position.

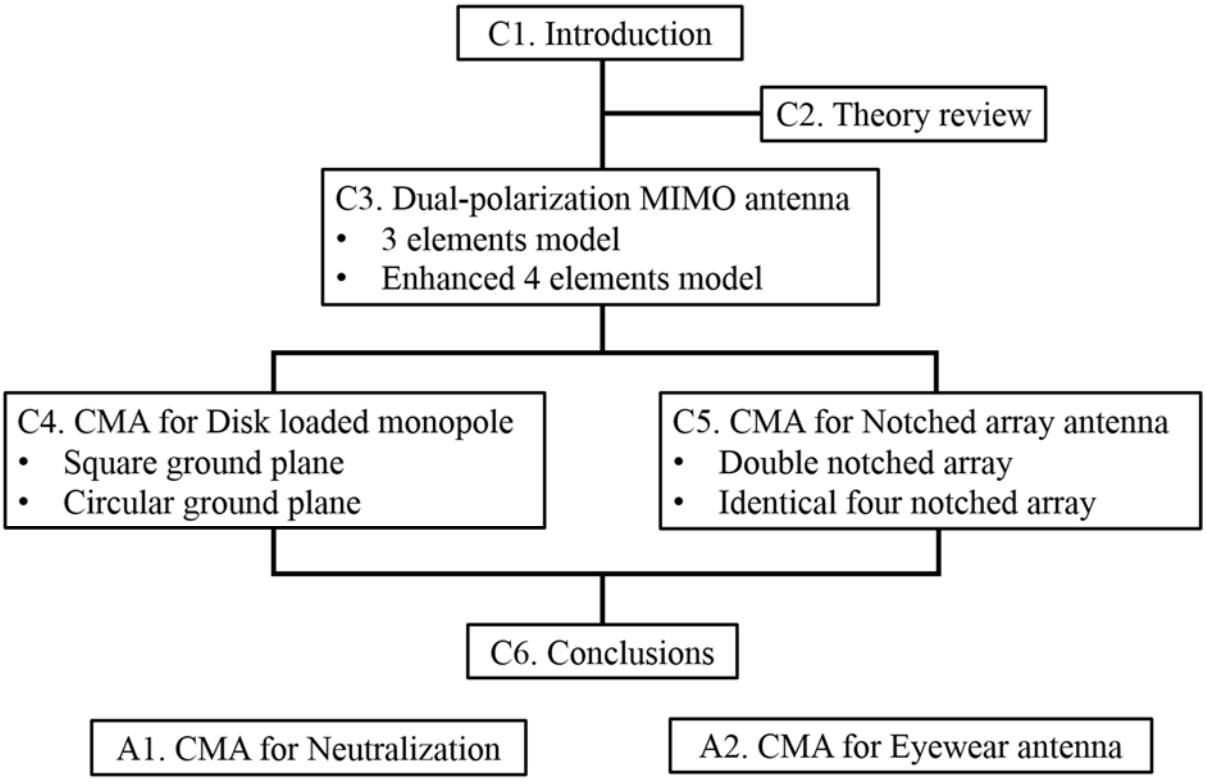

Figure 1. 3 The constitute of this thesis.

1.6 Characteristic Mode Analysis by FEKO[3]

As it will also be talked in Chapter 2, according to [15], the characteristic modes are defined by an eigenvalues equation. Characteristic eigenvalues, the most important coefficient in the theory of characteristic modes, are solved by the equation. If calculate the eigenvalues in Matlab, the linear equation is transformed into a mixed-potential integral equation (MPIE) [47] or a Rao-Wilton-Glisson (RWG) basis functions [48] using the MoM.

However, FEKO also started providing characteristic modes calculation function from September 2012 in its version 6.2 [49]. Considering convenience of antenna modeling, we utilize FEKO to calculate the characteristic modes in following Chapters. In addition, the FEKO updated Mode Tracking function in version 6.3 [50][51]. Since the modes may change with frequency, causing the mode index to switch if no tracking is implemented, as shown in Figure 1. 4 (a). Mode tracking is based on ordering the modes correctly at each frequency, relative to their rankings at the first frequency point. The new algorithm makes the working even more intuitive as shown in Figure 1. 4 (b). Moreover, it clarifies that the new version also extended to support dielectric and magnetic materials with the MoM with the surface equivalence principle, and apertures with the planar Green's function [50].

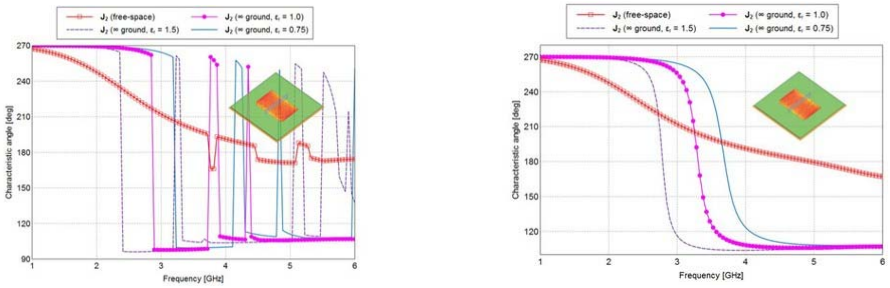

(a) (b)

Figure 1. 4 Characteristic angle plot with no tracking (a) and with tracking (b) [50][51].

[3] A commercial electromagnetic solutions software; linked to https://www.feko.info/

1.7 Summary

As the antenna geometry becomes more complicated, more often than not there is no closed formulation to analyze it. Under this circumstances, the time required for antenna design can be dramatically reduced by using computers and commercial simulators based on numerical methods. However, even with the support of computers, success of the final design still depends upon the intuition and previous experience of the designers. Actually in most cases, the final optimization is in fact made by “cut and try” methods. As a result, these days antenna design is very much governed by designers’ experience and know-how.

Because time-to-market is critical, efficiently antenna design is considerably important. The characteristic modes analysis is just such a method that can alleviate the problem.

What should be underline once again is that since characteristic modes are independent of any kind of excitation, they only depend on the shape and size of the conducting object. Thus, antenna design using characteristic modes can be performed in two steps. First, the shape and size of the radiating element are optimized. If the size of the element is scaled, the resonant frequency of the modes will be modified, whereas if the shape of the element is varied, not only the resonant frequency but also the radiating properties of the modes will change. Next, the optimum feeding configuration is chosen so that the desired modes may be excited.

In the following Chapter 2, we are going to concisely refine the MoM and the theory of characteristic modes.

CHAPTER 2
THEORY OF CHARACTERISTIC MODES

2.1 Introduction

The author[4] believe that almost all the antenna designers or researches would agree with an opinion that impedance problem is the most important issue to any antenna design.

An antenna can be represented by an equivalent impedance:

$$Z_A = R_A + jX_A \tag{2-1}$$

where

R_A = antenna resistance at feeding-point

X_A = antenna reactance at feeding-point

R_A is consisted of two parts:

$$R_A = R_r + R_l \tag{2-2}$$

[4] Shen Wang

where

R_r = radiation resistance of the antenna

R_l = loss resistance of the antenna

The equivalent impedance is attached at the feeding-point which is used to connect the antenna to a transmission line. Generally, this impedance is called the feeding-point impedance. However, when the antenna is radiating in an unbounded medium, in the absence of any other interfering elements or objects, the feeding-point impedance is the same as self-impedance of the antenna.

There are many methods that can be used to calculate the impedance of an antenna [52]. If ignore the approximate solutions for some high frequency cases, in general, these methods can be classified into four categories:

(1) Boundary value method;
(2) Transmission line method;
(3) Poynting vector method;
(4) Differential equation method;
(5) Integral equation method.

Extensive and brief discussions and comparisons of these methods have been reported in [52][53].

The boundary value approach is the most basic method. It treats the antenna as a boundary value problem. The solution to this method is obtained by enforcing the boundary conditions that usually the tangential electric field components vanish at the conducting surface. In turn, the current distribution and finally the impedance are determined as solutions to the problem. The principal disadvantage of this method is that it only has a few limited applications. It can only be applied and solved exactly on simplified geometrical shapes.

The transmission line method, which has been used extensively by Schelkunoff [54], treats the antenna as a transmission line. This method is most convenient for the biconical antenna. Since it utilizes tangential electric field boundary conditions for its solution. This technique

may also be classified as a boundary value method.

The basic approach of the Poynting vector method is to integrate the Poynting vector, which denotes power density, over a closed surface. The closed surface chosen is usually either a sphere with a very large radius R or a surface that coincides with the surface of the antenna. Here $R \geq 2D^2/\lambda$, and D is the largest dimension of the antenna. The method that utilizes the antenna surface was utilized for the calculation of antenna impedances [55]-[57].

The impedance of an antenna can also be calculated by using the Differential Equation method or the Integral Equation methods with a numerical technique solution, which has been briefly introduced in Chapter 1. Since the theory of characteristic modes is based on the MoM (Method of Moment), which is one of the Integral Equation methods, we ignore the Differential Equation method in this thesis.

The MoM, which in the late 1960s was extended to solve electromagnetic problems, is analytically simple [58]-[65]. Besides the electromagnetic problems, it is versatile that can be applied to various problems. However, it requires large amounts of computation. The limitation of this Integral Equation method is usually the speed and storage capacity of the computer, as that has been referred in Section 1.2 of the Chapter 1. Moreover, it is important that comparing with exact solutions based on extraordinarily complex Sommerfeld integral formulations [66], a method based on Equivalence Principle [67][68] is widely utilized. Due to its convenience, this approach is very general, and it can be used with today's modern computational methods and equipment to compute the characteristics of complex configurations of antenna elements, especially appropriate for dielectric materials, such as microstrip structures using substrate. Based on this method, characteristic modes of not only conductor but also dielectric materials are able to be calculated. In fact, the commercial simulator FEKO is using its numerical code with method based on the Equivalence Principle [50].

Section 2.2 will be an overview of electric field integral equation based on full equivalent current, and the MoM solution for the equivalent current. To demonstrate the approach, we will initially consider a specific antenna element using microstrip structure as example. In addition, because the characteristic modes are independent of any kind of excitation, we will only consider the self-impedance of the antenna element.

Section 2.3 provides a concise refinement of the theory of characteristic modes. This discussion will be separated to the derivation of the classical characteristic modes and the comparison of the characteristic modes analysis and the common antenna analysis.

Incidentally, in [52]-[65] there are many age-old books that difficult to acquire, nevertheless, some excerpts of the books can be read on the Internet[5].

2.2 E-Field Integral Equation and Method of Moment

As was introduced in Section 2.1, equivalence principle for the MoM can considerably simplify the complex and heavy computation. The core idea is to use the equivalence principle to replace all conducting bodies by equivalent surface electric currents, and all dielectrics by equivalent volume polarization currents. The respective boundary conditions on the conducting bodies and the dielectrics are utilized, establish two integral equations, and then use the MoM to solve for the electric current on the entire structure.

If appropriate primary function is selected, this approach is thought theoretically suitable for antennas with any structures. [68] presented some typical results to illustrate the effectiveness and potential of this method.

2.2.1 E-Field Integral Equation Based on Full Equivalent Current

In this section, we use the equivalence principle to establish electric field (E-field) integral equation based on full equivalent current to analyze a microstrip antenna element. The so-called Full Equivalent Current means that use free-space radiation from the equivalent surface

[5] http://ieeexplore.ieee.org/Xplore/home.jsp ; http://books.google.com/ ; etc.

currents to replace influence by the conductors, and free-space radiation from the equivalent polarization currents to replace influence by dielectrics. Both the equivalent surface currents and the equivalent polarization currents are currents that distribute in the free-space. Thus, the Green's function for free-space can be utilized to calculate equivalent E-field. As is known to all, the Green's function for free-space is the simplest one comparing to other situations. In following analysis, we strictly take the influence by finite ground plane into consideration.

Essentially, E-field integral equation is established by that tangential E-field on a perfect conductor surface is equal to 0. Figure 2. 1 shows a basic model for the E-field problems on perfect conductor.

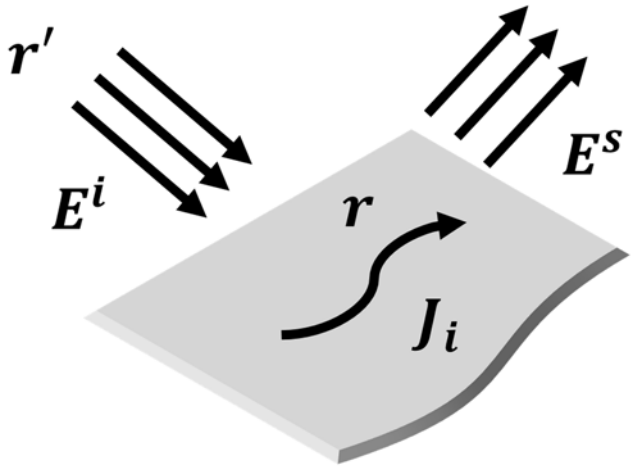

Figure 2. 1 A basic model for E-field problems.

Under the excitation of incident E-field, total E-field at arbitrary location $\boldsymbol{r}$ is:

$$\boldsymbol{E}(\boldsymbol{r}) = \boldsymbol{E}^{\boldsymbol{i}}(\boldsymbol{r}) + \boldsymbol{E}^{\boldsymbol{s}}(\boldsymbol{r}) \tag{2-3}$$

where

$\boldsymbol{E}^{\boldsymbol{i}}(\boldsymbol{r})$ = incident E-field at location $\boldsymbol{r}$

$\boldsymbol{E^s(r)}$ = scattered E-field at location $\boldsymbol{r}$

The scattered E-field $\boldsymbol{E^s(r)}$ consists of two components. The first component is due to the E-field produced by the induced current on the conductor due to the incident E-field $\boldsymbol{E^i}$, while the second component is due to the E-field produced by the induced volume polarization current in the dielectric. Hence:

$$\boldsymbol{E^s(r)} = L_c[\boldsymbol{J_c}] + L_d[\boldsymbol{J_d}] \tag{2-4}$$

where

$\boldsymbol{J_c}$ = the induced current on the conductor due to the incident E-field $\boldsymbol{E^i}$

$\boldsymbol{J_d}$ = the induced volume polarization current in the dielectric due to the incident E-field $\boldsymbol{E^i}$

$L[\boldsymbol{J}]$ = the E-field produced by $\boldsymbol{J}$

Figure 2. 2 shows a typical E-field problems for multi-layer structures such as microstrip

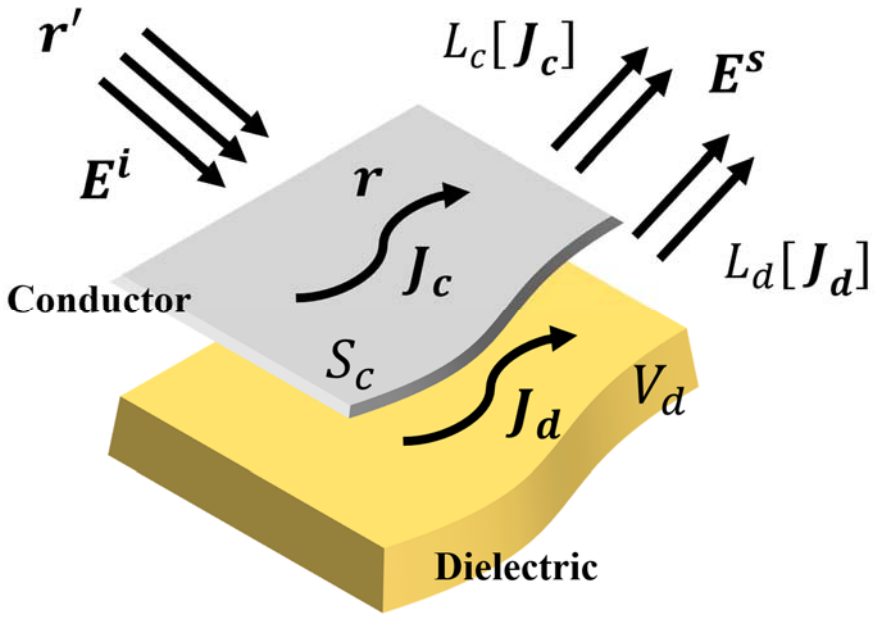

Figure 2. 2 E-field problems for multi-layer structures.

We have:

$$L_c[\boldsymbol{J_c}] = -j\omega \boldsymbol{A_c} - \boldsymbol{\nabla}\phi_c$$

$$= -\frac{j\omega\mu_0}{4\pi} \iint_{\text{conducter}} \boldsymbol{J_c}(\boldsymbol{r})\boldsymbol{G}(\boldsymbol{r},\boldsymbol{r}')ds' - \frac{\boldsymbol{\nabla}}{4\pi\varepsilon_0} \iint_{\text{conducter}} \rho_c(\boldsymbol{r}')\boldsymbol{G}(\boldsymbol{r},\boldsymbol{r}')ds' \tag{2-5}$$

where

$\boldsymbol{r}$ = field coordinate

$\boldsymbol{r}'$ = source coordinate

ω = angular frequency

ε_0 = permittivity of free space

μ_0 = permeability of free space

ρ_c = charge density on the conductors

$\boldsymbol{G}(\boldsymbol{r},\boldsymbol{r}')$ = Green's function of free space

and

$$\boldsymbol{G}(\boldsymbol{r},\boldsymbol{r}') = e^{-jk_0R}/R \tag{2-6}$$

where

$$R = \sqrt{(x-x')^2 + (y-y')^2 + (z-z')^2} \tag{2-7}$$

$$k_0 = \frac{2\pi}{\lambda_0} = \omega\sqrt{\varepsilon_0\mu_0} \tag{2-8}$$

According to the Equation of Continuity, the divergence of the current density $\boldsymbol{J}$ is equal to the negative rate of change of the charge density ρ. So, the charge density ρ_c on the conductors is related to the electric currents $\boldsymbol{J_c}$ on the conductors.

Thus, we have:

$$\rho_c = -\frac{\boldsymbol{\nabla}' \cdot \boldsymbol{J_c}}{j\omega} \tag{2-9}$$

Then, we can get the fields produced by $\boldsymbol{J_c}$ residing on all the conductors by combing (2-5), (2-8) and (2-9):

$$L_c[\boldsymbol{J_c}] = \frac{1}{j\omega 4\pi\varepsilon_0}\left[k_0^2 \iint\limits_{\text{conducter}} \boldsymbol{J_c}(\boldsymbol{r})\boldsymbol{G}(\boldsymbol{r},\boldsymbol{r}')ds' + \boldsymbol{\nabla} \iint\limits_{\text{conducter}} \boldsymbol{\nabla}' \cdot \boldsymbol{J_c}(\boldsymbol{r}')\boldsymbol{G}(\boldsymbol{r},\boldsymbol{r}')ds'\right] \tag{2-10}$$

This equation shows how to calculate the E-field produced by the induced current $\boldsymbol{J_c}$ on the conductor due to the incident E-field $\boldsymbol{E^i}$. On the other hand, the scattered field from the equivalent volume polarization currents $\boldsymbol{J_d}$ flowing in the dielectric regions can also be solved in similar style. That is:

$$L_d[\boldsymbol{J_d}] = \frac{1}{j\omega 4\pi\varepsilon_0}\left[k_0^2 \iiint\limits_{\text{volume}} \boldsymbol{J_d}(\boldsymbol{r})\boldsymbol{G}(\boldsymbol{r},\boldsymbol{r}')dV' + \boldsymbol{\nabla} \iiint\limits_{\text{volume}} \boldsymbol{\nabla}' \cdot \boldsymbol{J_d}(\boldsymbol{r}')\boldsymbol{G}(\boldsymbol{r},\boldsymbol{r}')dV'\right] \tag{2-11}$$

here the integration in this equation is carried out over the volume V_d instead of the surface S_d as in (2-10). S_d is the surface enclosing the volume V_d.

However, we have to enforce boundary condition for the dielectrics as:

$$\boldsymbol{\nabla}' \cdot \boldsymbol{J_d}(\boldsymbol{r}') \begin{cases} = 0, & \boldsymbol{r}' \in V_d \\ \neq 0, & \boldsymbol{r}' \in S_d \end{cases} \tag{2-12}$$

The boundary condition in (2-12) indicates that the current flowing in a homogeneous dielectric region is divergenceless, i.e. there is no charge density associated with this current in the interior of the dielectric except that at the interface of the inhomogeneous dielectric regions.

Hence, the second integral in (2-11) reduces to a surface integral:

$$L_d[\boldsymbol{J_d}] = \frac{1}{j\omega 4\pi\varepsilon_0}\left\{k_0^2 \iiint_{\text{volume}} \boldsymbol{J_d}(\boldsymbol{r})\boldsymbol{G}(\boldsymbol{r},\boldsymbol{r}')dV' + \boldsymbol{\nabla}\iint_{S_d}[-\boldsymbol{J_d}(\boldsymbol{r}')\cdot\boldsymbol{n}]\boldsymbol{G}(\boldsymbol{r},\boldsymbol{r}')dS'\right\} \tag{2-13}$$

here $\boldsymbol{n}$ represents the unit normal vector of the surface S_d.

On the conductor surface S_c, tangential E-field is 0. So, (2-3) is simplified as:

$$[\boldsymbol{E^i}(\boldsymbol{r}) + \boldsymbol{E^s}(\boldsymbol{r})]_{tan} = 0, \quad \boldsymbol{r} \in S_c \tag{2-14}$$

Combing (2-4), (2-10), and (2-11), the integral equation on the surface of the conductors is given by:

$$\boldsymbol{E^i}(\boldsymbol{r})_{tan} = -L_c[\boldsymbol{J_c}] - L_d[\boldsymbol{J_d}], \quad \boldsymbol{r} \in S_c \tag{2-15}$$

where $L_c[\boldsymbol{J_c}]$ is given by (2-10) and $L_d[\boldsymbol{J_d}]$ is given by (2-11).

In order to apply the E-field integral equation to the dielectric region, definition of the volume polarization current is utilized:

$$\boldsymbol{J_d}(\boldsymbol{r}) = j\omega\varepsilon_0(\varepsilon_r - 1)\boldsymbol{E}^{total}(\boldsymbol{r}), \quad \boldsymbol{r} \in V_d \tag{2-16}$$

where

$\boldsymbol{E}^{total}(\boldsymbol{r})$ = total E-field inside the dielectric regions denoted by V_d that we have

$$\boldsymbol{E}^{total}(\boldsymbol{r}) = \boldsymbol{E^i}(\boldsymbol{r}) + \boldsymbol{E^s}(\boldsymbol{r}), \quad \boldsymbol{r} \in V_d \tag{2-17}$$

ε_r = relative complex permittivity of the dielectric medium

By combing (2-16) and (2-17):

$$\boldsymbol{E^i(r)} = \frac{\boldsymbol{J_d(r)}}{j\omega\varepsilon_0(\varepsilon_r - 1)} - \boldsymbol{E^s(r)}, \quad \boldsymbol{r} \in V_d$$

(2-17)

Here the problem is to solve the total scattered fields $\boldsymbol{E^s(r)}$. Since it has been computed as before, from the two electric currents that are the surface currents on the conductors and the volume polarization currents on the dielectrics, it is same with (2-4) but $\boldsymbol{r} \in V_d$.

Hence in the dielectric regions, we can get:

$$\boldsymbol{E^i(r)} = \frac{\boldsymbol{J_d(r)}}{j\omega\varepsilon_0(\varepsilon_r - 1)} - L_c[\boldsymbol{J_c}] - L_d[\boldsymbol{J_d}], \quad \boldsymbol{r} \in V_d$$

(2-17)

So, finally we got two important equations (2-15) and (2-17). By given an incident E-field $\boldsymbol{E^i}$, we can utilize the coupled integral equations (2-15) and (2-17) to solve for the induced currents on the conductors $\boldsymbol{J_c}$, and the induced volume polarization currents in the dielectrics $\boldsymbol{J_d}$. Once the currents are known, any other indexes of interest can be obtained.

2.2.2 Overview of Method of Moment

If under some specific underlying assumptions, we can utilize Method of Moment (MoM) to obtain an approximate numerical solution of the coupled integral equations described by (2-15) and (2-17). In the case that we discuss above, the assumptions are:

I. The shapes of the conductors are only in the form of rectangular flat plates all located in one specific plane (something like *x*-*y* plane).
II. The dielectric regions exist as cubic elements and all inhomogeneous lossy dielectric regions consist of cubes.
III. The dielectric and permeability of every layer are constant.

Harrington introduced the MoM very in detail [59], thus in this thesis we just summarize some important points. One of them is about treatment of singular points in the medium volume integral equations. In the full equivalence current integral equation method based on the MoM for the analysis of microstrip antennas, whether in the conductor surface integral equation, or the integral equation of dielectric region, there are singular points exist due to the presence of Green's function. In order to save computational time, several studies proposed substituted analysis methods for that in the conductor surface integral equation [69][70] and the dielectric region integral equation [71], respectively.

A) General process

Generally, if try to use a diagram to overview the MoM, that will be Figure 2. 3. The original linear operator equation is:

$$L(x) = f \tag{2-18}$$

where

L = is a known linear operator

f = is a known excitation function

x = is basis function which is waiting to be determined

While the inverse problem is often intractable in closed form, the linearity of the operator L makes a numerical solution possible. The MoM requires that the unknown response function be expanded as a linear combination of N terms and written as

$$\sum_{n=1}^{N} u_n x_n$$

where each u_n is an unknown constant and each x_n is a known function usually referred to as a basis function. Substituting the combination into (2-18), and using the linearity of the L operator can reduce (2-18) to:

$$\sum_{n=1}^{N} u_n L(x_n) = f$$

(2-19)

The basis functions x_n are chosen, so that each $L(x_n)$ in (2-19) can be evaluated conveniently. The only task remaining then is to find the unknown constants u_n. The expansion of (2-19) leads to one equation with *N* unknowns. It alone is not sufficient to determine the *N* unknown u_n (*n* = 1, 2, . . . , *N*) constants.

To resolve the *N* constants, it is necessary to have *N* linearly independent equations. This can be accomplished by evaluating (2-19), e.g., applying boundary conditions, at *N* different points. This is referred to as point-matching (or in some books it is called as collocation). Thus, now provides an appropriate inner product $\langle \omega, f \rangle$. Inside the domain of the linear operator L, *N* weighting functions ω_m (*m* = 1, 2, . . . , *N*) are defined.

Thus, we have the inner product of ω_m and the (2-19):

$$\sum_{n=1}^{N} u_n \langle \omega_m, L(x_n) \rangle = \langle \omega_m, f \rangle$$

(2-20)

In matrix form, (2-20) can be expressed as:

$$[u_n][\Omega_{mn}] = [F_m]$$

(2-21)

Then the unknown coefficients u_n can be found by solving (2-21) using matrix inversion techniques, etc.

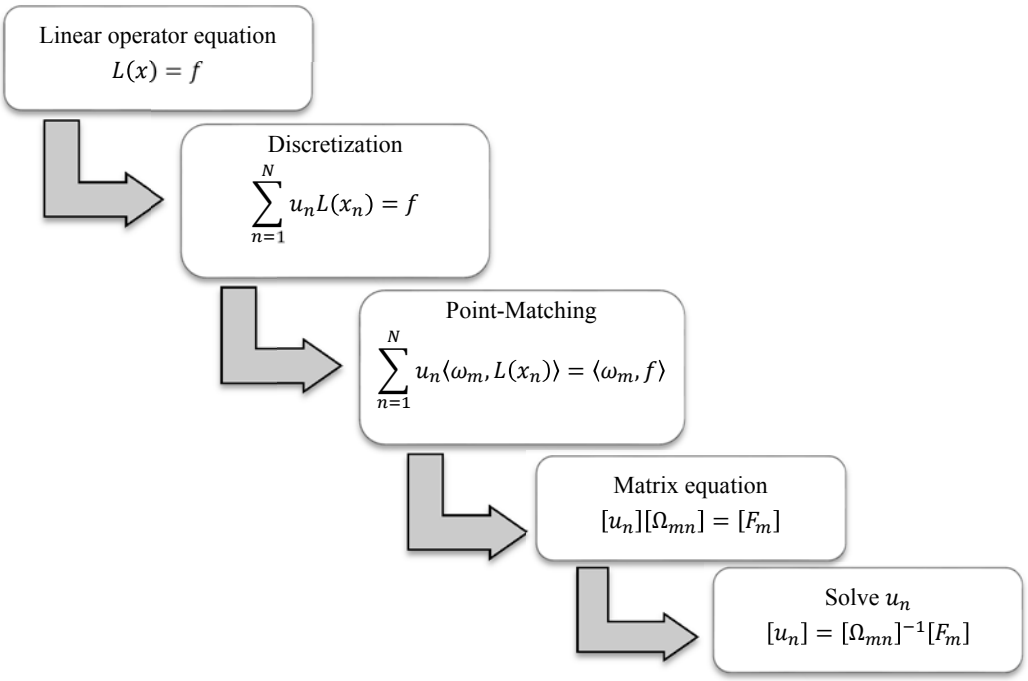

Figure 2. 3 Overview of general process of the MoM.

B) Basis functions

The choice of the basis functions x_n is a very important step in any numerical solution. In general, one chooses as basis functions the set that has the ability to accurately represent and resemble the anticipated unknown function, while minimizing the computational effort required to employ it.

Theoretically, there are many possible sets of basis functions. However, only a limited number are used in practice. These sets may be divided into two general classes. The first class consists of subdomain functions, which are nonzero only over a part of the domain of the function. Its domain is the surface of the structure.

The second class contains entire-domain functions that exist over the entire domain of the unknown function. The entire-domain basis function expansion is analogous to the well-known Fourier series expansion method.

Concerning the choice of the basis functions, more details can be found in [72]-[74].

C) RWG basis function

A very commonly used basis function that deserve to be mentioned is Rao-Wilton-Glisson (RWG) basis function, which was firstly proposed by S. M. Rao, D. R. Wilton and A. W. Glisson in [75] to solve electromagnetic scattering problems by conductor surfaces of arbitrary shape, and then was generalized inhomogeneous dielectric mediums by D. H. Schaubert [76].

By the RWG method, a lot of small planar triangular components are used to approximate the arbitrary surfaces. The model which is established by this method is called the Rao model. Linear superposition of unit currents along the three sides of any a triangle is used to approximate the constant vector current distribution inside the triangle area. This method can be calculated by using Matlab that S. Makarov provided a code package in 2002 [77], while many commercial simulators also utilize this basis function for the computation of the MoM. Figure 2. 4 shows an example that an oval-shaped surface is meshed in FEKO by small triangular components. More details about the RWG basis functions and derivations can be obtained from [75]-[77].

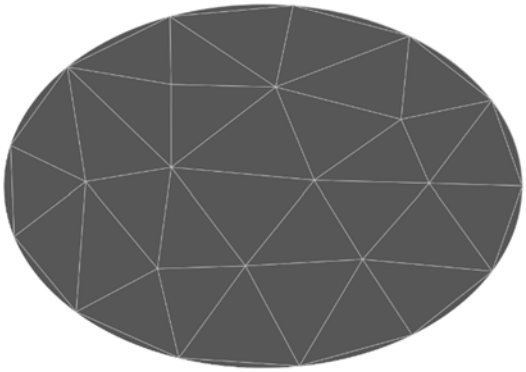

Figure 2. 4 An oval-shaped surface meshed in FEKO by small triangular components.

D) Weighting functions

The inner product of the weighting functions ω defined above (2-20) and the linear basis function $L(x)$, with that of ω and the excitation function f are found in (2-20). This two

inner product can be rewrite to integral form:

$$\begin{cases} \langle \omega, L(x) \rangle = \iint_S \omega^* \cdot L(x)\, dS \\ \langle \omega, f \rangle = \iint_S \omega^* \cdot f\, dS \end{cases} \tag{2-22}$$

where the asterisk ($*$) indicates complex conjugation, and S is the surface of the structure being analyzed. This is the core part of the MoM.

The point-matching process has solutions that can satisfy the electromagnetic boundary conditions only at discrete points. Between these points the boundary conditions may not be satisfied. However, the MoM can be utilized in conjunction with the inner product of (2-22), so that it forces the boundary conditions to be satisfied in an average sense over the entire surface S [58]-[65].

2.3 Theory of Characteristic Modes

An overview and early studies on applications of the theory of characteristic modes have been introduced in Section 1.3 and 1.4. In this Section, we summarize the classical theory which is the most important derivation of eigenvalue, eigen current, etc. of the characteristic modes [14]-[22], and derive correlated equations and definitions.

This Section will be divided into two parts. In 2.3.1, we derive the classical theory of characteristic modes which was firstly generalized to analyzing conductors in arbitrary shape by Robert J. Garbacz [14] and then summarized and improved by Roger. F. Harrington and Joseph R. Mautz [15][16]. In 2.3.2, we compare the theory of characteristic modes and the common antenna calculations based on the MoM. Since there are several paper can be referred to understand the generalized characteristic modes, we ignore this part. All the derivations in this Section are limited for only conductor surface.

2.3.1 Classical Theory of Characteristic Modes

A) Eigenvalues and Eigen Currents

Suppose *S* is the surface of a conductor. The tangential component of E-field on the surface is:

$$\left[L(\boldsymbol{J}) - E^i\right]_{tan} = 0 \tag{2-23}$$

where

E^i = incident E-field in the scatter problems, or input power in antenna problems

$\boldsymbol{J}$ = induced current on the conductor surface *S* due to the incident E-field or input power

$L(\boldsymbol{J})$ = scattered E-field due to the induced current $\boldsymbol{J}$

The operator L is defined by (2-10). While in the case of dielectrics, it is defined by (2-11) or (2-13).

Reorganize (2-23) to:

$$[L(\boldsymbol{J})]_{tan} = {E^i}_{tan} \tag{2-24}$$

Define $L(I)$ as:

$$Z(\boldsymbol{J}) = [L(\boldsymbol{J})]_{tan} \tag{2-25}$$

So (2-24) becomes:

$$Z(\boldsymbol{J}) = {E^i}_{tan} \tag{2-26}$$

This is an inhomogeneous equation. Its corresponding homogeneous equation is:

$$Z(\boldsymbol{J}) = 0$$

(2-27)

According to the theory of reciprocity, Z is a symmetric operator but not a Hermitian operator. In some sense, the Hermitian operator plays the role of the real numbers (being equal to their own "complex conjugate") and form a real vector space [78]. However, since Z is symmetric, its Hermitian component is real and can be expressed as:

$$R = \frac{1}{2}(Z + Z^*)$$

(2-28)

$$X = \frac{1}{2j}(Z - Z^*)$$

(2-29)

Here the asterisk ($*$) indicates complex conjugation, so we have:

$$Z = R + jX$$

(2-30)

R and X are real symmetric operators as well as the Hermitian operator. Then, we define weighting eigen equation as:

$$Z(\boldsymbol{J_n}) = (1 + j\lambda_n)M(\boldsymbol{J_n})$$

(2-31)

here

$1 + j\lambda_n$ = complex eigenvalue, and λ_n is real eigenvalue

$\boldsymbol{J_n}$ = eigen function as well as eigen current

M = weighting operator which is chosen

We choose $M = R$, and combine (2-30), (2-31):

$$(R + jX)(\boldsymbol{J_n}) = (1 + j\lambda_n)R(\boldsymbol{J_n})$$

(2-32)

Remove the common item $R(\boldsymbol{J_n})$, we obtain simplified weighting eigen equation:

$$X(\boldsymbol{J_n}) = \lambda_n R(\boldsymbol{J_n})$$

(2-33)

Moreover, the choice of R as a weighting operator in equation (2-33) is responsible for the orthogonality properties of characteristic modes. According to [14], the orthogonality properties can be summarized as:

$$\langle \boldsymbol{J_m}, R(\boldsymbol{J_n}) \rangle = \langle \boldsymbol{J_m}^*, R(\boldsymbol{J_n}) \rangle = \delta_{mn} \tag{2-34}$$

$$\langle \boldsymbol{J_m}, X(\boldsymbol{J_n}) \rangle = \langle \boldsymbol{J_m}^*, X(\boldsymbol{J_n}) \rangle = \lambda_n \delta_{mn} \tag{2-35}$$

$$\langle \boldsymbol{J_m}, Z(\boldsymbol{J_n}) \rangle = \langle \boldsymbol{J_m}^*, Z(\boldsymbol{J_n}) \rangle = (1 + j\lambda_n)\delta_{mn} \tag{2-36}$$

Where δ_{mn} is a Kronecker delta [79] that satisfies:

$$\delta_{mn} = \begin{cases} 1, & m = n \\ 0, & m \neq n \end{cases} \tag{2-37}$$

Consistent with (2-33), the *eigen current* $\boldsymbol{J_n}$ can be defined as the real currents on the surface of a conductor surface that only depend on its shape and size, and are independent of any specific source or excitation. Physically, R and X are the real and imaginary parts of the impedance operator Z. In practice, to compute characteristic modes of a particular conducting body, (2-33) needs to be reduced to matrix form, as explained in [15], using the Galerkin formulation [59]:

$$[X]\boldsymbol{J_n} = \lambda_n [R]\boldsymbol{J_n} \tag{2-38}$$

The term λ_n, in above equations, corresponds with the *eigenvalue* associated with the n^{th} characteristic mode. This eigenvalue is considerably important, because its magnitude gives information about how well the associated mode radiates. It is deduced that power radiated by modes is normalized to unit value [14]. In contrast, reactive power is proportional to the magnitude of the eigenvalue. Considering a mode is at resonance when its associated eigenvalue is zero, $\lambda_n = 0$, it is inferred that the smaller the magnitude of the eigenvalue, the more efficiently the mode resonates and radiates when excited. In addition, the sign of the eigenvalue determines whether the mode contributes to storing magnetic energy as an

inductance modes, that when $\lambda_n > 0$; or electric energy as a capacitance mode, that when $\lambda_n < 0$.

B) Modal Excitation

The content in this sub-section is called modal solutions in [15]. However, the author think modal excitation or modal synthesize may be more appropriate, because it indicates that how much a specific eigen current $\boldsymbol{J_n}$ of n^{th} characteristic mode can contribute itself to the actually excited antenna.

Suppose $\boldsymbol{J}$ is the induced current on the conductor surface which is excited by some specific excitation, and $\boldsymbol{J_n}$ is the eigen current of n^{th} characteristic mode defined in above sub-section. Also, $\boldsymbol{J_n}$ is seen as a basis function in the MoM. We assume $\boldsymbol{J}$ to be a linear superposition of the mode currents so that expand it as:

$$\boldsymbol{J} = \sum_{n=1}^{N} u_n \boldsymbol{J_n} \tag{2-39}$$

Where

u_n = weighting coefficient which is a coefficient to be determined

Substituting (2-39) into (2-26), since Z is a linear operator, we can get:

$$\sum_{n=1}^{N} u_n Z(\boldsymbol{J_n}) = {E^i}_{tan} \tag{2-40}$$

By using the MoM, the inner product of (2-40) with each $\boldsymbol{J_m}$ in turn is taken, giving the set of equations similar with (2-20) that we have:

$$\sum_{n=1}^{N} u_n \langle \boldsymbol{J_m}, Z(\boldsymbol{J_n}) \rangle = \langle \boldsymbol{J_m}, {E^i}_{tan} \rangle, \qquad m = 1,2,\dots,N$$

(2-41)

If only observe one mode, so let $m = n$, substitute (2-36) into (2-41):

$$\sum_{n=1}^{N} u_n(1 + j\lambda_n) = \langle \boldsymbol{J_n}, {E^i}_{tan} \rangle$$

(2-42)

Define:

$$\langle \boldsymbol{J_n}, {E^i}_{tan} \rangle = V_n^i$$

(2-43)

We call V_n^i as *modal excitation coefficient*. This coefficient obviously indicates that how much the specific eigen current $\boldsymbol{J_n}$ of n^{th} characteristic mode can contribute itself to the actually excited antenna.

Combining (2-39), (2-42) and (2-43), we obtain the induced current $\boldsymbol{J}$ on the conductor surface:

$$\boldsymbol{J} = \sum_{n=1}^{N} \frac{V_n^i \boldsymbol{J_n}}{1 + j\lambda_n}$$

(2-44)

This equation expresses the composition of the total current $\boldsymbol{J}$ induced by some specific excitation. And, both the modal excitation coefficient V_n^i and the eigenvalue λ_n denote contribution degree, or weight of the eigen current $\boldsymbol{J_n}$ of n^{th} characteristic mode to the total current more clearly. The two coefficients are demonstrated as following, respectively.

V_n^i --- reflects the relationship between mode *n* and the chosen specific excitation. The modal excitation coefficient accounts for the way the position, magnitude and phase of the applied excitation influence the contribution of each mode to the total current. Consequently, the term $V_n^i \boldsymbol{J_n}$ in (2-44) indicates the coupling between the excitation and the *n*th characteristic mode. In short, it determines if a particular mode is excited by the antenna feeding or the incident field.

λ_n --- reflects resonance degree of mode *n* itself. Its magnitude expresses information about how well the associated characteristic mode resonates and radiates when the mode is fully excited.

C) Modal Significance and Characteristic Angle

Since the modal expansion of the current described in (2-44) is inversely dependent upon the eigenvalues, it seems more consistent to analyze the variation of the term

$$MS = \left|\frac{1}{1 + j\lambda_n}\right| \tag{2-45}$$

rather than the variation of the isolated eigenvalue. This term is usually called *modal significance (MS)*, as it represents the normalized amplitude of the current modes [28]. Same with the eigenvalue, this normalized amplitude only depends on the shape and size of the conducting object, and it does not account for excitation.

Deriving from the eigenvalue, we can find the domain of the modal significance is

$$0 < MS \leq 1$$

Identically, a mode is at resonance when its associated modal significance is $MS = 1$. It is inferred that the closer the modal significance to 1, the more efficiently the mode resonates and radiates when excited. However, the sign of the modal significance cannot determine whether the mode contributes to storing magnetic energy as an inductance modes or electric energy as a capacitance mode, like the eigenvalue.

There is another representation, *characteristic angle*, that more convenient to use. The characteristic angle is defined in [26] by:

$$\alpha_n = 180° - tan^{-1}\,\lambda_n \tag{2-46}$$

From a physical point of view, the characteristic angle indicates the phase difference between a characteristic current $\boldsymbol{J_n}$ and the associated characteristic field $\boldsymbol{E_n}$. Also, because the coefficient is from the eigenvalue, it is able to represent the status of modes. That is, a mode

resonates when its characteristic angle is $\alpha_n = 180°$. Therefore, when the characteristic angle is close to $180°$, the mode is a good radiator. Thus, the radiating bandwidth of a mode can be obtained from the slope at $180°$ of the curve described by the characteristic angles vs. frequencies. When the characteristic angle is near $90°$ or $270°$, the mode mainly stores energy. Moreover, different with the modal significance, the value of the characteristic angle can indicate whether the mode contributes to storing magnetic energy as an inductance modes, that when $90° < \alpha_n < 180°$; or electric energy as a capacitance mode, that contrarily when $180° < \alpha_n < 270°$.

The three important coefficients of characteristic mode are summarized in Table 2. 1.

Table 2. 1
Summary of the three coefficients of characteristic mode

Eigenvalue $\boldsymbol{\lambda_n}$	Modal Significance $\boldsymbol{MS}$	Characteristic Angle $\boldsymbol{\alpha_n}$	Mode Status
$\boldsymbol{\lambda_n > 0}$	$0 < MS < 1$	$90° < \alpha_n < 180°$	Inductive
0	1	$180°$	Resonant
$\boldsymbol{\lambda_n < 0}$	$0 < MS < 1$	$180° < \alpha_n < 270°$	Capacitive

2.3.2 Comparison of Characteristic Modes Analysis and Common Antenna Analysis Based on MoM

There is an important question worth to answer that what is the difference between the theory of characteristic modes and the common antenna analysis based on the MoM. The two methods are same on the calculating process, which is the integral equation method based on the MoM. However, there are merely two key parts in the MoM, the discretization process and the point-matching process, to transform a linear operator equation to a matrix equation.

To a common antenna analysis problem, we have two important known conditions that are the structure of the antenna and the excitation, or the incident E-field. Thus, the calculation based on the MoM is the most principle procedure to obtain remaining indexes such as radiation resistance, current distribution, radiation pattern, etc.

While to the characteristic modes analysis problem, we have only one known condition that is the structure of the antenna. Since both the excitation and the incident wave are not considered in this theory, the most remarkable feature of the theory is the existing of a lot of possibilities. In other words, there are a lot of characteristic modes with different current distributions as well as different possible feeding style to excite these modes. Nevertheless, as one of the characteristic modes, it has to satisfy the requirements given by (2-34), (2-35) and (2-36), and where $m = n$. That is to say, as characteristic modes, their eigen currents must be orthogonal to each other over source region, and the characteristic E-fields are orthogonal to each other over spherical surface at infinity. Then, the eigenvalue, $\boldsymbol{\lambda_n}$ is used to stamp the status of each mode. This procedure looks like a qualification verification procedure.

Figure 2. 5 shows overview and comparison of procedure of the two analysis.

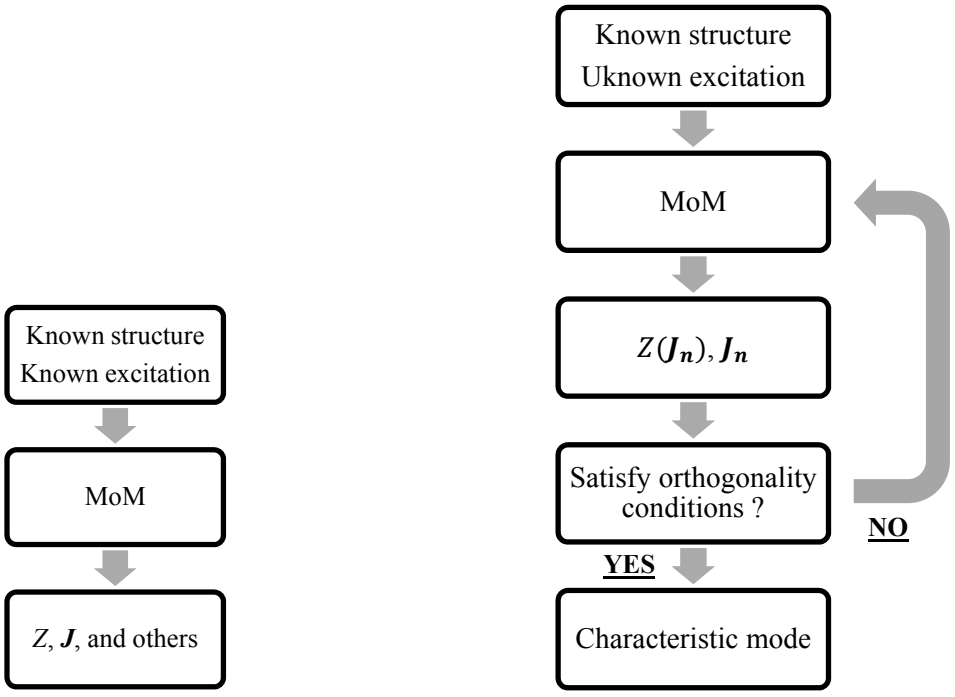

Figure 2. 5 Overview and comparison of (a) common antenna analysis and (b) characteristic modes analysis.

2.4 Summary

In this Chapter, firstly, we introduced the E-field integral equation based on the theory of full equivalent current to find induced current density on conductor surfaces or induced polarization current density in dielectric bodies, by a known incident E-field or an excitation when in most of the antenna problems. Secondly, the method of moment (MoM), which is a very versatile method that can be applied to various problems including electromagnetic problems, is briefly concluded. The discretization and point-matching are the most important processes in the MoM, to create appropriate matrixes and integral equations. The procedure of the MoM can be described as assembling the current density at each point on the antenna to find total current distribution. Finally, as the theme of this thesis, the classical theory of characteristic modes is summarized. As the condition of judging a current mode is a characteristic mode or not, its eigen current must be orthogonal at the source region to any other characteristic mode. Figure 2. 6 summarizes the three subjects in Chapter 2.

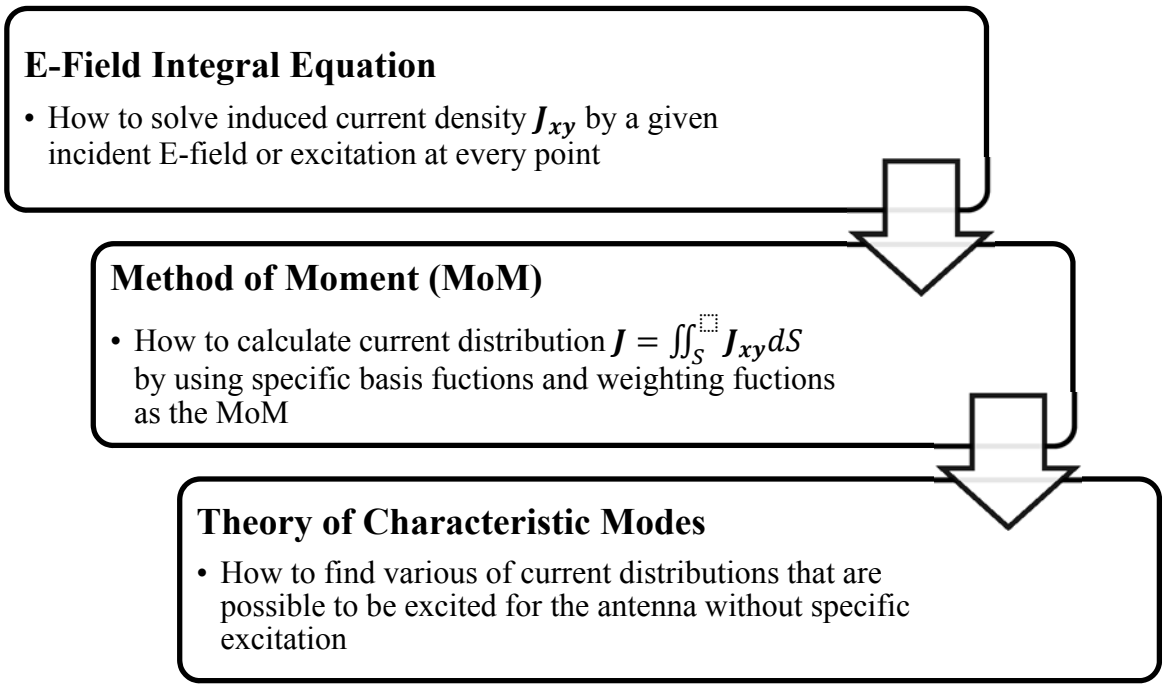

Figure 2. 6 Summary of the content in Chapter 2

CHAPTER 3
COMPACT DUAL-POLARIZATION MIMO ANTENNA

3.1 Introduction

In recent years, Multiple-Input Multiple-Output (MIMO) system becomes a noticeable technology due to its communication speed enhancement without extra frequency band, especially in multipath fading environment, and the resulting demand. The selection and design for MIMO antennas are extraordinarily important to realization of the MIMO system. When considering MIMO technology, Line-of-Sight (LOS) propagation is a problem that increase correlation of channels, and lead to bad performance of the system. The LOS cannot be ignored especially in indoor environment. Figure 3. 1 shows a 2×2 MIMO concept map which indicates operating principle of the MIMO system. Two signals $[s_0, s_1]$ are input into an encoder at the same time, distributed to two routes and radiated by two transmitter antennas. On the other side, two receiver antennas receive signals respectively from the transmitter antennas through channels $[h_{00}, h_{10}]$ and $[h_{01}, h_{11}]$. The received signals are $[r_0, r_1]$, which are converted by the air channel. Then, these received new signals are inversed by a decoder to returning to the original signals $[s_0, s_1]$.

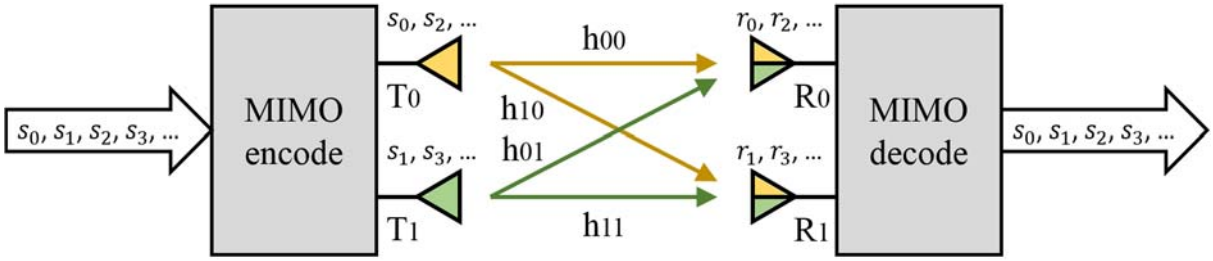

Figure 3. 1 A 2×2 MIMO concept map.

The process of transmitting from the encoder to the decoder can be denoted by a matrix equation as:

$$\begin{bmatrix} r_0 \\ r_1 \end{bmatrix} = \begin{bmatrix} h_{00} & h_{01} \\ h_{10} & h_{11} \end{bmatrix} \begin{bmatrix} s_0 \\ s_1 \end{bmatrix} \tag{3-1}$$

which has a simplified form as:

$$[R] = [H][S] \tag{3-2}$$

Hence, the inversed process which decodes the $[R]$ to the $[S]$ is:

$$[S] = [H]^{-1}[R] \tag{3-3}$$

It is clear that if want to decode the $[R]$ to the $[S]$, we must solve the inversion of $[H]$. However, the inversion will be difficult if correlation coefficient of $[H]$ is large. Generally, the correlation coefficient between multipath channels is small, while the LOS make it large. Unfortunately, the LOS usually occurs in an indoor environment because of the limited space in a room.

Until now, spatial multiplexing antenna has been applied as most of the MIMO antennas. However, to reduce the impact caused by the LOS, space between the component antennas of spatial multiplexing antenna should be large enough. In general, a distance longer than half

wavelength is considered appropriate. That is why just as people's impression that the MIMO antenna usually has big entire size, involving large space between the components. Nevertheless, dual-polarization antenna, which combines a pair of component antennas with orthogonal polarizations, is proved one of the best choices for MIMO system because it provides very low correlation coefficient between its component antennas even in a very limited space [80], as shown in Figure 3. 2.

Various dual-polarization antennas have been proposed. All these antennas can be classified into two types according to their constitution. As one type, same component antennas are installed orthogonally to radiate orthogonally polarized waves like which is shown in Figure 3. 2 (b). As a typical example, an antenna composed of two orthogonal print dipoles and a PIN-diode switch circuit is proposed in [81].

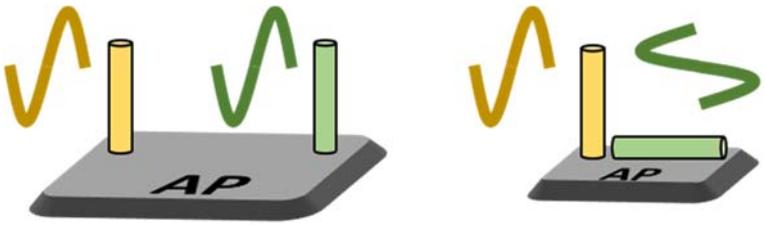

(a) (b)

Figure 3. 2 Spatial multiplexing antenna (a) and dual-polarization antenna (b).

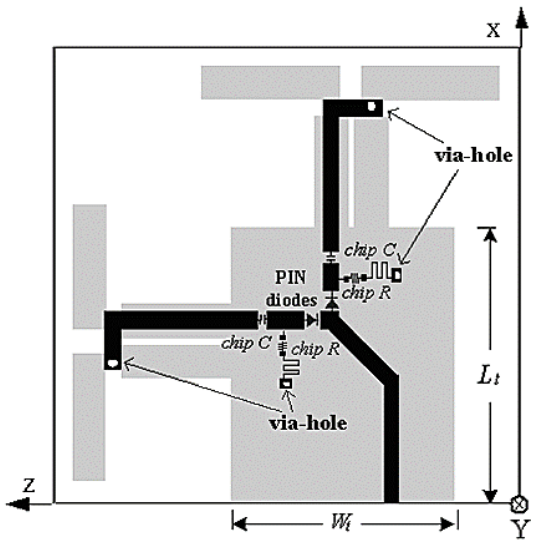

Figure 3. 3 A dual-polarized antenna composed of two orthogonal print dipoles .

However, the component antennas of most of the dual-polarized antenna in this type quoted above are not able to radiate same pattern. The component antennas used for MIMO base station is supposed to have radiation patterns in same shape. Although this is not a necessary condition, radiation patterns in same shape are helpful for power covering.

Correspondingly, antennas of the other type solved this problem. Such as an antenna comprising a wire-loop antenna and a notch array was calculated and discussed in [82]. It was proved that this combined antenna with component antennas in different types can radiate orthogonally polarized waves with same pattern. The structure of the wire-loop antenna is simple but bandwidth is very narrow. Besides, it is better to use microstrip lines as a power divider to feed the notched array antenna. Characteristics of notched array antenna using microstrip lines was discussed in [83]. A compactly composed polarization diversity antenna has been proposed and designed at lower frequency band for vehicle communication systems [84]. Even if the operating frequencies are different, the antenna size in [84] is pretty big comparing with the antenna which is proposed in this thesis.

In the initial stage of this subject, some earlier proposals have been discussed [85][86]. In [85], bandwidth of vertical polarized component is very narrow, and mutual coupling is large due to its one-piece structure. While in [86], separated component antennas was proposed. However, the adjacent arrangement cannot provide us satisfactory radiation patterns.

As another way to place the two component antennas, overlapped arrangement is proposed, and practically confirmed to realize compact conformation. Moreover, the overlapped arrangement is considered able to enhance the uniformity of radiation patterns in horizontal pane. This proposal will be shown and discussed in Section 3.2. A further upgraded model is then proposed for commercialized application. This sample antenna, which will be introduced in Section 3.3, is composed of redesigned component antennas providing very wide bandwidth as well as excellently uniform radiation patterns in the horizontal plane. The performance of the enhanced antenna satisfy the requirement of indoor MIMO base station.

Finally in Section 3.4, we conclude this Chapter.

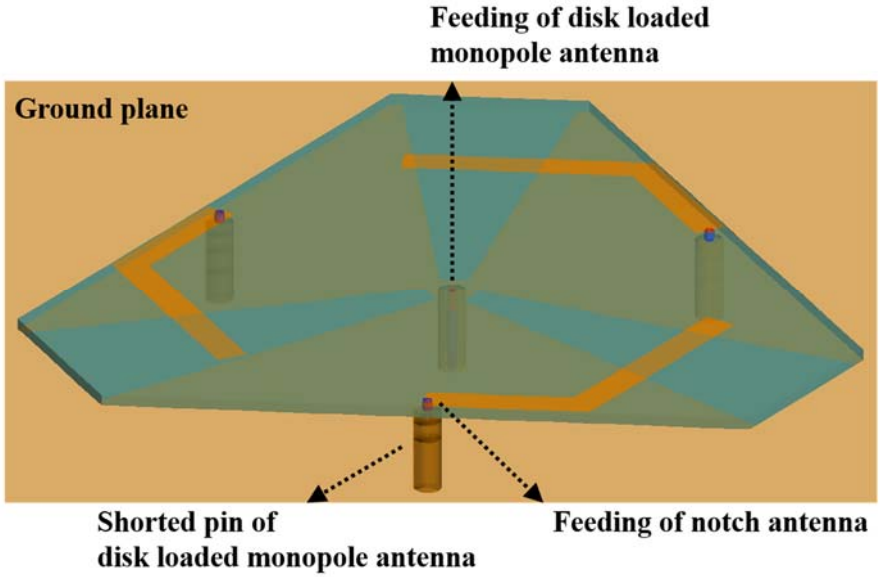

Figure 3. 4 The one-piece structure proposed in [85].

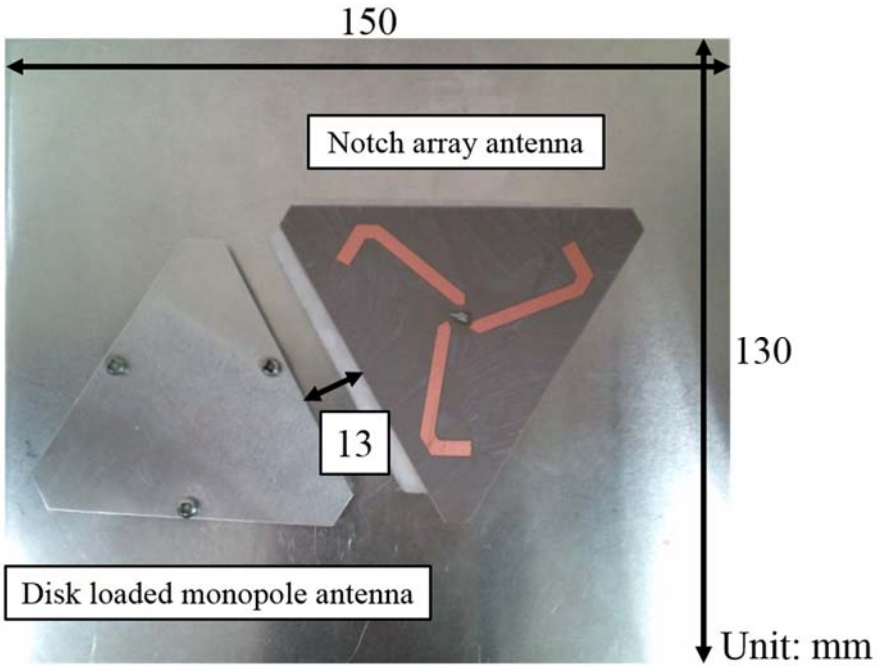

Figure 3. 5 The adjacent arrangement proposed in [86].

3.2 A Compact Orthogonally Polarized Antenna

In this Section we present a combined antenna with dual-polarization which composed of a vertically polarized disk loaded monopole antenna and a horizontally polarized notched array antenna. Both of their radiation patterns of the principle polarization is omni-directional in horizontal plane, similar in shape with that of a monopole set on semi-infinite ground. In respect of bandwidth, the wide bandwidth of 210 MHz of the vertical polarization component makes itself possible to cover the whole 2 GHz band defined by IMT-2000, which is wider than any other vertical polarization components in [82][84][85][86]. On the other side, double layer of microstrip parasitic elements is proposed for the horizontal polarization component to provide double resonances that they cover uplink band as well as downlink band separately. The two components will be separately presented in 3.2.1 and 3.2.2, and the combined model will be in 3.2.3.

3.2.1 Vertical Polarization Component

A vertically polarized disk loaded monopole antenna is used to be the vertical polarization component because it behaves excellent performance that e.g. the antenna usually has same bandwidth in spite of half antenna height, comparing with a traditional inverted-F antenna, for the conductor plate provides bigger distributed capacitance and smaller distributed inductance to cause reduced Q-value. The proposed disk loaded monopole antenna in the thesis consists of a triangular conductor plate, a feeding pin, three shorted pins and a ground plane. As shown in Figure 3. 6, the feeding point is located at the center of the triangular plate, and the three shorted points are placed around it central-symmetrically.

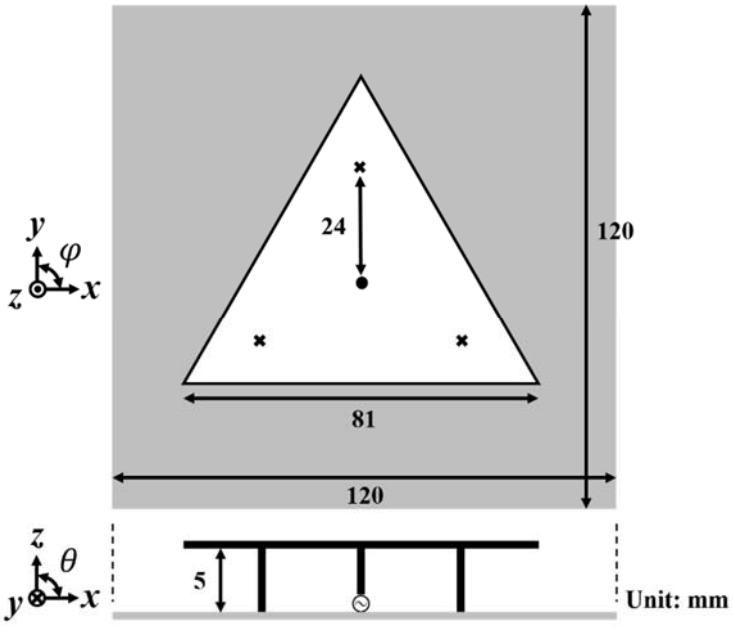

Figure 3. 6 Geometry of the disk loaded monopole antenna.

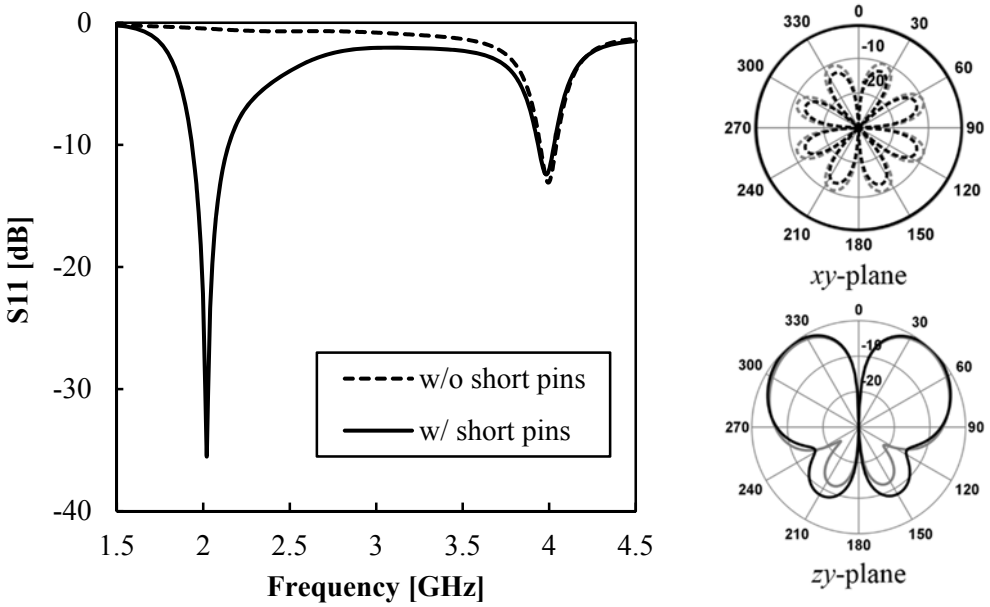

Figure 3. 7 Input responses of the disk loaded monopole, and radiation patterns when short pin is used. Solid lines denote $\boldsymbol{E_\theta}$ and dotted lines denote $\boldsymbol{E_\varphi}$. Lines in black stand for 1.95 GHz, lines in gray stand for 2.14 GHz.

Radiation characteristic of the disk loaded monopole antenna mainly depends on the current flowing through the feeding pin and the shorted pins. Comparing with a wavelength, when distance between the feeding pin and the shorted pin is sufficiently small, the radiation pattern in vertical plane is similar with that of a monopole antenna. The conductor plate is a non-radiating element because of image current produced by the ground plane. However, the electrical size of the conductor plate impacts on frequency response of the antenna.

It is found that the height of antenna and the edge length of the triangular conductor plate basically influence resonant frequency of the antenna, because they handle path of the current flowing through the feeding pin and shorted pins. The resonant frequency increases along with reducing of the antenna height or the edge length of the triangular conductor plate. At the meantime, the height of antenna relates to the impedance bandwidth. The bandwidth broadens along with increased antenna height, since higher antenna height provides larger electrical size of the main radiating part of the antenna. When the antenna height is 6 mm, the bandwidth can reach 13 %. Another parameter, the space between feeding pin and shorted pins, is a key factor that it handles the input impedance of antenna. In addition, the diameter of the pins also impact on the input impedance more or less.

The disk loaded monopole antenna has two dominant modes, one is called coaxial mode and the other is patch mode. The coaxial mode occurs only when the shorted pins exist and are close enough to the feeding pin, whereas the patch mode occurs when there are no shorted pins, or they are far away from the feeding pin. The input response of the antenna is shown in Figure 3. 7. It is observed that the coaxial mode appears at 2 GHz when the shorted pins are used, while disappears when there is no shorted pins. However, the patch mode always appears at 4 GHz whatever the shorted pins exist or not. The coaxial mode of the disk loaded monopole antenna is the desired mode to be excited for this low frequency mode enables a 60% smaller antenna size than the patch mode. Moreover, when the antenna works at 4GHz, the patch mode, horizontally polarized radiation strongly increase due to the resonant patch. While the radiation pattern forms similar with a monopole antenna when the antenna works at 2GHz band, the coaxial mode, as is shown in Figure 3. 7.

3.2.2 Horizontal Polarization Component

A notched array antenna used for the horizontal polarization antenna will be introduced in this Section. Although a horizontally placed dipole is able to easily provide horizontally polarized radiation pattern, the radiation pattern cannot be satisfied as being a base station antenna. Three or more centrally symmetry horizontally placed dipoles can provide us omni-directional radiation pattern in the horizontal plane, while the total volume cannot answer the requirement of miniaturization, especially for indoor base station. Selection of a horizontally polarized antenna with omni-directional radiation pattern is considered a problem.

As an excellently proposed antenna which radiate omni-directional as well as horizontally polarized waves, notched array antenna has been proposed by some researchers [82]-[84]. The antenna's well performances have been proved in the references. However, the problem of the antenna miniaturization is one of most important tasks which is solved in this thesis. The miniaturization relates to that resolve contradiction between antenna height and bandwidth.

The notched array antenna combining three notched radiators which are placed symmetrically is shown in Figure 3. 8. The three notches are cut on bottom conductor layer of a dielectric substrate, and three microstrip lines feed the notches, respectively, on the top layer. A feed point is placed at the center of the antenna connecting the microstrip lines to feed the notches separately. For this antenna with dimensions recorded in Table 3. 1, a ground plane is used as the ground of the disk loaded monopole antenna as well as a reflector plate to reduce the impact caused by installing place of the base station. Whereas, the conductor ground plane intensely influences the input characteristic of a horizontally polarized antenna which is close to the ground. It is known that the antenna's resonant frequency rises when the antenna height reduces, as is shown in Figure 3. 9. If consider the antenna and the ground plane as an entirety, the phenomenon can be explained by reduced entire size. However, although the input impedance and the resonant frequency can be readjusted by optimized width and length of the microstrip line, the impedance bandwidth becomes narrow when antenna height reduces.

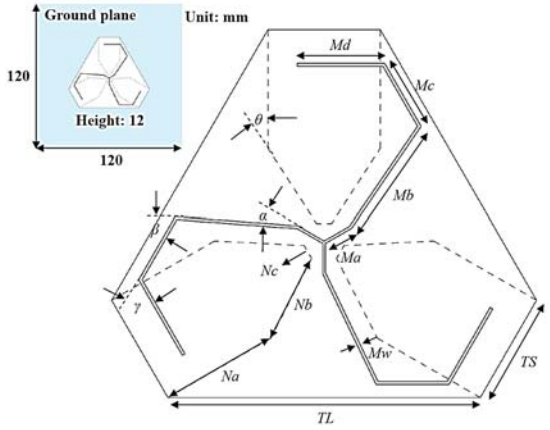

Figure 3. 8 Geometry of a designed notched array antenna with integrate power divider. Part in gray is on the top layer and parts drawn by dotted lines are the layout of the bottom layer. Dielectric coefficient is 2.6, and substrate thickness is 0.8 mm.

Table 3. 1

Dimensions of the notched array antenna shown in Figure 3. 9.

Parameter	*TL*	*TS*	*Na*	*Nb*	*Nc*	*Ma*	*Mb*
Values [mm]	50	18	19	14	2.4	4.8	21.1
Parameter	*Mc*	*Md*	*Mw*	*α*	*β*	*γ*	*θ*
Values [mm, deg.]	10.1	19.5	5	25.7	64.3	60	33.6

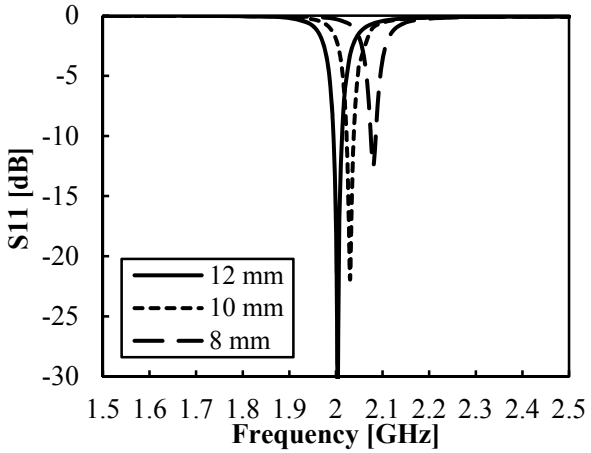

Figure 3. 9 Input response of the notched array antenna with changed antenna height.

As what has been shown in Figure 3. 9, the bandwidth of such a horizontally polarized antenna closely placed to the ground plane is very narrow. Physically, the radiation of antenna is affected by the reflection wave with approximate 180° changed phase. And, coupling current and surface wave on the reflector board consume the power of the antenna. The power divider, which is simply equipped, causes the bandwidth to become narrower. Because the bandwidth of only 1% of the notched array antenna is too narrow to use, approach to widening bandwidth is necessary.

Parasitic elements are widely applied in antenna designs as one of the most significant approaches to exciting another resonance or widening the bandwidth [87]. Some printed antennas with printed parasitic elements located at the same layer have been introduced [88]-[93].

For the notched array antenna, three pairs of parasitic microstrip lines is installed to the outboard blank space in both layers of the dielectric substrate, as shown in Figure 3. 10. In this figure, outline of the antenna indicates the shape of the dielectric substrate. The notched array shown by dotted lines is cut on the bottom conductor layer, and microstrip lines are cut on the top conductor layer to feed the three notches. Three pieces of wide microstrip lines (PL × PW) are cut on the top layer and close to the notches. If we only add this three parasitic elements on the top face, the bandwidth of antenna can be broadened to 40 MHz, which is shown in Figure 3. 11. Producing another resonance is one of the most feasible approaches to cover both the uplink and downlink frequency bands specified by the IMT-2000. Consequently, another set of parasitic elements on the bottom layer is added and shown in Figure 3. 10. Central lines of the two set of parasitic elements on two layers are overlapped. Both terminals of the parasitic microstrip lines on the bottom layer turn by a corner of 60°, and extend outside of the range of parasitic elements on the top layer. Another resonance which is caused by mutual coupling between the parasitic elements on the two layers appears can be found in Figure 3. 11. By using optimized dimensions recorded in Table 3. 2, the double resonances are adjusted to cover both the uplink band of 1.94~1.96 GHz and the downlink band of 2.13~2.15 GHz.

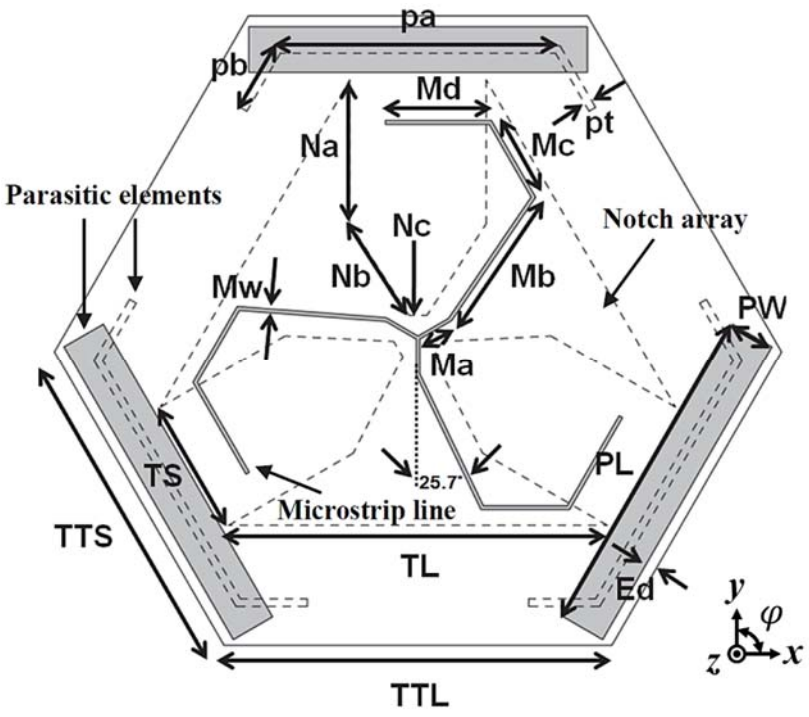

(a)

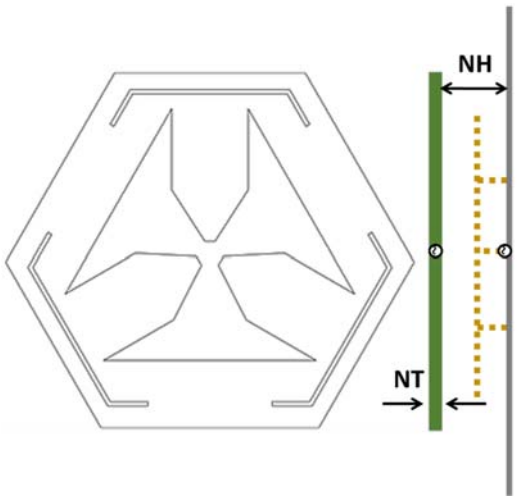

(b)

Figure 3. 10 Geometry of the notched array antenna with parasitic elements. (a) Parts in gray are in the top layer and parts by dotted lines are the layout of the bottom layer; (b) separately shows the layout of the bottom layer and side view including the disk loaded monopole antenna.

Table 3. 2

Dimensions of the notched array antenna shown in Figure 3. 10.

Parameter	*TL*	*TS*	*Na*	*Nb*	*Nc*	*Ma*	*Mb*	*Mc*	*Md*	*Mw*
Values [mm]	50	18	19	14	2.4	4.8	19.7	11.7	14	0.5
Parameter	*TTL*	*TTS*	*Ed*	*NT*	*NH*	*PL*	*PW*	*pa*	*pb*	*pt*
Values [mm]	51.2	44.8	0.7	0.8	12	44.7	7	37.5	10	1

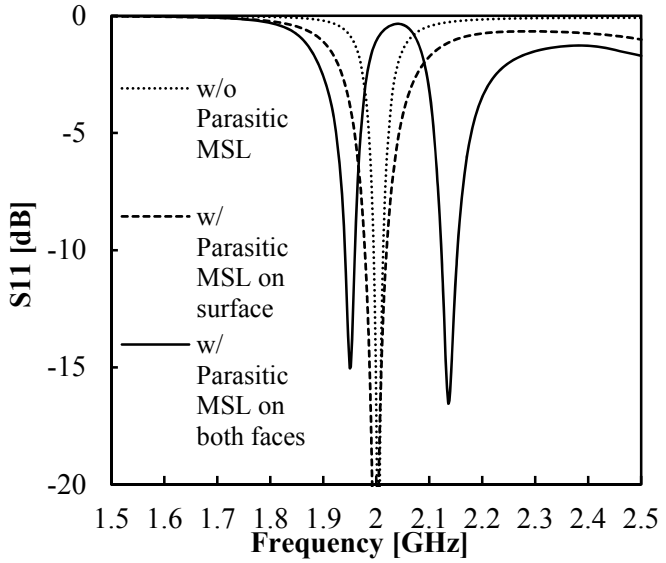

Figure 3. 11 Input response of the notched array antenna.

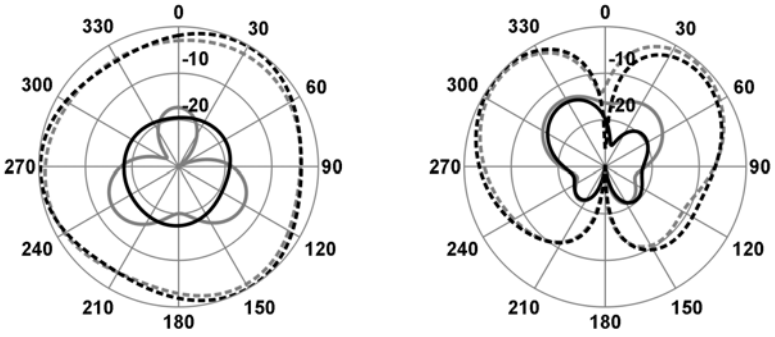

(a) (b)

Figure 3. 12 Radiation patterns of notch array antenna. (a) Horizontal plane, (b) Vertical plane. Solid lines denote $\boldsymbol{E_\theta}$ and dotted lines denote $\boldsymbol{E_\varphi}$. Lines in black stand for 1.95 GHz, lines in gray stand for 2.14 GHz.

The radiation patterns of the notched array antenna working at the uplink band and the downlink band are shown in Figure 3. 12. Because of the in-phase excitation, the radiation pattern of the notch array antenna is similar with that of a monopole antenna. In addition, because the linear parasitic elements are too close to main radiator, the notched array, they only slightly increase the amplitude of the outboard composite waves. This causes the circularity degree of the radiation patterns in the horizontal plane is maintained.

3.2.3 Characteristic Modes Analysis for Antenna Elements Combination

Structure of a composite antenna which is composed of the two component antennas is introduced in this part. Because of the increased size of notched array antenna with parasitic elements, an adjacent arrangement will cause a larger total size of the composite antenna. As another way to arrange the two component antennas, an overlapped arrangement is proposed, practically confirmed that can realize not only a compact conformation but also uniform radiation patterns in horizontal plane. Figure 3. 13 shows side view and top view of the proposed composite antenna. Because of the existence of its feeding pin and shorted pins, the disk loaded monopole antenna has to be arranged to the under layer.

Characteristic modes of the antenna elements is calculated to investigate mutual influence due to their combination. Figure 3. 14 and Figure 3. 15 show current distribution and characteristic angles of two primary modes of the disk loaded monopole. Detailed illustration about the two modes can be found in Chapter 4. Figure 3. 16 and Figure 3. 17 show current distribution and characteristic angles of three primary modes of the notch array with ground plane. After the combination, it can find light frequency move shown by solid lines in Figure 3. 18; frequency of the notch array increase due to conductor plate of the disk loaded monopole, while frequency of the disk loaded monopole reduce because of volume increasing of the whole antenna system. Figure 3. 19 shows S-parameters of the composite antenna.

To find more information, two patterns I and II are also calculated and results are shown in Figure 3. 20 and Figure 3. 21. The resonant frequency of $\boldsymbol{J_1}$ of the disk loaded monopole is adjusted to coincide with that of $\boldsymbol{J_1}$ and $\boldsymbol{J_3}$ of the notch array before combination, respectively, for the pattern I and II, by increasing or reducing size of the conductor plate of disk loaded monopole. By observing the results, we can find the frequency shift become larger

after the combination. It is interesting that frequencies of the modes of notched array vary in approximately same degree. This can be considered as interlock between the modes because of their common resonant components. Moreover, S21 become larger because more mutual influence produced when the two element antennas are combined.

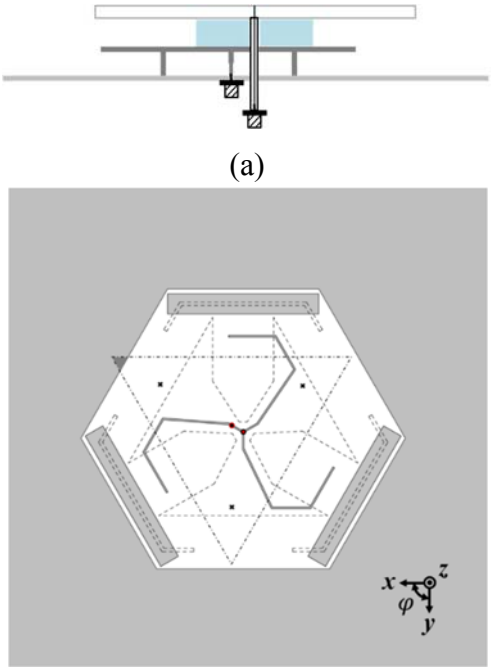

(a)

(b)

Figure 3. 13 (a) Side view and (b) top view of proposed composite antenna.

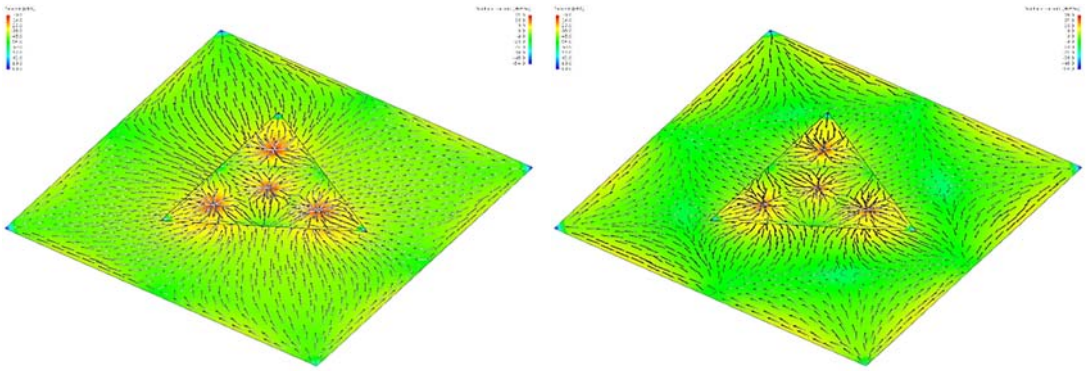

(a) (b)

Figure 3. 14 Characteristic current distribution of (a) $\boldsymbol{J_1}$ and (b) $\boldsymbol{J_2}$ of the disk loaded monopole.

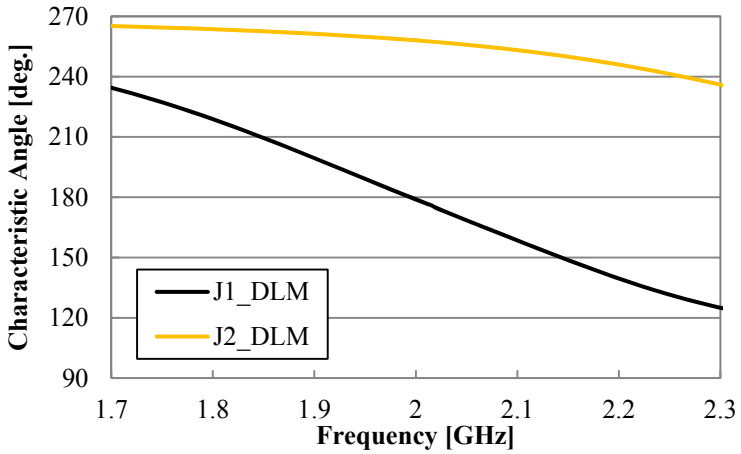

Figure 3. 15 Characteristic angle of J_1 and J_2 of the disk loaded monopole.

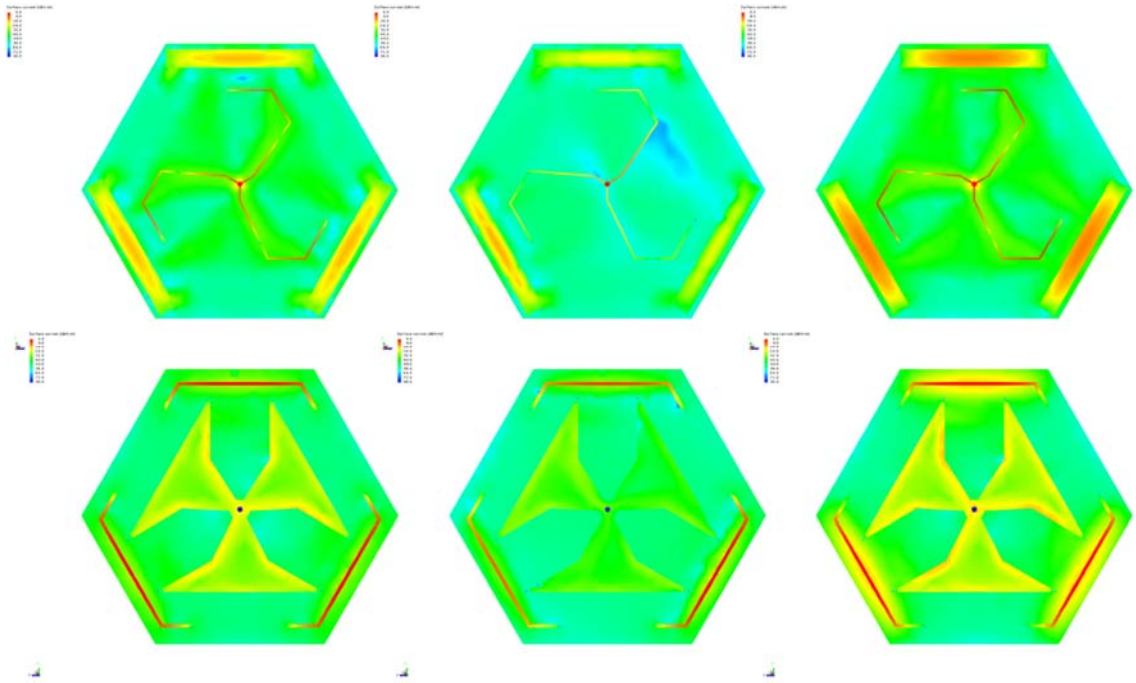

(a) (b) (c)

Figure 3. 16 Characteristic current distribution of (a) J_1, (b) J_2 and (c) J_3 of the notch array. Upper and lower sides show the two surface, respectively.

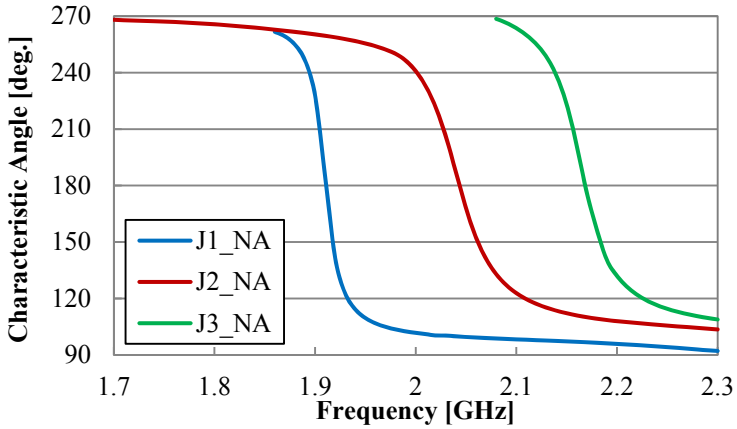

Figure 3. 17 Characteristic angle of J_1, J_2 and J_3 of the notch array.

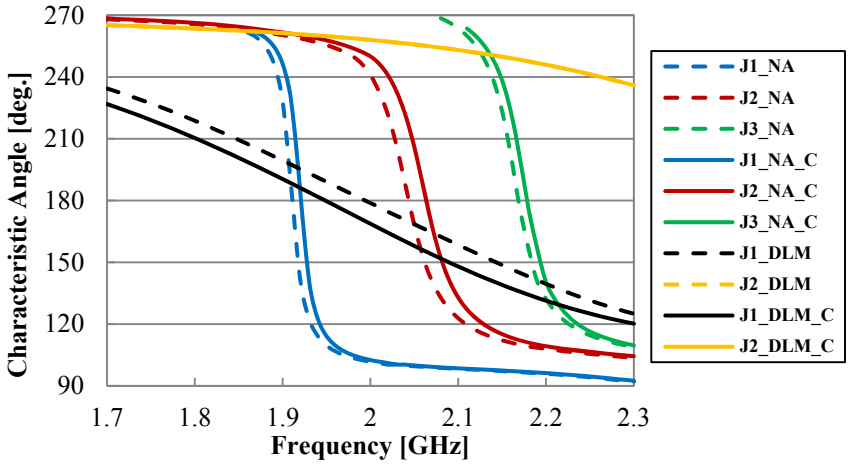

Figure 3. 18 Characteristic angle of each mode before and after (*_C) combining.

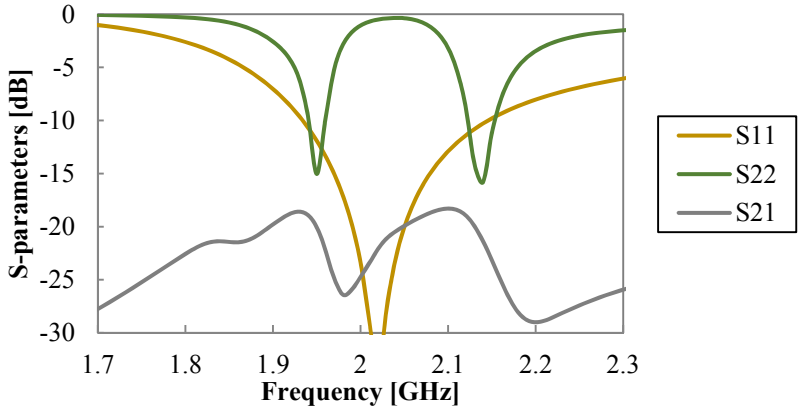

Figure 3. 19 Calculated S-parameters of the composite antenna.

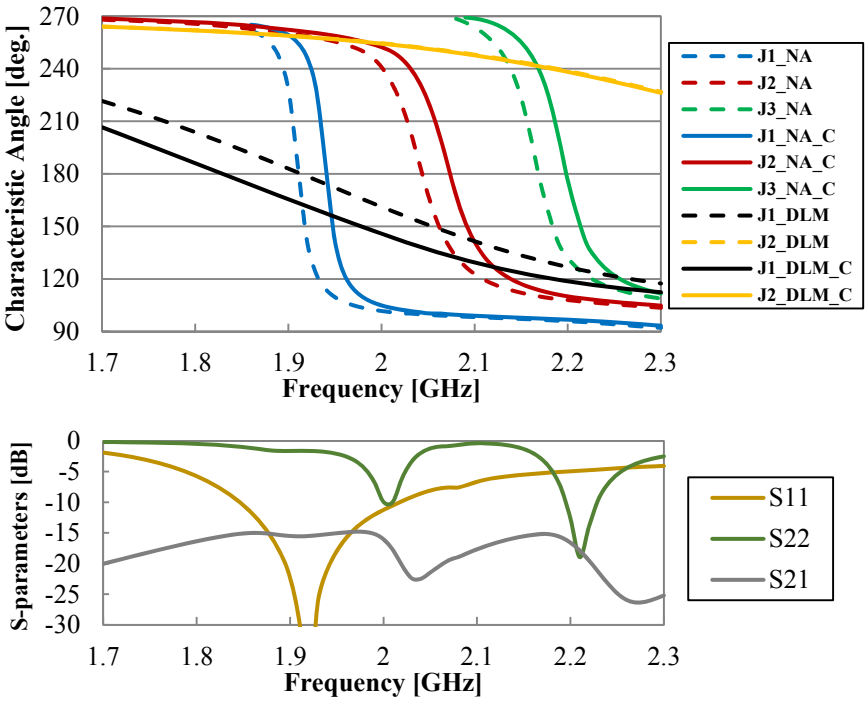

Figure 3. 20 Characteristic angles and S-parameters of Pattern I.

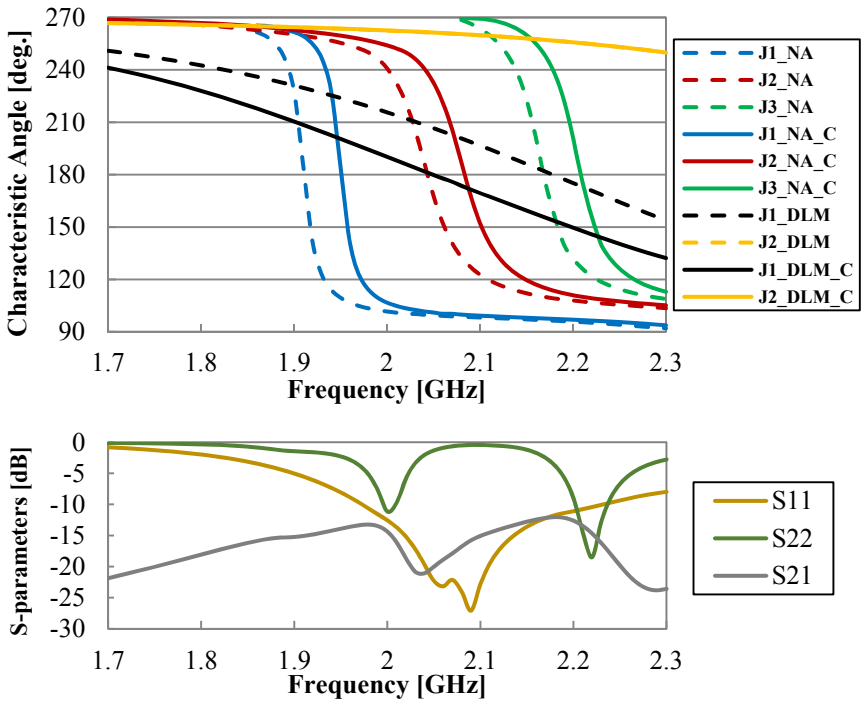

Figure 3. 21 Characteristic angles and S-parameters of Pattern II.

3.2.4 Composite Antenna and Experiment

To the notched array antenna which is arranged to the upper layer, an appropriate way to feeding it by using a thin coaxial cable is necessary to think about. As one of the applicable ways which is shown in Figure 3. 13, the thin coaxial cable connects the center part of the microstrip line and conductor plate on which the notched array antenna is cut, passing through two holes made in the plate of disk loaded monopole antenna and the ground plane, before finally connecting to input port at the other end. The radius of holes is 1 mm, while the distance between the hole and the feeding pin of the disk loaded monopole antenna is 5 mm. Because the hole is not on main current route, the current distribution of the disk loaded monopole almost not change. It has been verified that the input impedance of the disk loaded monopole antenna has little affected by the existence of hole and coaxial cable.

The designed notched array antenna with parasitic elements is fabricated and shown in Figure 3. 22, and the combined composite antenna is shown in Figure 3. 23.

Figure 3. 22 Fabricated sample of the notched array antenna with parasitic elements.

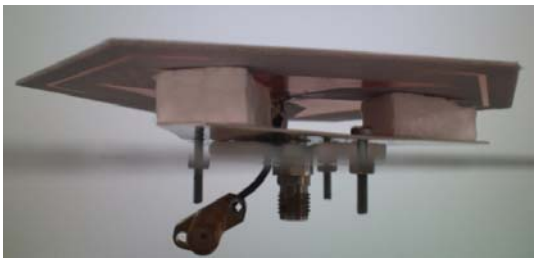

Figure 3. 23 Proposed composite antenna.

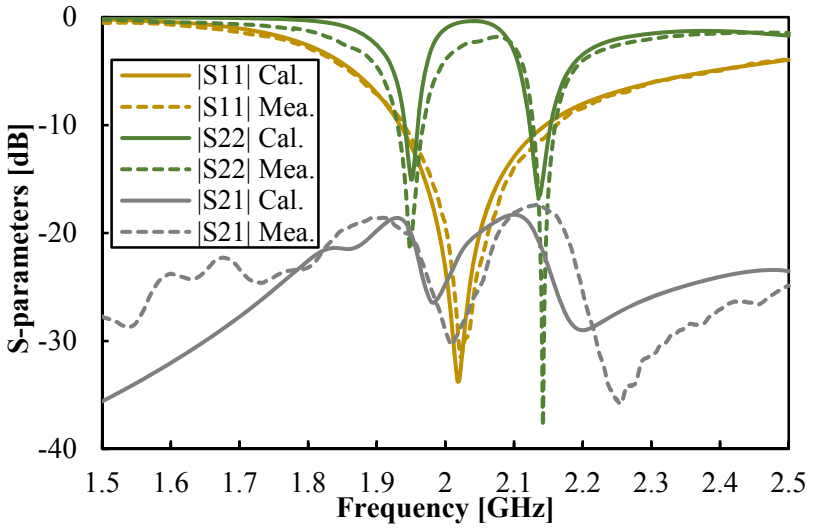

Figure 3. 24 Input response of port 1: disk loaded monopole; and port 2: notched array.

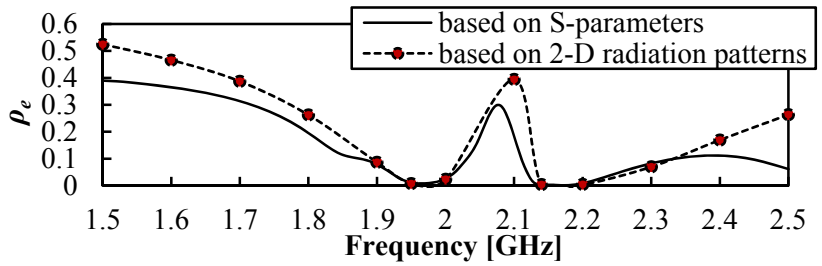

Figure 3. 25 Calculated correlation coefficient between the two component antennas.

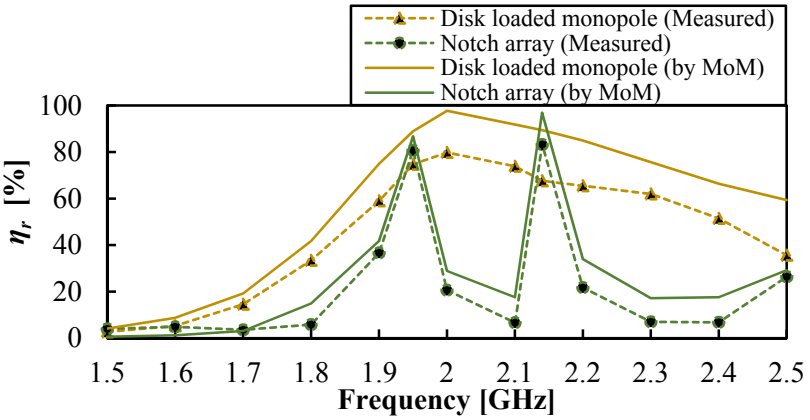

Figure 3. 26 Radiation efficiency of the two component antennas.

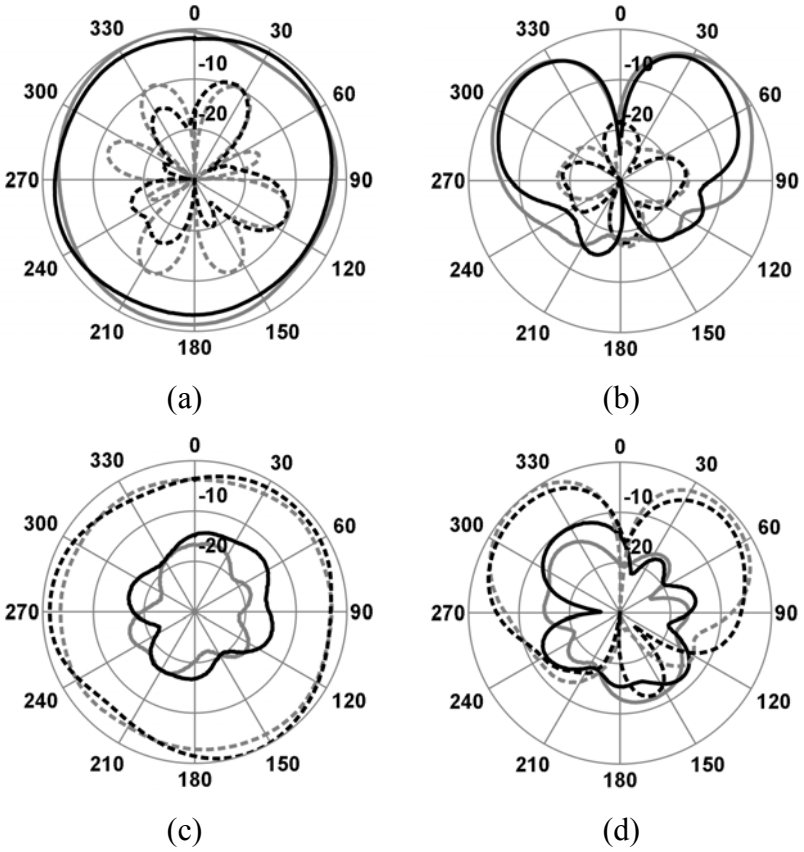

Figure 3. 27 Measured radiation patterns of the disk loaded monopole (a, b) and the notched array (c, d); (a, c) are in horizontal plane and (b, d) are in vertical plane. Solid lines denote $\boldsymbol{E_\theta}$ and dotted lines denote $\boldsymbol{E_\varphi}$. Lines in black denote 1.95 GHz, lines in gray denote 2.14 GHz.

The input responses of the two component antennas and the mutual coupling characteristic determined by both calculation and experiment are shown in Figure 3. 24. It clearly shows the measured results agree with the calculated results very well. Both the uplink band and downlink band are covered by the composite antenna. Moreover, the mutual coupling coefficient in both of the operation bands is less than -18 dB, which is low enough to be a MIMO antenna.

In order to investigate the correlation between the two component antennas, correlation coefficient is calculated in two ways which are solved by utilizing 2-D radiation patterns and S-parameters, respectively. It should be noticed that using 3-D radiation patterns and the S-parameters may obtain coincident results [94]. The correlation coefficient calculated by utilizing the 2-D radiation patterns in horizontal plane is given by:

$$\rho_e \simeq \frac{\left[\int_0^{2\pi}\left(\boldsymbol{E_{\theta 1}E_{\theta 2}^*} + \boldsymbol{E_{\varphi 1}E_{\varphi 2}^*}\right)d\varphi\right]^2}{\int_0^{2\pi}\left(\boldsymbol{E_{\theta 1}E_{\theta 1}^*} + \boldsymbol{E_{\varphi 1}E_{\varphi 1}^*}\right)d\varphi \cdot \int_0^{2\pi}\left(\boldsymbol{E_{\theta 2}E_{\theta 2}^*} + \boldsymbol{E_{\varphi 2}E_{\varphi 2}^*}\right)d\varphi}$$

(3-4)

Results given by this equation are shown by black solid line in Figure 3. 25.

On the other hand, the correlation coefficient calculated by utilizing the S-parameters is given by:

$$\rho_e \simeq \frac{|S_{11}^* S_{12} + S_{21}^* S_{22}|}{[1-(|S_{11}|^2 + |S_{21}|^2)][1-(|S_{22}|^2 + |S_{12}|^2)]}$$

(3-5)

Here the antenna is assumed to be a lossless antenna. Results given by this equation are shown by black dotted line with red marks in Figure 3. 25.

The low level of the correlation coefficients sufficiently proves the effectiveness of the proposed antenna of reducing correlation as a MIMO antenna, even having such a 12 mm close space between the two component antennas.

Besides, radiation efficiency is calculated by MoM, and measured in the experiment by measuring *Total Radiated Power* (TRP) of the fabricated antenna. The radiation efficiency calculated by TRP is given by:

$$\eta_r \simeq \frac{P_{TRP}}{P_{TRP}|_s}$$

(3-6)

where

P_{TRP} = Measured TRP of the antenna under test

$P_{TRP}|_s$= Measured TRP of a standard dipole antenna

The P_{TRP} is calculated by the integral of *Effective Isotropic Radiated Power* (EIRP) over the entire solid angle surrounding the antenna [95], that is given by:

$$P_{TRP} = \frac{1}{4\pi}\int_0^{2\pi}\int_0^{\pi}\left[EIRP_\theta(\theta,\varphi) + EIRP_\varphi(\theta,\varphi)\right]d\theta d\varphi$$

(3-7)

While for those antennas which has identical or approximatively identical radiation power in the φ-plane, equation (3-7) can be simplified to:

$$P_{TRP} \simeq \frac{1}{2}\int_0^{\pi} \left[EIRP_{\theta}(\theta,\varphi) + EIRP_{\varphi}(\theta,\varphi)\right] d\theta$$

(3-8)

Moreover, it improves precision of the result if solve an average of the P_{TRP} measured from two orthogonal φ-planes. The results given by measuring the *zx*-plane and the *zy*-plane of the two component antennas are shown in Figure 3. 26 by dotted lines with marks. The measured η_r of disk loaded monopole antenna are lower than calculated valued because of the not very well physical coupling of the fabricated sample.

Finally, radiation patterns of the two component antennas are shown in Figure 3. 27. The radiation patterns in both uplink band and downlink band of both the antennas are similar with monopole antenna's radiation pattern.

This composite antenna is patented[6].

3.3 Enhanced Orthogonally Polarized Antenna for Indoor MIMO Base Station

Comparing with the proposed orthogonally polarized antenna in Section 3.2, a further upgraded composite antenna is proposed in this Section for commercialized application. This sample antenna, which is technically fabricated, is composed of redesigned component antennas providing very wide bandwidth as well as excellently uniform radiation patterns in the horizontal plane. The component antennas operate at the 2 GHz band of IMT-2000 that are1.94 ~ 1.96 GHz for uplink and 2.13 ~ 2.15 GHz for downlink; the enhanced impedance bandwidths of over 300 MHz for the disk loaded monopole antenna and 155 MHz for the notched array

[6] Huiling Jiang, Keizo Cho, Hiroyuki Arai, Shen Wang, "Antenna," P2013-46331A, Japan Patent Office, 2013/03/04

antenna. The performance of the enhanced antenna is confirmed that can satisfy the practical requirement of indoor MIMO base station.

As proposed in [84]-[86] and the previous Section, the disk loaded monopole generally consists of a top loaded conductor plate, a feed pin, one or more shorted pins and a ground plane. However, when using plural shorted pins, we can also use multiple feed pins, as is shown in Figure 3. 28. In this case, there is almost no current flowing on the center part of the conductor plate so that it is non-radiating. So, it does not impact antenna characteristics even though a hole is punched at the center of the conductor plate.

On the other hand, different with the notched array antenna in the previous Section, we arrange four notched array symmetrically on the bottom conductor layer of the dielectric substrate to further improve the omni-directionality. As shown in Figure 3. 29, there are four notches cut on the bottom conductor layer, and four microstrip lines feeding them, respectively, on the upper layer. The quantity of the parasitic elements is also added to four sets.

This composite antenna sample is enhanced and fabricated by Nihon Dengyo Kosaku Co., Ltd.[7] with NTT DOCOMO, Inc.[8] Photographs of the manufactured composite antenna sample are shown in Figure 3. 30 and Figure 3. 31. The notched array antenna is placed above the disk loaded monopole antenna. The feed pins of disk loaded monopole are in-phase fed by microstrip lines distributing on the top layer of the bottom substrate. Matching circuit is made on the transmission lines for better impedance matching. The notched array antenna is fed by a coaxial post which is placed through the hole punched on the center of the disk loaded monopole antenna. The composite antenna is fixed on a mounting plate, and covered by a radome (not shown in the figures).

The imput responses of the two component antennas are shown and compared with that of the previous design in Figure 3. 32. To the narrow band antenna, the notched array, the bandwidth widened from 70 MHz to 155 MHz. The bandwidth enhanced due to the increment of notches' quantity. To the disk loaded monopole, its bandwidth widened due to the usage of the matching circuit. S21 is confirmed still lower than -17 dB, shown in Figure 3. 33. Radiation patterns of the two component antennas are shown in Figure 3. 34. In horizontal plane, circularity of the disk loaded monopole is 1.92 dB at 1.95 GHz and 1.53 dB at 2.14 GHz; the value of the notched array is 1.59 dB at 1.95 GHz and 1.28 dB at 2.14 GHz. The identity of both the antennas in the horizontal plane becomes better than the previously proposed antenna.

[7] 7-4, Nissai Hanamizuki, Sakado, Saitama, 350-0269, Japan
[8] 3-6, Hikari-no-oka, Yokosuka, Kanagawa, 239-8536, Japan

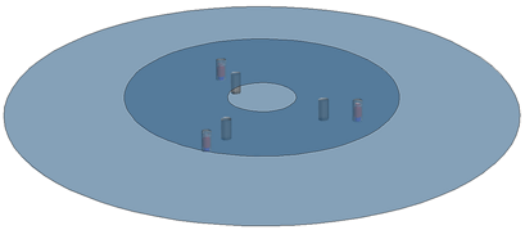

Figure 3. 28 Geometry in 3-D view of the enhanced disk loaded monopole antenna.

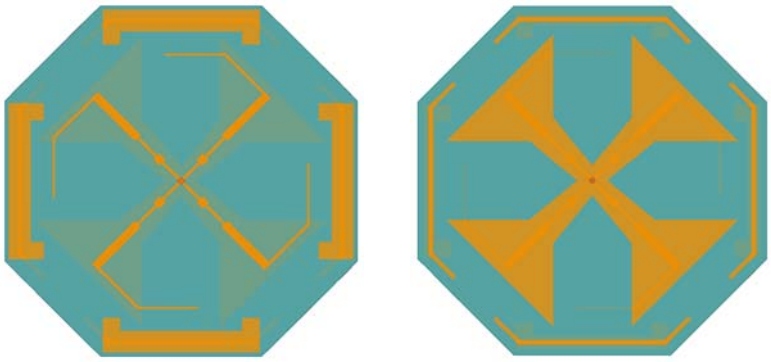

(a) (b)

Figure 3. 29 Geometry of enhanced notched array antenna; (a) Top view and (b) bottom view.

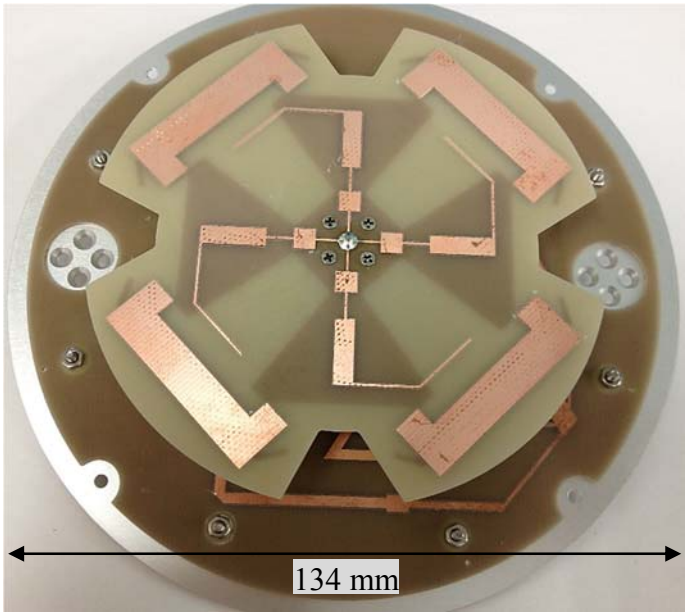

Figure 3. 30 Photographs of the manufactured composite antenna in top view.

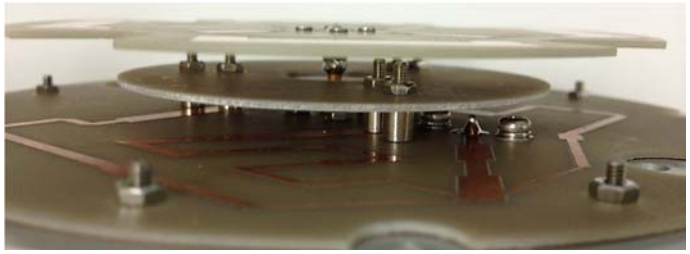

(a)

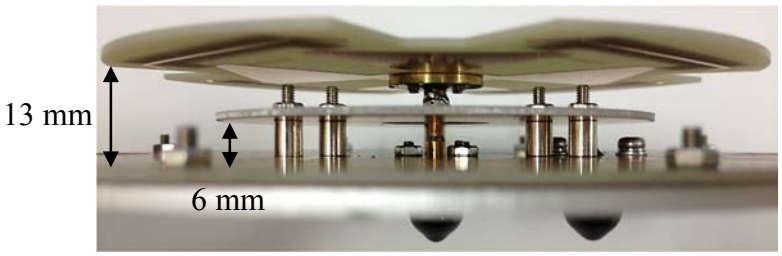

(b)

Figure 3. 31 Photographs of the manufactured composite antenna in side view; (a) Details about microstrip transmission line and (b) feeding posts of the antennas.

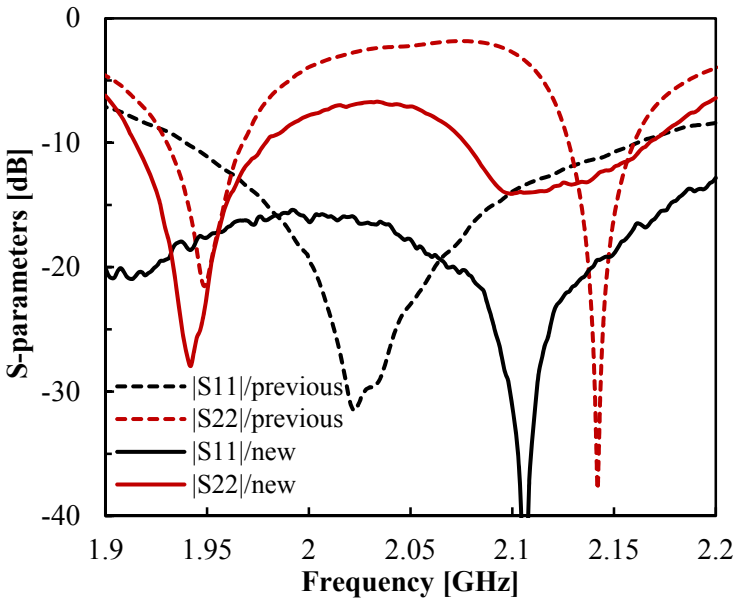

Figure 3. 32 Measured input responses of the two component antennas of previous design and new design. Port 1 denotes the disk loaded monopole and port 2 denotes the notched array.

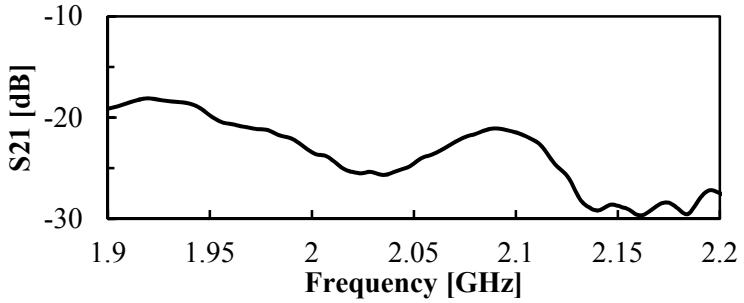

Figure 3. 33 Measured mutual coupling response between the two component antennas.

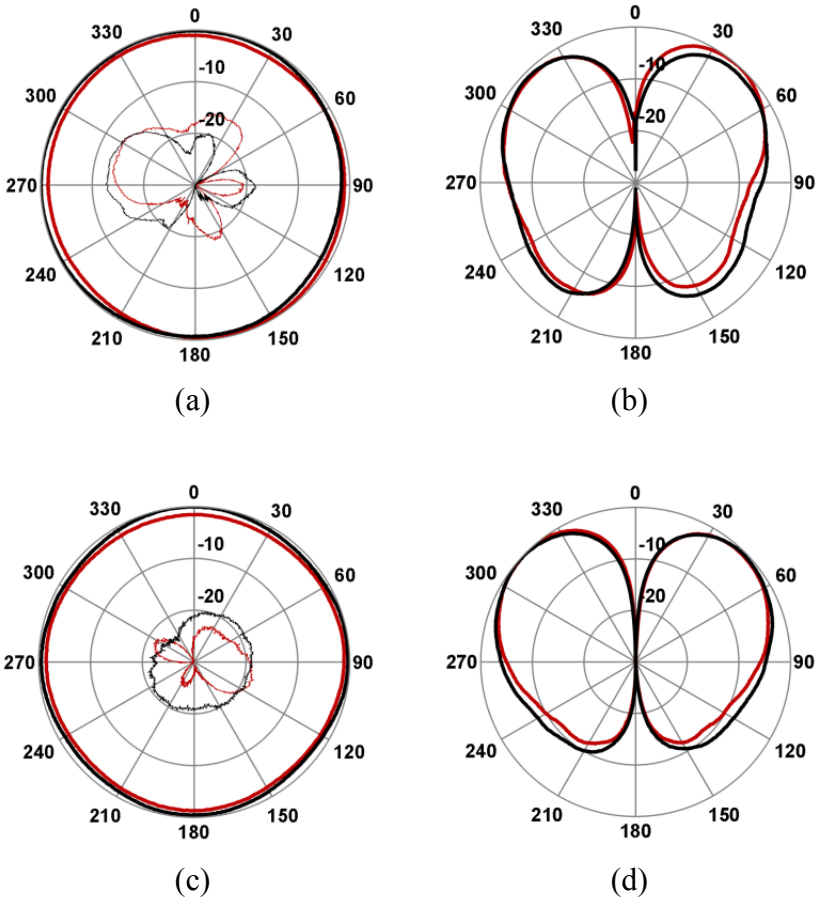

Figure 3. 34 Measured radiation patterns of the two component antennas. (a), (b) are patterns of the disk loaded monopole; (c), (d) are patterns of the notched array. (a), (c) are in horizontal plane and (b), (d) are in vertical plane. Black lines are at 1.95 GHz and red lines are at 2.14 GHz. Thinner lines denote patterns of cross-polarization.

3.4 Summary

A compact composite antenna composed of two orthogonally polarized component antennas is proposed to reduce correlation and realize miniaturization. The two low-profile component antennas, a disk loaded monopole antenna and a notched array antenna are utilized for the vertical polarization component and horizontal polarization component, respectively. Characteristic modes analysis is used to confirm mutual influence between the two components when they are combined. The interlock phenomenon between different modes is confirmed that is very important to antenna combination.

The proposed antennas has further miniaturized size and improved isolation. The whole antenna is developed for covering 2 GHz of IMT-2000, that is uplink band of 1.94~1.96 GHz and downlink band of 2.13~2.15 GHz. Parasitic elements are utilized for bandwidth enhancement of the narrow band notched array antenna. Correlation coefficient between the component antennas is confirmed very low in the two operating bands. Moreover, radiation efficiency and radiation patterns show good status of the antenna. Due to the overlapped arrangement, which is used to combining the double component antennas, the composite antenna has a finally designed size of $0.8\lambda \times 0.8\lambda \times 0.08\lambda$ (ground plane included).

As an enhanced model for indoor MIMO base station, a further upgraded composite antenna is proposed. This technically fabricated sample antenna is composed of redesigned component antennas providing very wide bandwidth as well as excellently uniform radiation patterns in the horizontal plane. Impedance bandwidth of the disk loaded monopole antenna is improved to 300 MHz for, and 155 MHz bandwidth is provided by the notched array antenna. The performance of the enhanced antenna is confirmed that is able to satisfy the practical requirement of indoor MIMO base station.

CHAPTER 4
CHARACTERISTIC MODES ANALYSIS FOR CROSS-POLARIZATION REDUCTION OF DISK LOADED MONOPOLE

4.1 Introduction

So far, studies and application approaches of the characteristic modes almost concentrated on discussing the question how the characteristic modes impact on the excited antennas resonance characteristics. It is true that frequency response of the modes is directly related to antennas resonance response when specific excitation is decided. If an antenna is resonant without any external matching component, e.g. a matching circuit, there must be one mode or multiple modes resonate at the nearby frequency. This special insight property of the characteristic modes analysis make itself significantly useful for the problems about antennas resonance characteristics.

However, reports about relationship between the characteristic modes and the radiation pattern of antennas with specific excitations are seldom seen. It is known that similar with the antennas resonance response, radiation pattern of an antenna with specific excitation will

perform resemble patterns of the excited modes. Nevertheless, with regard to the modes which are unexcited by the specific excitation, it is not very clear how they can impact the antennas radiation pattern.

Theoretically, if a current mode $\boldsymbol{J_n}$ which cannot be excited by the given antenna feeding, the associated modal excitation coefficient in (2-43):

$$V_n^i = \langle \boldsymbol{J_n}, {E^i}_{tan} \rangle = 0 \tag{4-1}$$

The inner product of $\boldsymbol{J_n}$ and the incident E-field (in this case it is the excitation by antenna feeding) ${E^i}_{tan}$ is 0, so it indicates the mode does not contribute to the excited antenna's current as well as radiation pattern at all.

However, there are quite a number of modes are excited more or less, especially when the antenna size is electrically large. In this case, there are more modes existing in the concerned frequency band. As a matter of fact, we often observe this phenomenon, the existent undesired current and undesired radiation, in ordinary antenna designs. As a simple example combing the theory of characteristic modes to illustrate in detail, Figure 4. 1 shows a microstrip antenna. We discuss three modes occurring on the patch.

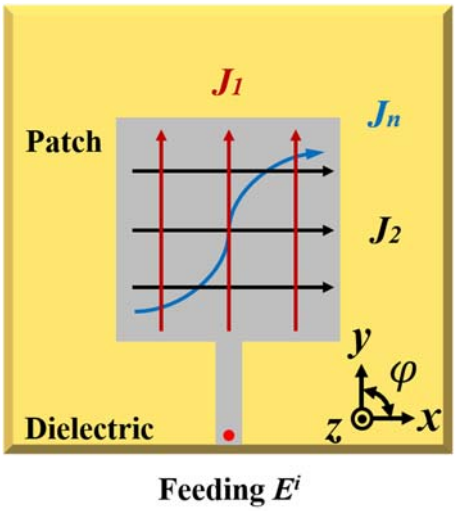

Figure 4. 1 A microstrip patch antenna and three modes occurring on it.

$\boldsymbol{J_1}$ and $\boldsymbol{J_2}$ are the two modes parallel with the edges (along *y*-axis and *x*-axis), and orthogonal with each other, respectively shown as the figure. $\boldsymbol{J_n}$ is an arbitrary mode other than the first two modes, and we assume the current has both *y*-axis and *x*-axis components. Then we consider the patch antenna is fed by microstrip line along the *y*-axis, and at the center of one of the edges. Although it is impossible in the reality, particularly, we ignore the influence to the characteristic modes from this feeding structure. Moreover, suppose all the edges have half wave length.

In this case, obviously we have:

$$V_1^i > \cdots > V_n^i > \cdots > V_2^i \tag{4-2}$$

This expression indicates $\boldsymbol{J_1}$ is the most excited mode by the given feeding, among the three modes and even among all the possible modes occurring on the patch. Correspondingly, $\boldsymbol{J_2}$ is believed the worst excited mode, or can be called unexcited mode. However, due to its *y*-axis component, $\boldsymbol{J_n}$ will be excited by the given feeding to a certain degree.

Therefore, we face two questions so common in most of the antenna design procedures that worth to consider about:

(1) How to modify an antenna to excite a desired mode which is now inadequately excited?
(2) How to reduce excitation for an undesired mode as far as possible?

This two question also have practical meaning for the study of characteristic modes. The answer to the questions may be simple: revise the structure of the antenna or change the feeding. Nevertheless, in practical antenna design, this simple answer is not an eligible answer but one of the most significant problems and tasks. Hence, it is necessary to find answer from the characteristic mode itself. To the both question (1) and (2), we are going to demonstrate practical solutions to illustrate how to apply characteristic modes analysis for cross-polarization reduction and for radiation pattern optimizations, in this Chapter and the next Chapter.

In this Chapter, we calculate the characteristic modes of the disk loaded monopole antenna proposed in 3.2.1 of previous Chaper, and analysis radiation properties of the modes to discuss how to reduce the cross-polarization component radiated by the antenna.

Generally, the cross-polarization component radiated by the disk loaded monopole or just a monopole with square ground plane of finite size is not very small. When the antenna is with dimension shown in Figure 3. 6, the cross-polarization, horizontal polarization, is near to -10 dB which can be confirm by observing Figure 3. 7. However, it is found if the size of ground plane becomes bigger, the cross-polarization will become larger. Figure 4. 2 shows the geometry of the disk loaded monopole antenna with a bigger square ground plane which has a 150×150 mm size. The size of the triangular conductor plate is also lightly changed to make the antenna resonate at 2.05 GHz covering the uplink band and the downlink band. Figure 4. 3 shows radiation pattern of the antenna in horizontal plane (*xy*-plane). When the ground plane size is 150×150 mm, maximum gain of the cross-polarization increase to about -5 dBi. Large cross-polarization will reduce antenna polarization purity, and increase the correlation with other component antenna, which is the horizontal polarization component in the previous Chapter. Therefore, it is necessary to discuss how to reduce the cross-polarization component radiated by the disk loaded monopole antenna.

The horizontal polarization component of this antenna is considered radiated by the ground plane. Because the square side length of 150 mm is near to one wavelength related to 2 GHz. Hence, the strong horizontal polarization component may be radiated by the side part of the ground plane. However, it is difficult for general antenna parameters, such as input response, radiation pattern, and current distribution, to provide more information about the resonance of the ground plane. We exactly need to know the characteristic of this resonance to find a way by which to avoid the resonance. The characteristic modes analysis is exactly a great method to quantitatively show the whole insight of this ground mode. Hence, in this Section 4.2, we calculate the characteristic modes of the disk loaded monopole antenna and focus on the mode associated with the ground plane. Then in Section 4.3, we propose circular ground plane to replace the square one and explain why circular ground reduces the cross-polarization radiation.

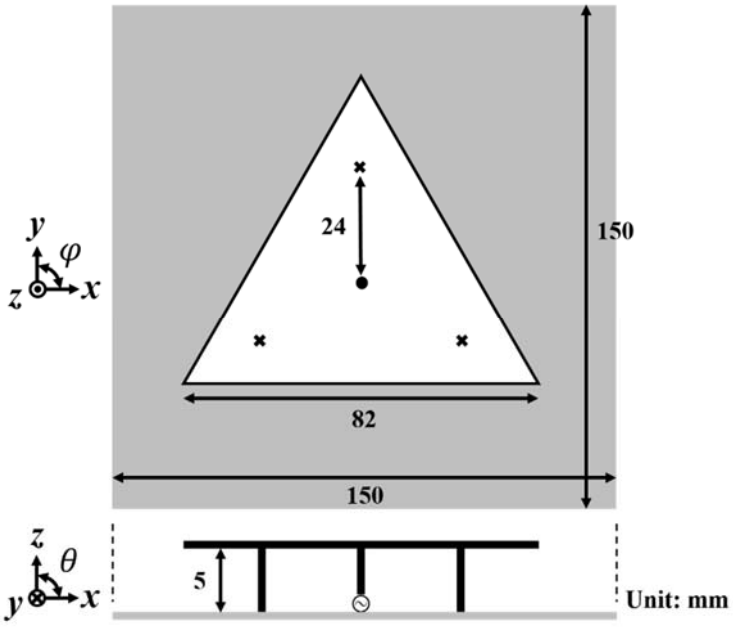

Figure 4. 2 Geometry of the disk loaded monopole antenna with 150×150 mm square ground plane.

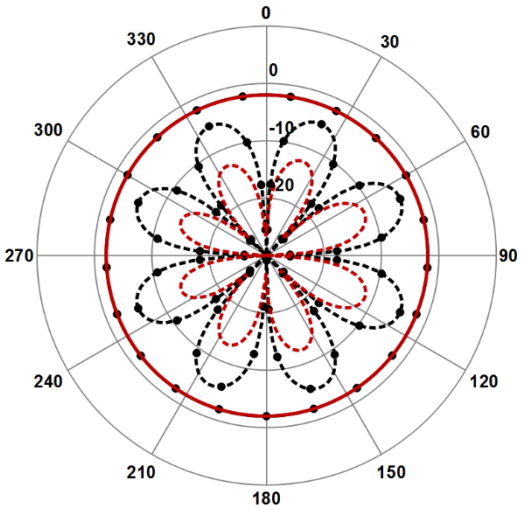

Figure 4. 3 Radiation gain patterns of the disk loaded monopole antenna in *xy*-plane. Red lines are with a 120×120 mm square ground plane, and black lines with marks are with a 150×150 mm square ground plane. Solid lines denote $\boldsymbol{E_\theta}$ and dotted lines denote $\boldsymbol{E_\varphi}$.

4.2 Characteristic Modes Analysis for Disk Loaded Monopole Antenna

A disk loaded monopole antenna consisting of a triangular conductor plate, a feeding pin, three shorted pins and a ground plane is an evolution of monopole antenna. In spite of the very low profile, the antenna has wide bandwidth. However, same with the monopole antenna, a conductor ground plane is necessary to the disk loaded monopole antenna. A ground plane with finite size obliquely upward reflects antenna radiation, and obliquely downward leaks some radiation.

First of all, we observe the first 6 modes occurring on a 150×150 mm conductor plate in 1.5 GHz ~ 2.5 GHz band. Figure 4. 4 shows current distribution of the modes, and Figure 4. 5 shows frequency response of characteristic angle of each mode. From the characteristic angle it can confirm only $\boldsymbol{J_5}$ and $\boldsymbol{J_6}$ are in capacitive status in the band, while other modes are in inductive status. Moreover, only $\boldsymbol{J_5}$ and $\boldsymbol{J_6}$ is possible to be excited because they all have minima of current distribution at their center position, and a capacitive coupler such as the disk loaded monopole should be placed at this position to excite the mode [42]. $\boldsymbol{J_2}$ and $\boldsymbol{J_3}$ also have minima of current distribution at their center position, whereas their current distribution is asymmetric so that difficult to be excited due to feeding structure of the disk loaded monopole.

As shown in Figure 4. 3, the antenna radiates horizontal polarization component, which is the cross-polarization, in *xy*-plane. This component is thought radiated by the ground plane. To further investigate the radiation, we calculate characteristic modes of the antenna. Two characteristic modes occurring on the antenna, $\boldsymbol{J_1}$ and $\boldsymbol{J_2}$, are confirmed strongly excited by the used feeding type. Current distribution of the two modes is shown in Figure 4. 6. In both the modes, current flowing on feeding pin and shorted pins is in phase and strong, especially in the $\boldsymbol{J_1}$ mode. It can also be observed that current flow on the ground plane and is relatively

concentrated in area near four edges of the ground plane. In middle area near the edge, the current change orientation, and current amplitude (density) is small. By carefully observation, we find the current distribution on the ground of $\boldsymbol{J_1}$ is similar with the $\boldsymbol{J_5}$ of single conductor plate, while the current distribution on the ground of $\boldsymbol{J_2}$ is similar with the $\boldsymbol{J_6}$ of single conductor plate.

Horizontally polarized radiation patterns of $\boldsymbol{E_\varphi}$ associated with the two modes are shown in Figure 4. 7. Both the pattern has eight beams with maximum radiation in the horizontal plane. The horizontally polarized radiation of $\boldsymbol{J_2}$ mode is strong, while the radiation of $\boldsymbol{J_1}$ mode is weak. Actually, the horizontally polarized radiation patterns of $\boldsymbol{J_1}$ and $\boldsymbol{J_2}$ are similar with that of the $\boldsymbol{J_5}$ and the $\boldsymbol{J_6}$ of single conductor plate, caused by the strong current flowing on the area near the edges of the square ground plane.

Frequency response of characteristic angle of the two modes comparing with the $\boldsymbol{J_5}$ and the $\boldsymbol{J_6}$ of single conductor plate shown in Figure 4. 8, in 1.5 GHz ~ 2.5 GHz. In summary of what was analyzed above, we consider $\boldsymbol{J_1}$ to be a mode containing excited form of the ground's $\boldsymbol{J_5}$, while $\boldsymbol{J_2}$ to be a mode containing excited form of the ground's $\boldsymbol{J_6}$. However, feeding pin and shorted pins are the main part in both $\boldsymbol{J_1}$ and $\boldsymbol{J_2}$, by observing the current distributions.

Figure 4. 9 shows input response of the antenna which resonate at 2.05 GHz. This frequency is close to the resonance frequency of $\boldsymbol{J_1}$. It obviously shows $\boldsymbol{J_1}$ is dominant mode, while $\boldsymbol{J_2}$ is subsidiary mode. Actually, it seems that $\boldsymbol{J_2}$ substantially correlates with the ground plane, whereas $\boldsymbol{J_1}$ approximately does not correlate with the ground plane, at least in the frequency band higher than 2.1 GHz.

If turn back to observe the $\boldsymbol{J_5}$ and the $\boldsymbol{J_6}$ of single conductor plate again, we can find another common point except the strong current flowing on the area near the edges; current around the center area is radial. This kind of radial current exactly makes it possible to be excited by the disk loaded monopole. Nevertheless, the current near the center area is not absolutely radial since the square is not centrosymmetry, and the semi-radial current may exactly cause the current near edge due to voltage difference. Therefore, in next Section, we discuss a centrosymmetry ground plane, a circle, on which a mode with absolutely radial current distribution exist that can be excited.

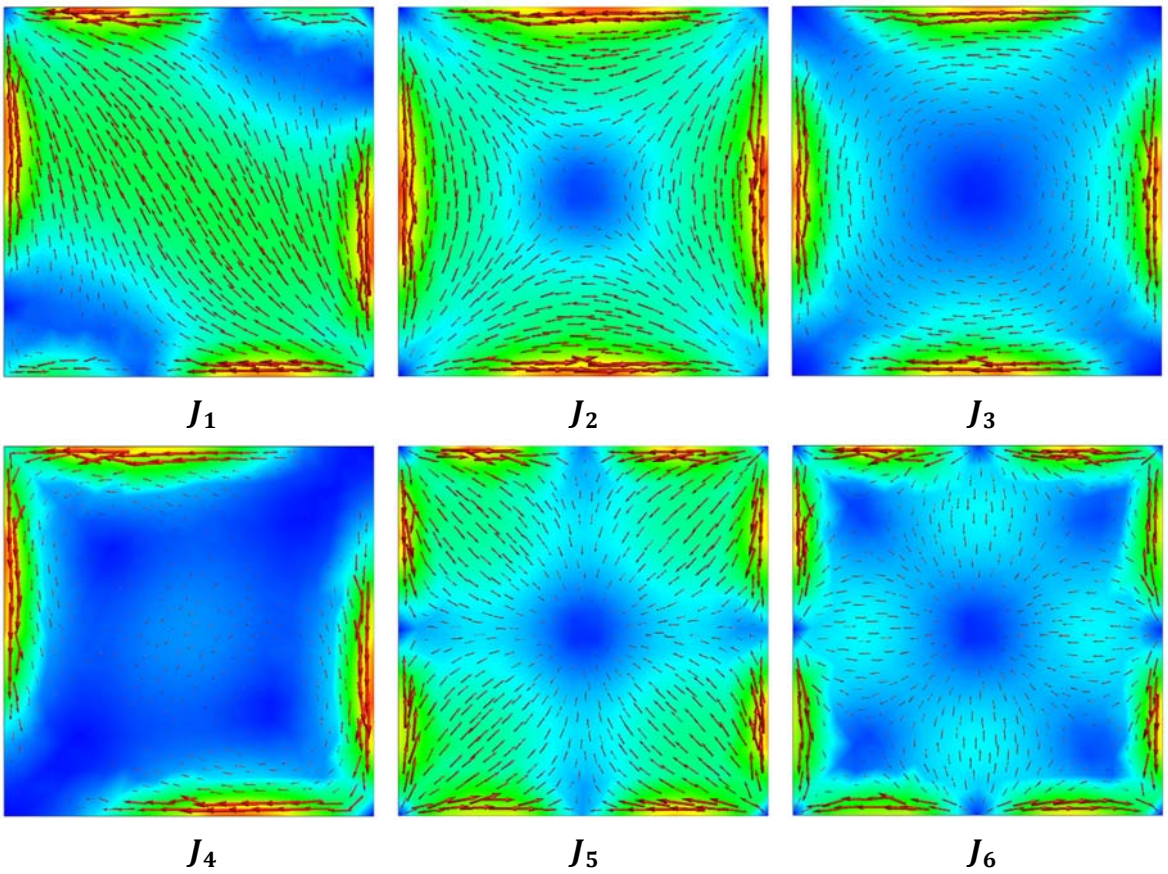

Figure 4. 4 First 6 characteristic modes of a 150×150 mm conductor plate.

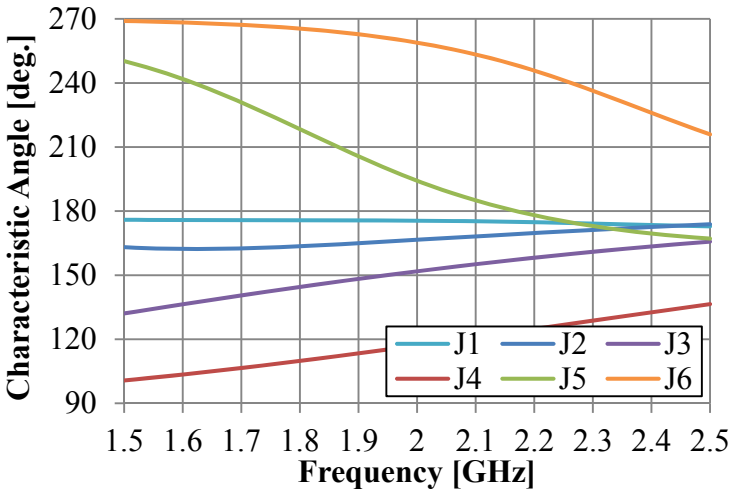

Figure 4. 5 Characteristic angle response of the 6 modes of the 150×150 mm conductor plate.

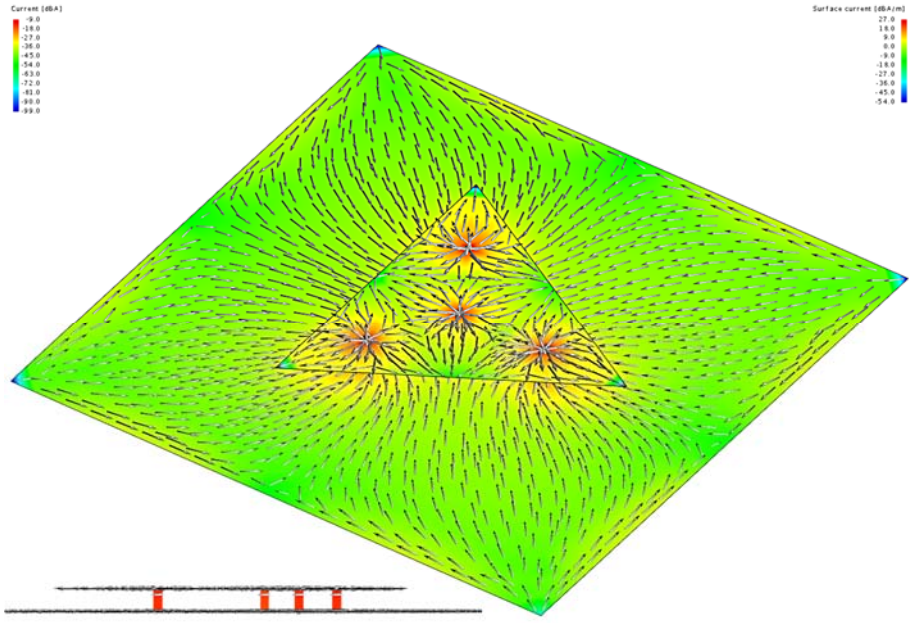

(a)

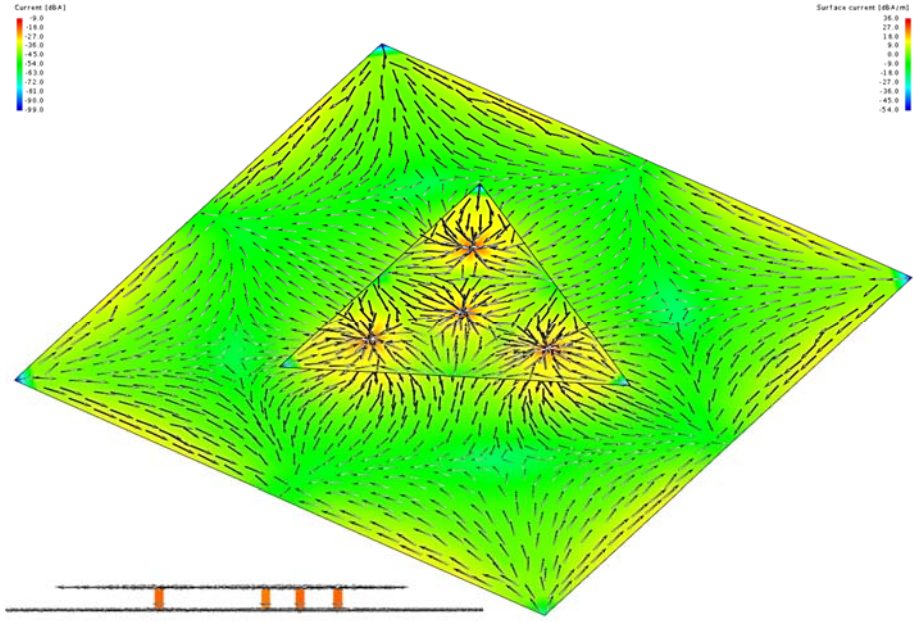

(b)

Figure 4. 6 Eigen current distribution (a) $\boldsymbol{J_1}$ and (b) $\boldsymbol{J_2}$ of the disk loaded monopole.

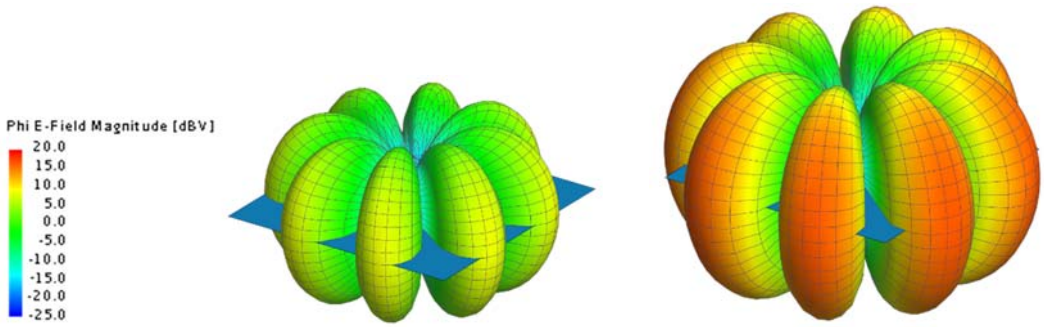

(a) (b)

Figure 4. 7 Horizontal polarized $\boldsymbol{E_{\varphi}}$ characteristic radiation pattern of (a) $\boldsymbol{J_1}$ and (b) $\boldsymbol{J_2}$.

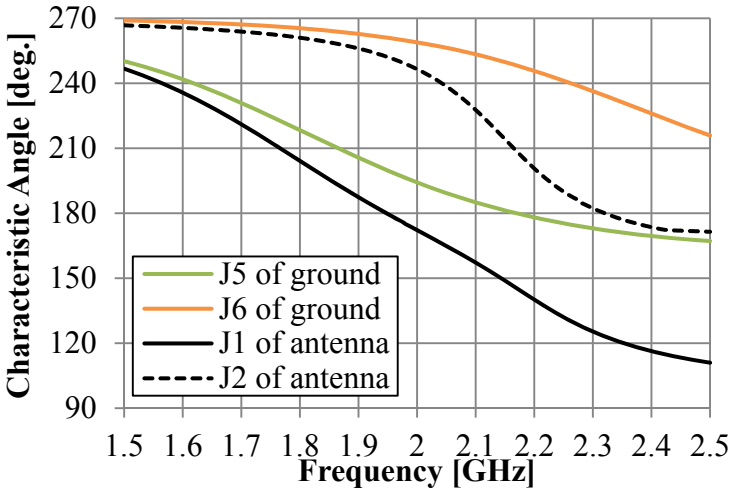

Figure 4. 8 Characteristic angles of the modes of antenna and that of single ground.

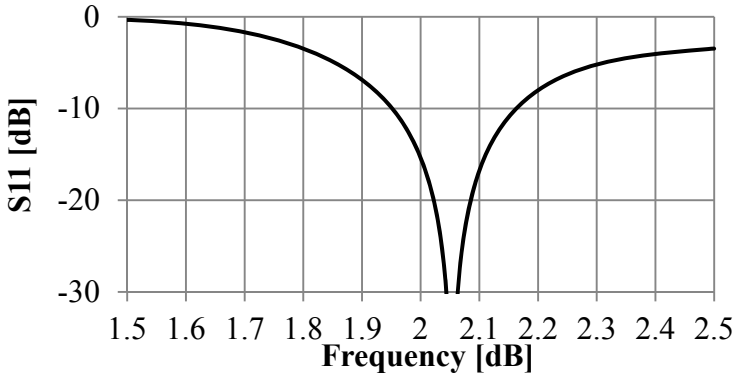

Figure 4. 9 Input response of the disk loaded monopole antenna.

4.3 Cross-Polarization Reduction Due to Circular Ground Plane

In previous Section, we discussed the cross-polarized radiation component of the disk loaded monopole antenna in the case of utilizing a square ground plane. The feeding of disk loaded monopole antenna usually excite the characteristic mode of a ground in which radial current distribute around the center area. When utilize a square ground plane, the current near the center area is not absolutely radial since the square is not centrosymmetry. The semi-radial current may exactly cause the current near four edges due to voltage difference. In this Section, we discuss a circular ground, which is centrosymmetry, to find whether the cross-polarization reduce due to exciting a mode with absolutely radial current distribution.

The first 6 modes occurring on a circular conductor plate with perimeter of 600 mm in 1.5 GHz ~ 2.5 GHz band. The perimeter equals to that of the square ground plane discussed in the previous Section for comparison. Figure 4. 10 shows current distribution of the modes, and Figure 4. 11 shows frequency response of characteristic angle of each mode. From the current distribution, we find $\boldsymbol{J_6}$ has strong radial current around the center area. This mode radiates little component of horizontal polarization. Figure 4. 12 shows current distribution of two characteristic modes, $\boldsymbol{J_1}$ and $\boldsymbol{J_2}$, occurring on the antenna utilizing the circular ground plane. It is noticed that in both the modes, current flowing on the ground plane is radial style which is similar with that of the $\boldsymbol{J_6}$ belonging to the single circular plate. This result indicates $\boldsymbol{J_6}$ is the only mode excited by the feeding of disk loaded monopole. Figure 4. 13 shows horizontally polarized radiation pattern $\boldsymbol{E_\varphi}$ of $\boldsymbol{J_1}$ and $\boldsymbol{J_2}$. Both the radiation level is extraordinarily small because the $\boldsymbol{J_6}$ ground mode originally radiates little horizontally polarized E-field. Characteristic angle of the two modes comparing with the $\boldsymbol{J_6}$ of circular conductor plate is shown in Figure 4. 14, and input response of the antenna is shown in Figure 4. 15. It indicates $\boldsymbol{J_1}$ is still the dominant mode, while $\boldsymbol{J_2}$ is subsidiary high order mode.

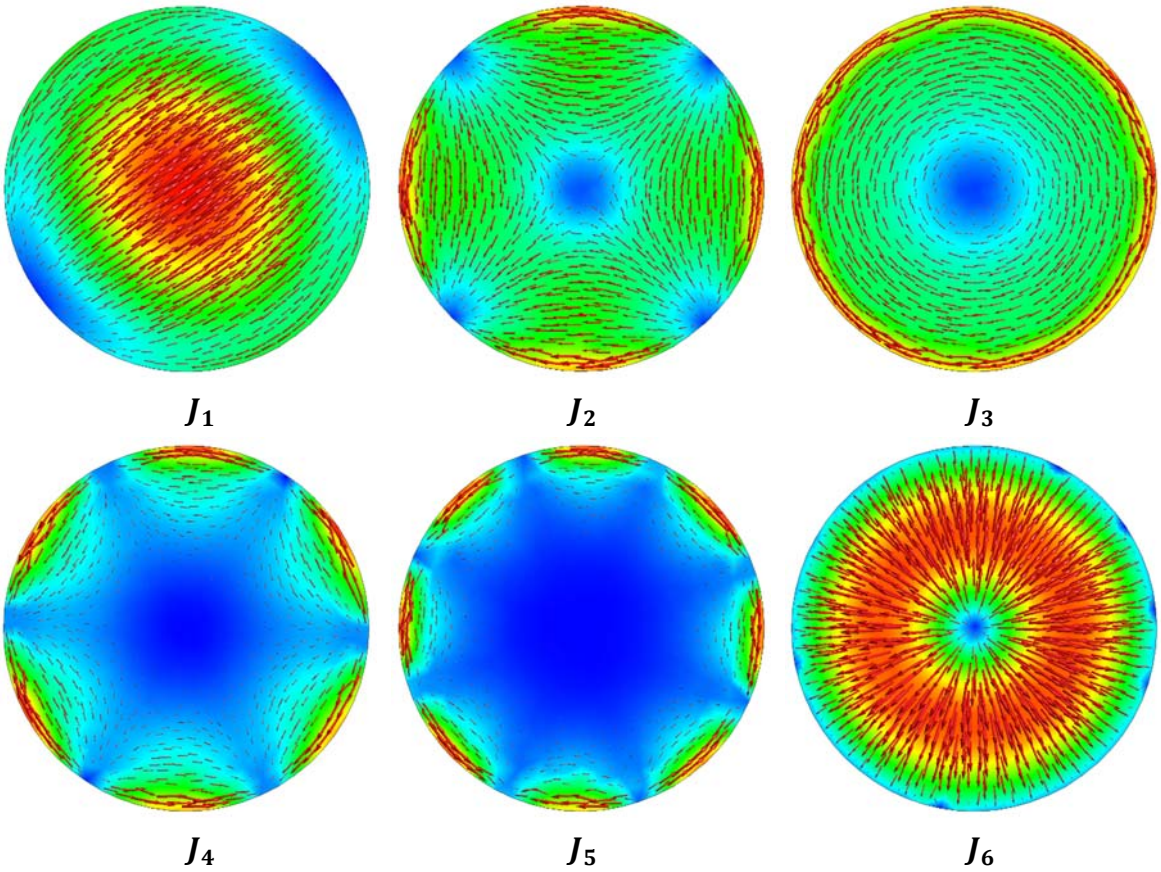

Figure 4. 10 First 6 characteristic modes of circular conductor plate with perimeter of 600 mm.

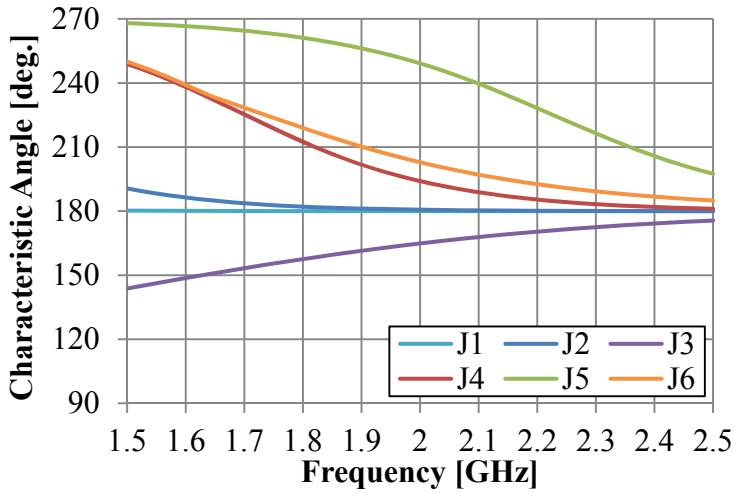

Figure 4. 11 Characteristic angle response of the 6 modes of the circular conductor plate.

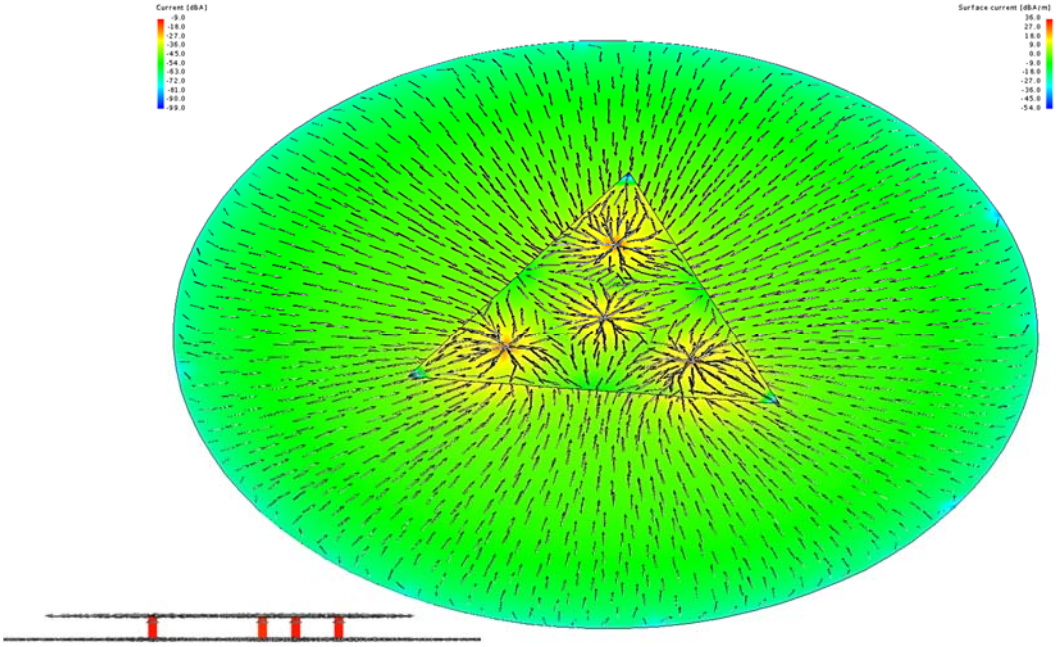

(a)

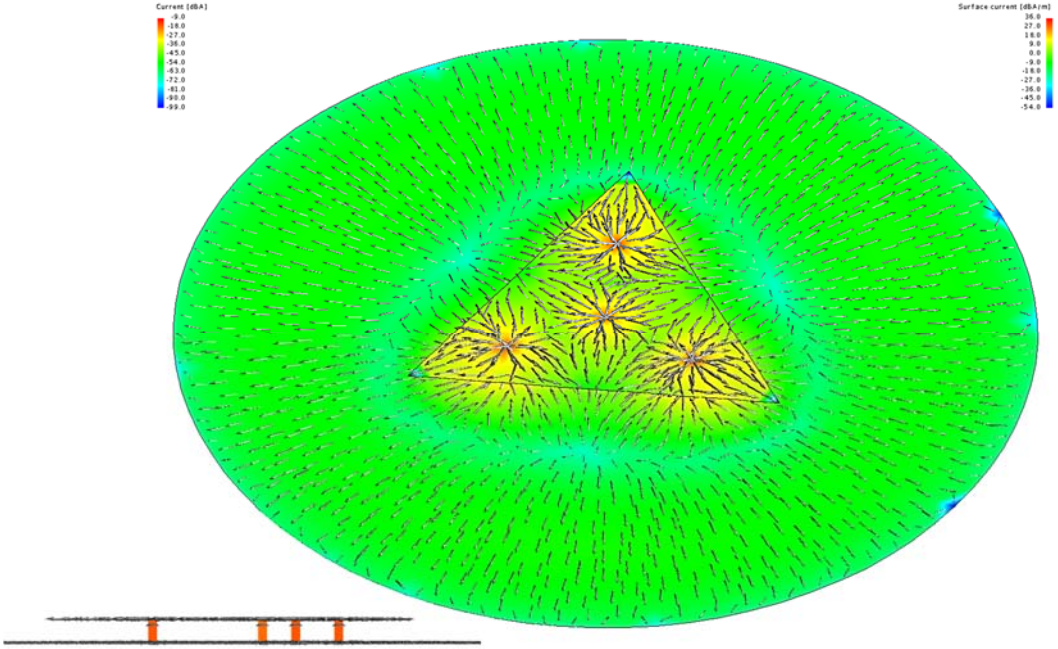

(b)

Figure 4. 12 Eigen current distribution (a) $\boldsymbol{J_1}$ and (b) $\boldsymbol{J_2}$ of the disk loaded monopole.

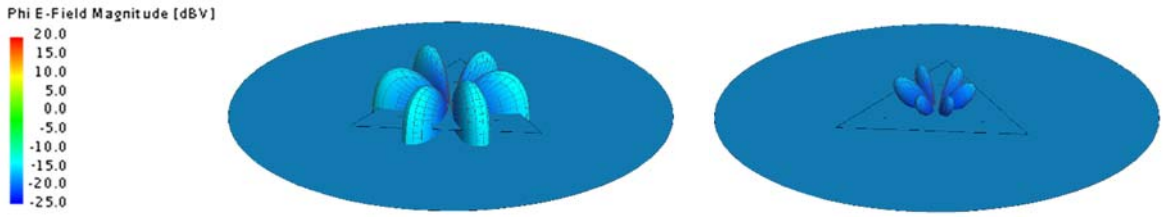

(a) (b)

Figure 4. 13 Horizontal polarized E_{φ} characteristic radiation pattern of (a) J_1 and (b) J_2.

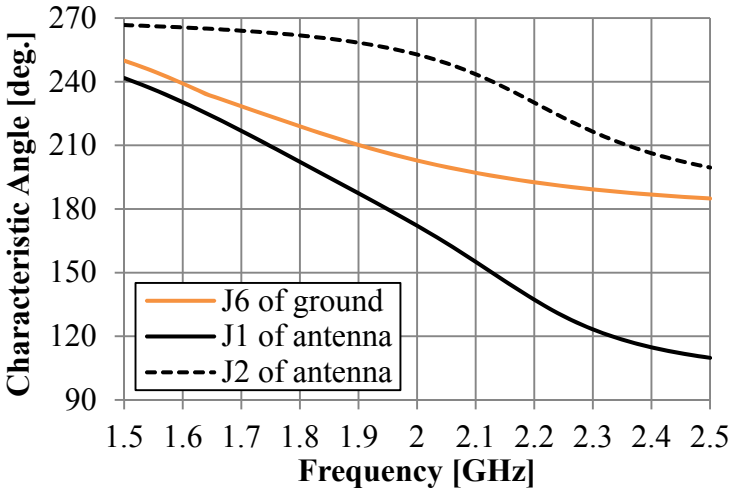

Figure 4. 14 Characteristic angles of the modes of antenna and that of single ground.

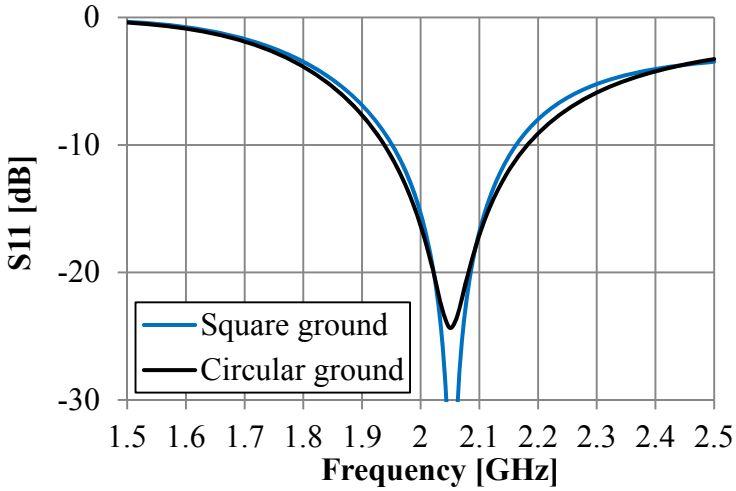

Figure 4. 15 Input response of the disk loaded monopole antenna.

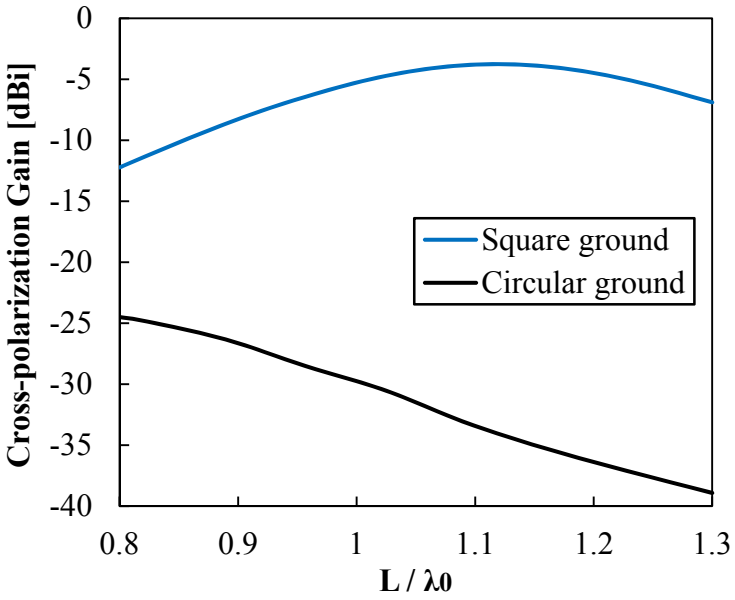

Figure 4. 16 Cross-polarization gain of the disk loaded monopole antenna along with variant **L** which denotes the side length of the square ground plane or a quarter of perimeter of the circular ground plane. **λ0** is wavelength corresponding to 2.05 GHz.

We calculated a series of cross-polarized radiation gain of the disk loaded monopole antenna utilizing the square ground plane and the circular ground plane, respectively, with different size. The results are shown in Figure 4. 16. In this figure, horizontal axis represents **L**, which denotes the side length of the square ground plane or a quarter of perimeter of the circular ground plane, normalized by **λ0**, which is wavelength corresponding to 2.05 GHz. The range of **L / λ0** is 0.8 ~ 1.3, because too small ground plane causes strong downward radiation, while too big ground plane cannot satisfy the miniaturization of antenna. In the case of utilizing the square ground plane, cross-polarization gain varies in -4 ~ -12 dBi and has a peak when **L** is 1.12**λ0**. While if utilize the circular ground plane, cross-polarization gain greatly reduces to -24 ~ -39 dBi and decreases along with increased **L**. The reduced cross-polarization gain is considered due to the excited J_6 ground mode which has absolutely centrosymmetry radial current distribution. Increased **L** decreases resonant frequency of the J_6 to close to the operating band so that this non-horizontal-polarization mode provides antenna decreased cross-polarization component.

4.4 Summary

In this Chapter, we used the characteristic modes analysis to discuss the problem of cross-polarization of the disk loaded monopole antenna. The antenna feeding excites characteristic modes of the ground plane so that horizontally polarized E-field is radiated by the ground plane to be the cross-polarization component in the antenna radiation pattern.

Since its feeding structure, the disk loaded monopole tends to excite those modes have radial current distribution from center area to edge areas of the ground plane. Although it is not a centrosymmetry shape, a square ground plane has two characteristic modes provide the radial current. However, the radial current distributions are not uniform due to the ground plane's shape; and the imbalanced semi-radial current causes voltage difference on the edge areas so that strong current distribute along the edge areas to radiate horizontally polarized E-field. When the antenna is fed and the ground mode is excited, the horizontal polarization component will be radiated by the ground so that mutual coupling between the disk loaded monopole and the horizontally polarized notched array will increase.

In order to reduce the horizontal polarization component radiated by the ground plane, a ground mode providing absolutely uniform radial current distribution is desired, because this current distribution radiates little horizontally polarized E-field. A centrosymmetry circular ground plane is conformed that involve the characteristic mode and can be excited by the antenna. The uniformly radial current flowing on the ground plane make the horizontal polarization radiation component greatly reduce to a very low level.

CHAPTER 5
CHARACTERISTIC MODES ANALYSIS FOR RADIATION PATTERN OPTIMIZATION OF NOTCHED ARRAY

5.1 Introduction

In Chapter 4, we discussed conductor plates with different geometries providing different characteristic modes. In Chapter 5, we discuss how to move specific characteristic modes by revising local dimensions, and to optimize antenna radiation pattern. The notched array antennas are used for examples in this Chapter and separated to two step; firstly, we calculate the characteristic modes of a double notched antenna to show how to change antenna radiation pattern by exciting desired mode or removing undesired mode, while keeping primary geometry; secondly, we apply the method to a four notched array that help to propose a horizontally polarized reference antenna with perfectly identical radiation pattern in horizontal plane.

A notched antenna can be regarded as an evolution from a slot antenna. Due to its good performances, the slot antennas are widely used, especially in the case of low-profile

requirements, such as airplanes or satellites. Figure 5. 1 (a) shows a general model of slot antenna using a conductor plate. The slot can well resonate when the length is about $\lambda_0/_2$, and ignore the width. However, effectively the width is certainly existent so that the length is usually not exactly $\lambda_0/_2$. The slot antenna can be fed by a coaxial cable, or a microstrip line when it is fabricated by dielectric substrate. Whatever the slot antenna is fed, the feeding position will impact on antenna input impedance. If the feeding is at the center of slot, the impedance is about $500\,\Omega$. Thus, the feeding position is usually offset as shown in the figure.

On the conductor surface, current distribute around the slot as shown in the figure. When a time-varying current is distributed around the slot, a time-varying magnetic field is excited inside the slot and surround the conductor plate. Then, electric field is excited. Electromagnetic wave is radiated all around, and the maximum radiation is along the $\pm z$-axis.

The notched antenna which is originally proposed in [96] can be imagined as the half of slot antenna as shown in Figure 5. 1 (b). Extremely similar with a monopole antenna, an image is symmetrically formed at the other side of the open end, where the disappeared part. The notched antenna can be considered as the complementation of a monopole antenna, too. In other words, the radiation pattern can also be contrastively analyzed as the magnetic radiation pattern of the monopole. Also, oppositely with that the radiation of a monopole antenna is partly reflected by the finite ground plane, the radiation of a notch antenna partly scatters toward the free space due to the disappearance of the other side.

The above analysis can be verified by simulating a notched antenna shown in Figure 5. 2 (a). Its radiation patterns in (b) *xy*-plane and (c) *zx*-plane indicate lightly strong radiation scattering toward the $+x$-axis, that pointing to the free space. Cross polarization which can be found in (d) *zy*-plane is considered the radiation of the wire feeding used for excitation of the notched antenna.

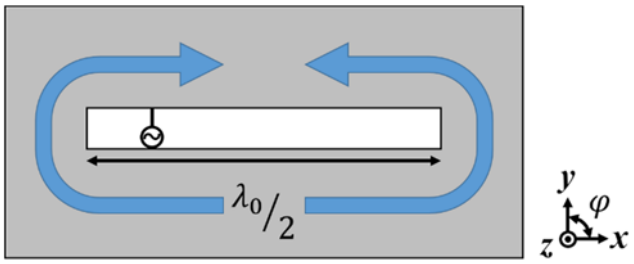

(a)

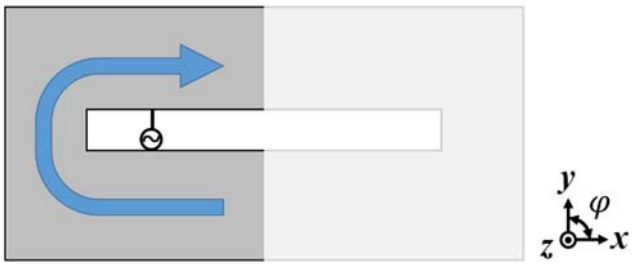

(b)

Figure 5. 1 Slot antenna (a) and notched antenna (b).

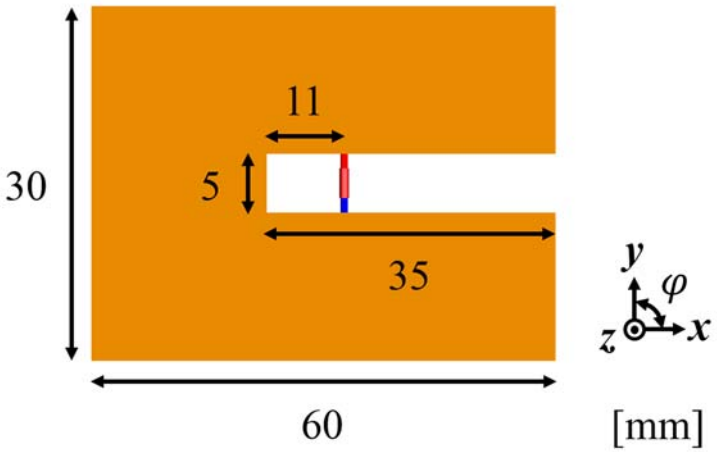

(a)

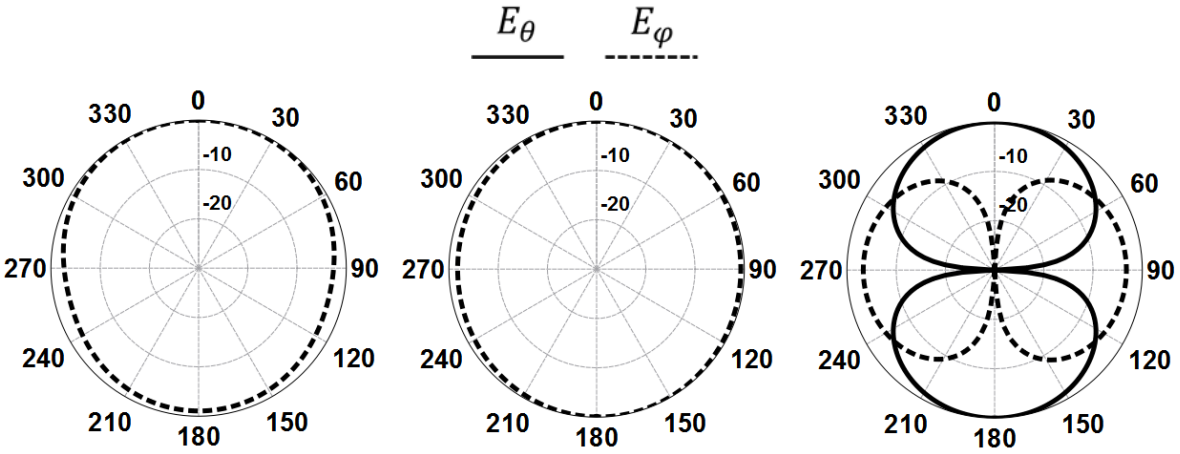

(b) (c) (d)

Figure 5. 2 A notched antenna in free space and the simulated radiation patterns

5.2 Double Notched Antenna

Two collinear notched antennas can be arranged symmetrically in opposite direction to provide varied performance. This kind of antenna has been proposed in [97] and [98] applying to common cellular system in highway tunnel. Figure 5. 3 shows the proposed antenna geometry in [98], two notched antennas cut on one of the conductor plates of a dielectric substrate above a ground plane are excited by two inversely orientated probes in simulation. This double notched antenna has two operating modes, patch mode and probe mode. In low frequency band, due to the half wavelength length, the conductor plate resonates and radiate bi-directional $\boldsymbol{E_\varphi}$ pattern to $\pm y$-axis; in high frequency band, due to a quarter wavelength active length (the length of the probes in simulation), the active part of microstrip lines resonate as two monopoles, and radiate bi-directional $\boldsymbol{E_\varphi}$ pattern to $\pm x$-axis. In this case, since its size does not match the resonant frequency of microstrip line, the two notches does not dominantly resonate. However, the antenna maybe radiate to both $\pm x$-axis and $\pm y$-axis like double orthogonal "8" if the notches resonate together with the conductor plate under a revised geometry.

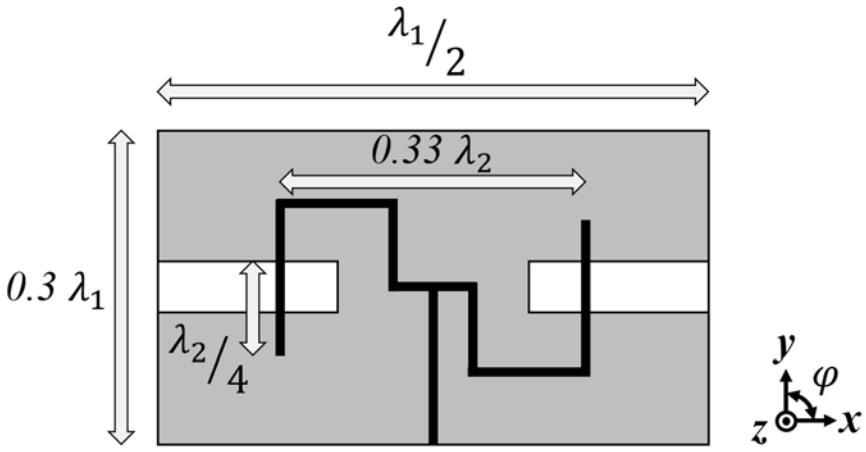

Figure 5. 3 The bi-directional notched antenna (ground not included) proposed in [98]. Gray part denotes conductor plate where the notches are cut on; black lines denote microstrip lines.

The double notched antennas proposed in [97][98] are low gain antenna that installed in short tunnels of less than 2 km with about 200 m interval [99], while for long tunnels longer than 2 km, another approach with higher gain is proposed [100]. Similar with that in [98], the proposal in [100] also has bi-directional radiation pattern in both *xy* -plane and *zy* -plane (same with the *xy*-plane and *zy*-plane in Figure 5. 3). The high gain of about 5 dBi is obtained for the probe mode by using directors placed on both sides of the notches as that in a Yagi-Uda array.

In this Chapter, we also use a double notched antenna as an example to illustrate how to use characteristic modes to analyze antenna and contribute to realizing required performances by exciting desired characteristic modes. Different with the previous designs in [97]-[100], this time an electrically small conductor plate is attempted for the discussion to reduce characteristic modes occurring on the antenna. Figure 5. 4 shows the geometry of the proposed antenna. As is mentioned in its caption, two wide mouth notches is cut on the bottom conductor sheet of a dielectric substrate, and a microstrip line is on the top conductor sheet used for feeding the notches. Dielectric constant of substrate is 2.6, and the thickness is 0.8 mm.

Comparing with the previous antennas, space between the two notches is very narrow so that the notches are close to each other. As a result, maximum radiation to ± *x*-axis is difficult because of the mutual out-phase radiation by the two elements.

The antenna is fed from the center of the microstrip line. The size of an original type (in this thesis) is recorded in Table 5. 1. The original type is designed to working at 1.5 GHz. This is an arbitrary frequency without any supposed application. Input characteristic vs. frequency is shown in Figure 5. 5. The antenna has well matching, but the bandwidth is merely 3.3% because of the small conductor ground plate. Figure 5. 6 shows antenna's radiation pattern at 1.5 GHz, in *xy*-plane and *zy*-plane, respectively. Thus, it can confirm the maximum radiation is on ± *y*-axis. Radiation on ±*x*-axis is weak because of the short space between the two inversely orientated elements so that radiation from them cancel each other on ±*x*-axis. In addition, the maximum radiation is in both E-plane and H-plane.

However, the radiation pattern in *xy*-plane indicates the antenna is neither omni-directional nor absolutely bi-directional in the horizontal plane. In order to change the antenna's radiation pattern, in next Section we calculate the characteristic modes occurring on the antenna to study its operating mechanism.

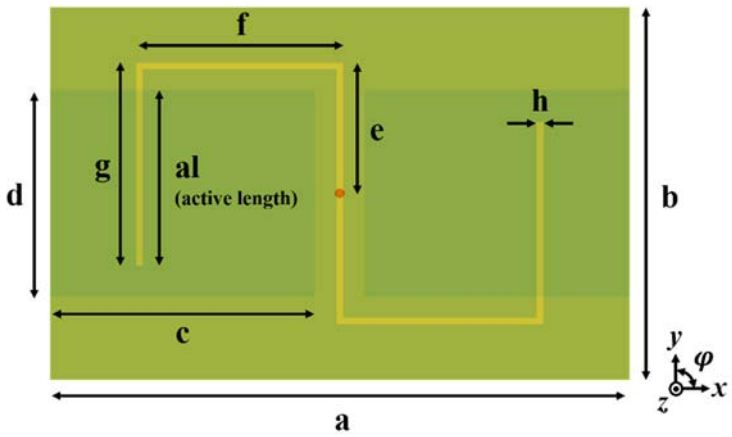

Figure 5. 4 Geometry of the double notched antenna. Microstrip line (e, f, g, etc.) is on top face and notches (c, d, etc.) are on bottom face.

Table 5. 1

Size of the original type double notched antenna.

a	b	c	d	e	f	g	al	h
70	45	32	25	15	25	24	21.5	0.8

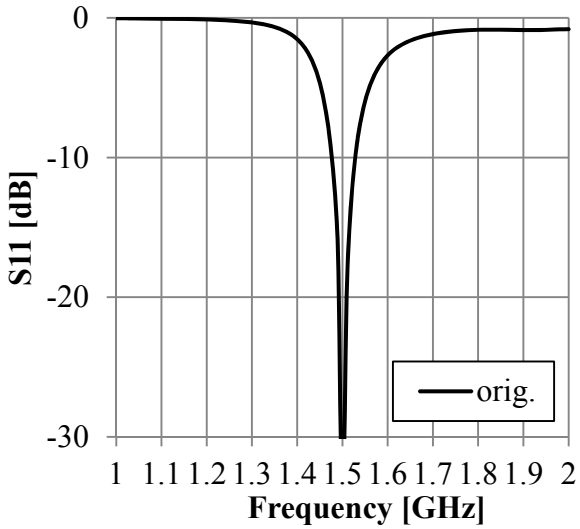

Figure 5. 5 Input characteristic of the original type double notched antenna.

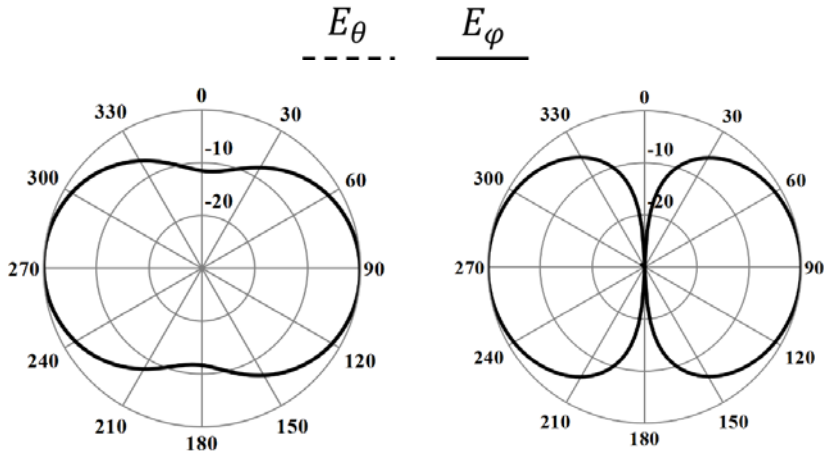

xy-plane *zy*-plane

Figure 5. 6 Radiation pattern of the original type double notched antenna at 1.5 GHz.

5.2.1 Characteristic Modes Analysis for Double Notched Antenna

Characteristic modes of the antenna in spectrum of 1~2 GHz are calculated. Although antenna excitation is not taken into account in the theory of characteristic modes, in this case, since the feeding position is established and certain, we calculate the model with center feeding pin to reduce investigation range.

There are two important characteristic modes, $\boldsymbol{J_1}$ and $\boldsymbol{J_2}$, are found by observing calculation results. Although there are several other modes observed in the concerned band, only this two modes are possible to be excited by the supposed feeding style we use. So, it is sufficient to discuss only $\boldsymbol{J_1}$ and $\boldsymbol{J_2}$. Figure 5. 7 shows characteristic current distribution of the two modes. It is noticed that current on the conductor ground plane (bottom face) is strong in the $\boldsymbol{J_1}$ mode, while relatively weak in the $\boldsymbol{J_2}$ mode. And, current of the $\boldsymbol{J_2}$ mode relatively concentrate on the microstrip line. Figure 5. 8 shows the top view of 3-D characteristic radiation pattern, which are horizontally polarized patterns, of the two modes. The radiation pattern of the $\boldsymbol{J_1}$ mode approximates to omni-directional, while that of $\boldsymbol{J_2}$ is similar with practically excited antenna's radiation pattern that approximates to bi-directional.

Frequency response of characteristic angles of this two significant modes are shown in Figure 5. 9 to provide resonance information. Since a mode is at resonance status when its characteristic angle is close to 180°, we can be informed of the resonant frequency of the two modes; $\boldsymbol{J_1}$ mode resonates at 1.09 GHz, while $\boldsymbol{J_2}$ mode resonates at 1.54 GHz. If combining the excited antenna's input response property shown in Figure 5. 5, the $\boldsymbol{J_2}$ mode would be considered the dominant mode, because its resonant frequency is close to the excited antenna's resonant frequency. Besides the frequency, the radiation pattern of $\boldsymbol{J_2}$ which is similar with the practically excited antenna's radiation pattern is also an important hint.

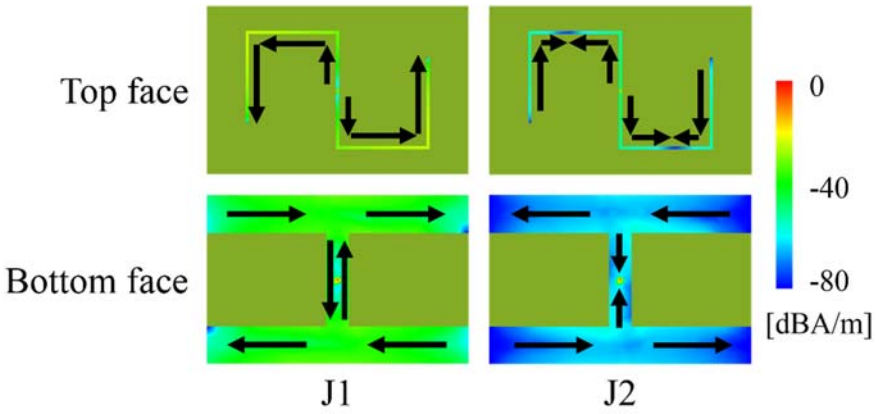

Figure 5. 7 Characteristic current distribution of the two modes. Black arrows represent current orientations.

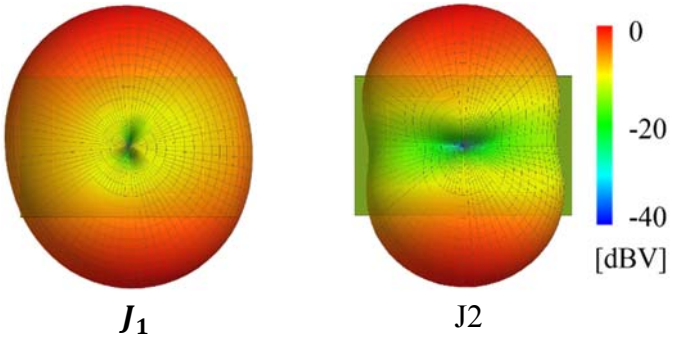

Figure 5. 8 Top view of 3-D E_φ characteristic radiation patterns of the two modes.

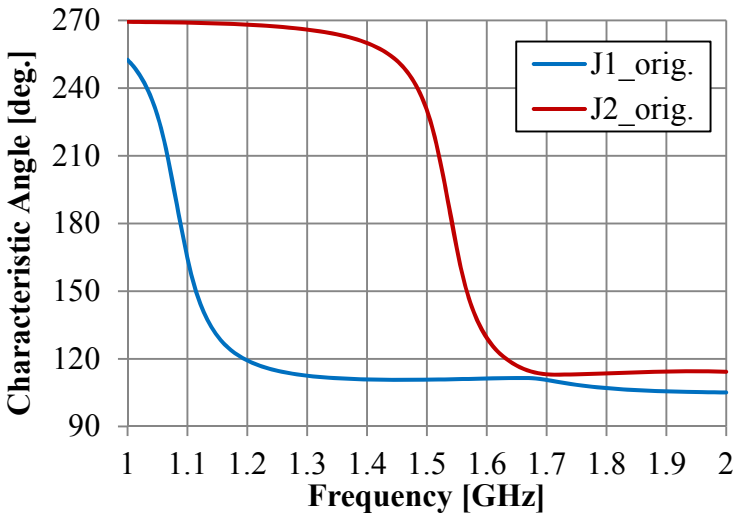

Figure 5. 9 Characteristic angles of the two modes.

However, the antenna's practical resonance should be explained as a cooperation which is contributed by both the two modes, for the resonant frequency is little lower than that of $\boldsymbol{J_2}$ due to the existent of the $\boldsymbol{J_1}$ mode.

Nevertheless, it is difficult to get more information for antenna parameters adjustment in next step depending on only the characteristic current distributions and frequency responses of the two modes. We have to know which part of the antenna respectively causes the modes. Therefore, some parameter studies are supplemented for obtaining more details. Figure 5. 10 ~ Figure 5. 17 show the results of parameter studies.

Figure 5. 10 and Figure 5. 11 show variations on the characteristic angles and the input response caused by different **g**, the length of the last part of microstrip line, respectively. Along with shortened **g**, the frequency response of both $\boldsymbol{J_1}$ and $\boldsymbol{J_2}$ ascend, and the antenna's input response ascend, too. However, the fluctuation ratio of $\boldsymbol{J_2}$ is larger than that of $\boldsymbol{J_1}$. This result indicates $\boldsymbol{J_2}$ depends on the microstip line more than $\boldsymbol{J_1}$.

Figure 5. 12 and Figure 5. 13 show the variations caused by different **f**, the length of the second part of microstrip line. Similar with **g**, shortened **f** also make the frequency response of $\boldsymbol{J_1}$, $\boldsymbol{J_2}$, and the antenna's input response ascend. However, this time the fluctuation ratio of $\boldsymbol{J_1}$ is almost same with that of $\boldsymbol{J_2}$, because the **f** relates to both microstrip line length and its feeding position on the notches.

Figure 5. 14 and Figure 5. 15 show the variations due to different **a**, the length of the conductor ground plane. This result is interesting because increased **a** causes the frequency response of $\boldsymbol{J_1}$ ascend, while that of $\boldsymbol{J_2}$ descend, and finally the antenna's input response a little descend by the same fluctuation ratio with $\boldsymbol{J_2}$. This result indicates $\boldsymbol{J_1}$ much more relates to the microstrip line's feeding position, and $\boldsymbol{J_2}$ has correlation with the ground's length.

Figure 5. 16 and Figure 5. 17 show the variations caused by different **c**, the length of the notches. Shortened **c** causes frequency response of both the modes ascend, especially $\boldsymbol{J_1}$, because $\boldsymbol{J_1}$ is considered deeply depending on the microstrip line's feeding position.

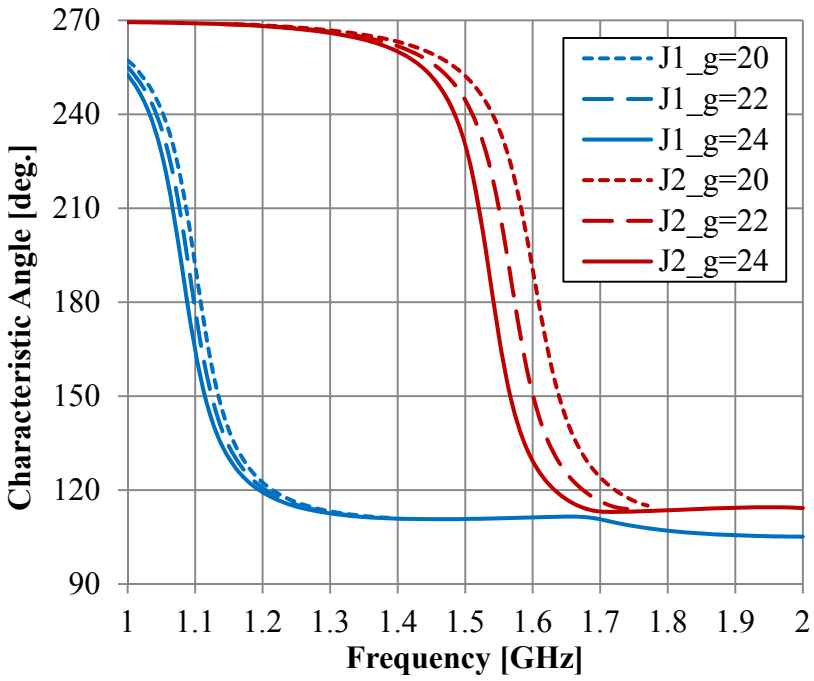

Figure 5. 10 Characteristic angles according to different **g**.

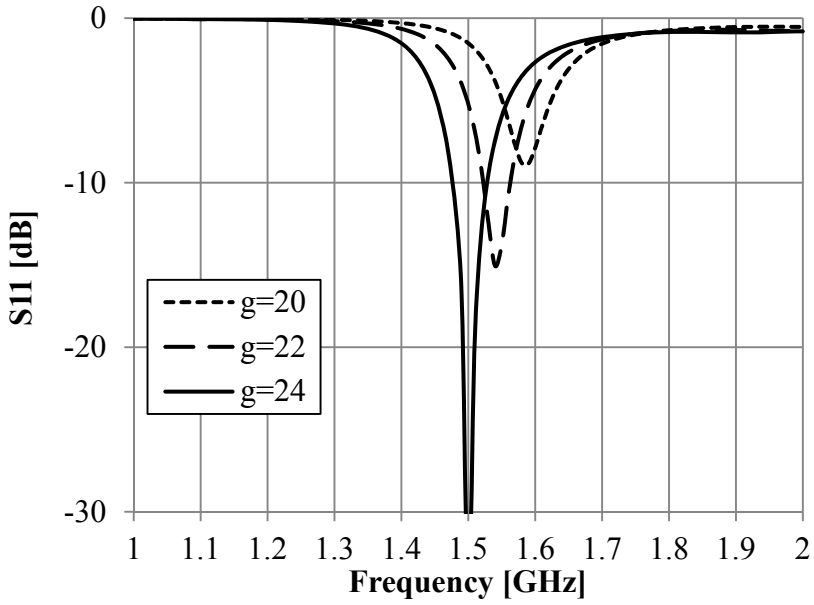

Figure 5. 11 Antenna input response according to different **g**.

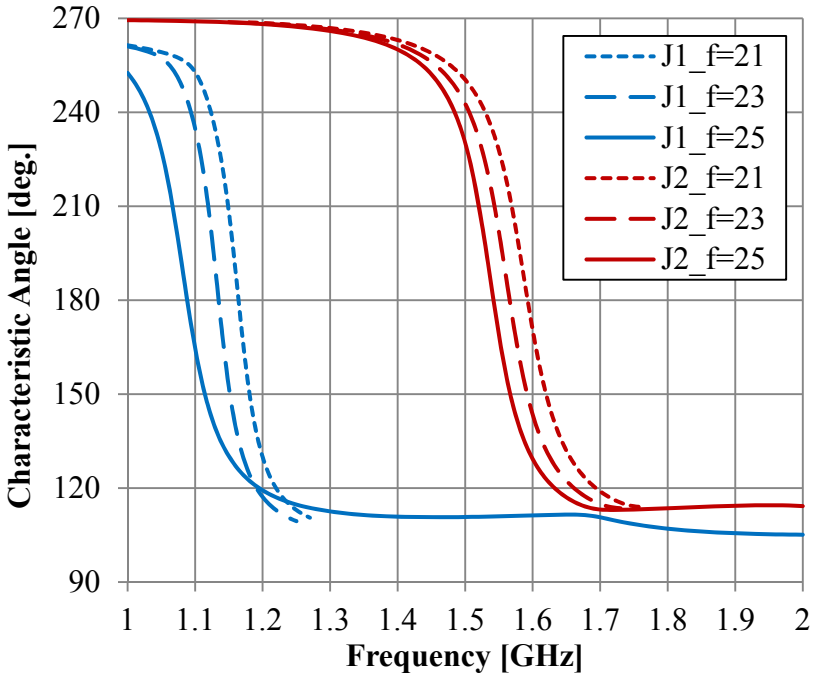

Figure 5. 12 Characteristic angles according to different **f**.

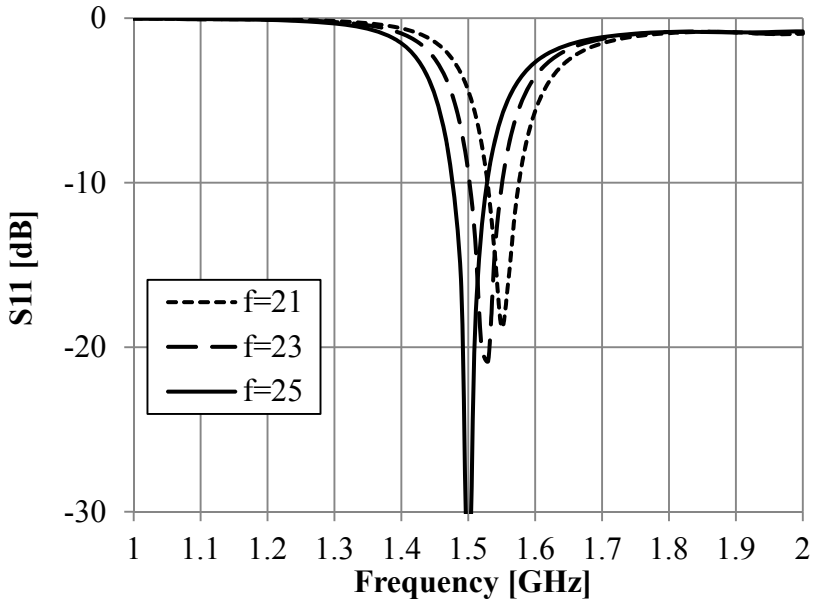

Figure 5. 13 Antenna input response according to different **f**.

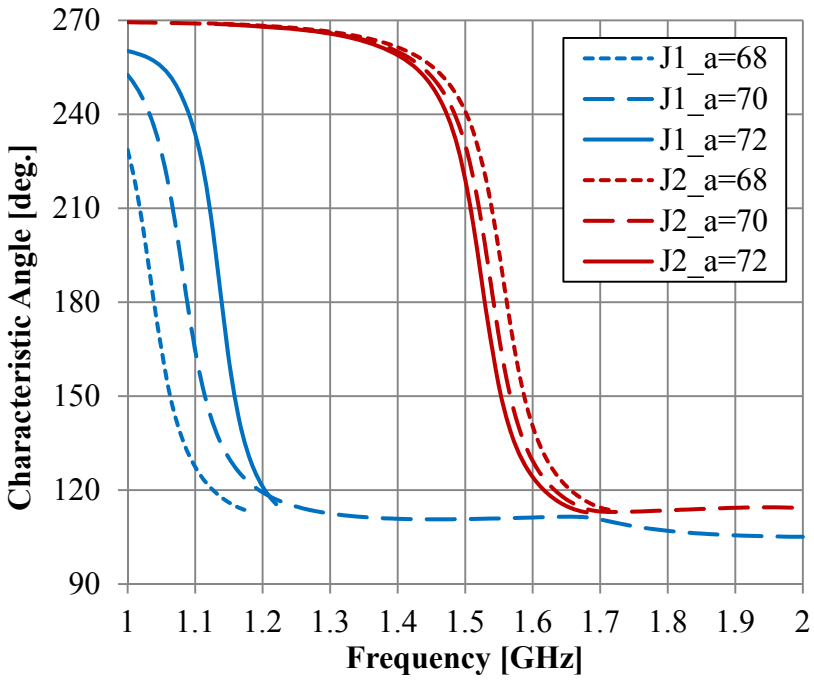

Figure 5. 14 Characteristic angles according to different **a**.

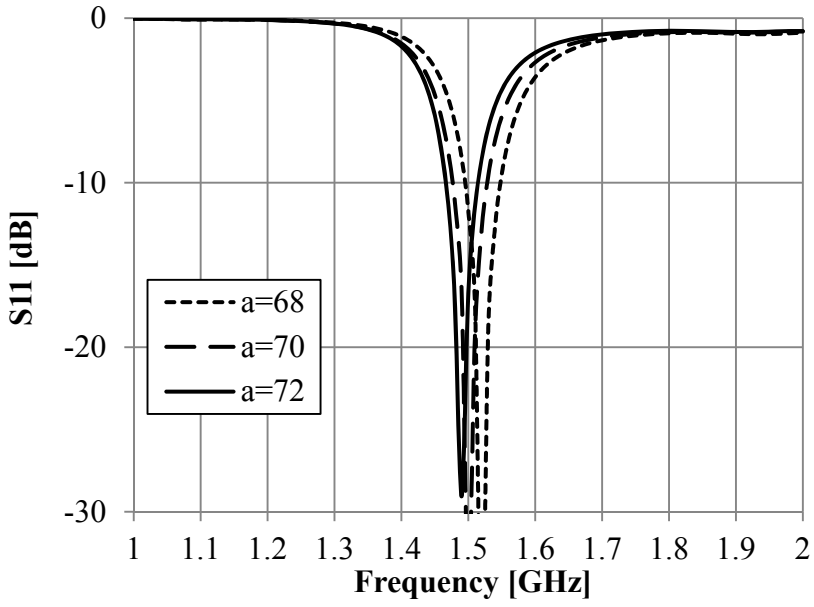

Figure 5. 15 Antenna input response according to different **a**.

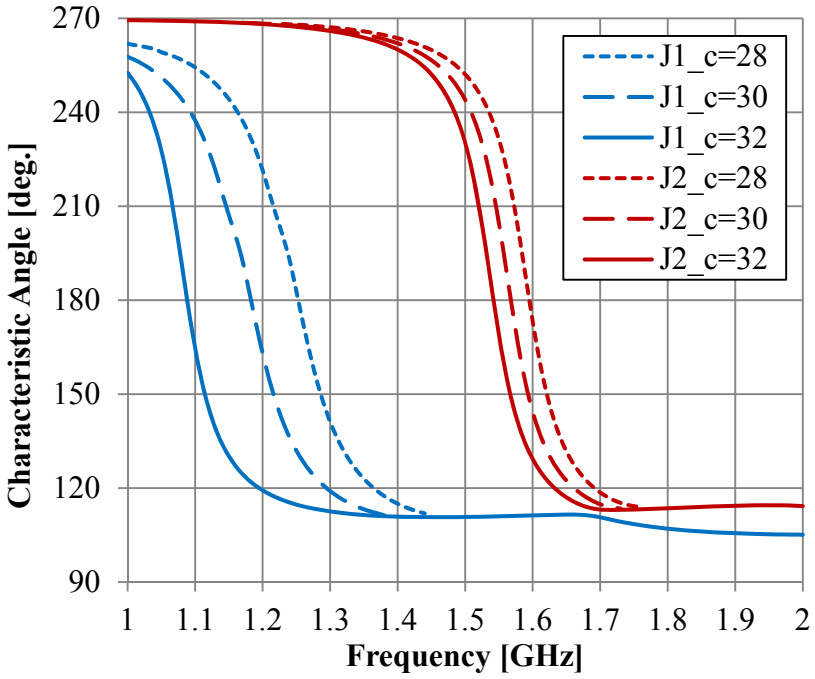

Figure 5. 16 Characteristic angles according to different **c**.

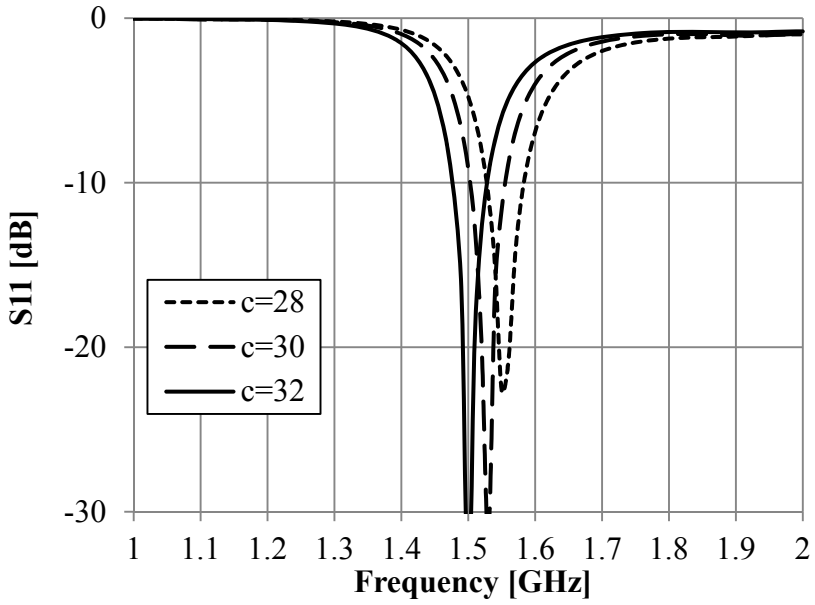

Figure 5. 17 Antenna input response according to different **c**.

By analyzing the parameters study results, we understand the following key points, and use these points to guide parameter adjustment to excite desired mode or restrain undesired mode.

i. Both $\boldsymbol{J_1}$ and $\boldsymbol{J_2}$ relate to the current flowing on both the microstrip line and the ground plane. This is also indicated by the current distributions.
ii. $\boldsymbol{J_1}$ correlates with the current on ground plane more, particularly the surrounding current under the microstrip line and close to the two notches.
iii. $\boldsymbol{J_2}$ almost depend on every part of the antenna, and this is why it's the principle mode directly leading to antenna resonance.

5.2.2 Radiation Pattern Adjustment by Controlling Characteristic Modes

From the characteristic modes analysis in last Section, we know adjusting the length of ground plane and the notches move the frequency response of $\boldsymbol{J_1}$ and at the same time slightly move that of $\boldsymbol{J_2}$. And, adjusting the length of microstrip line's last part mostly move response of $\boldsymbol{J_2}$, while the middle part **f** correlates the feeding position of the notches so that relate to both the two modes. Besides, it should be noticed that the part **al** shown in Figure 5. 4 is active part to excite the notches. So, only changing **al** can effectively move the response of $\boldsymbol{J_2}$. That means changing the length of microstrip line's beginning part **e** will lead to the change of the **al**, so that this change causes opposite result with changing **g**.

Once we know these important points, we can obtain desired characteristics by efficient adjustment. In this case, we expect two possible type as targets. Considering the radiation pattern of the $\boldsymbol{J_1}$ mode approximates to omni-directional, and the radiation pattern of $\boldsymbol{J_2}$ is similar to bi-directional; hence, one type is omni-directional antenna in which the $\boldsymbol{J_1}$ mode is supposed to be excited, while oppositely the other type is bi-directional antenna by restraining $\boldsymbol{J_1}$ mode. Therefore, we shorten the length of the ground plane, lengthen the microstrip line, and at the same time keep the size of notches to obtain omni-directional pattern. The size of the

omni-directional type is shown in Table 5. 2. On the other hand, we lengthen the length of the ground plane and shorten the microstrip line to obtain bi-directional pattern. The size of the bi-directional type is shown in Table 5. 3.

When the antenna is omni-type, resonant frequencies of $\boldsymbol{J_1}$ and $\boldsymbol{J_2}$ close to each other at about 1.1~1.2 GHz, shown by blue lines in Figure 5. 18. $\boldsymbol{J_1}$ can be also excited due to its approach to the dominant mode $\boldsymbol{J_2}$. Therefore, bi-resonance is observed by blue line in Figure 5. 19. Omni-directional radiation pattern of $\boldsymbol{E_\varphi}$ in *xy*-plane is shown by blue line in Figure 5. 20. Ripple of the pattern in *xy*-plane is ±1.06 dBi at 1.11 GHz, and ±1.23 dBi at 1.22 GHz (not shown).

When the antenna is bi-directional type, resonant frequency of $\boldsymbol{J_1}$ reduces slightly but that of $\boldsymbol{J_2}$ is almost invariant. It is observed that the resonant frequency of the antenna slightly descends while bandwidth decreases, as in Figure 5. 19. Bi-directional radiation pattern of $\boldsymbol{E_\varphi}$ in both *xy*-plane and *zy*-plane is obtained due to the larger interval between the two modes. Additionally, the radiation patterns in *zy*-plane are almost same because the geometries of the all three types at ±*y*-axis are almost invariant.

Table 5. 2
Size of the omni-directional type double notched antenna.

a	**b**	**c**	**d**	**e**	**f**	**g**	**al**	**h**
50	45	22	25	15	21	30	27.5	2

Table 5. 3
Size of the bi-directional type double notched antenna.

a	**b**	**c**	**d**	**e**	**f**	**g**	**al**	**h**
80	45	32	25	15	25	22	19.5	0.8

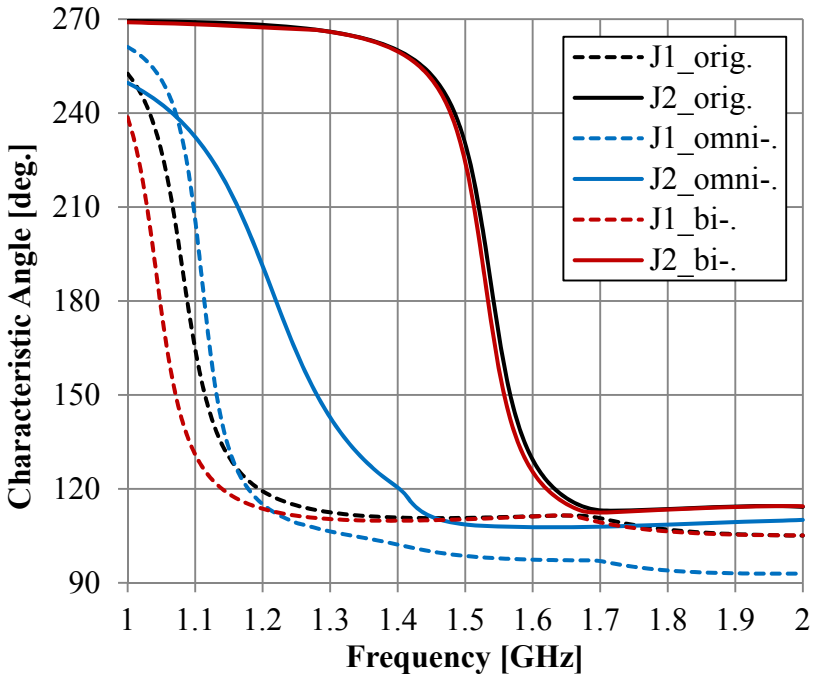

Figure 5. 18 Characteristic angles of the two modes. Black lines denote the original, blue lines denote the omni-directional and red lines denote the bi-directional type.

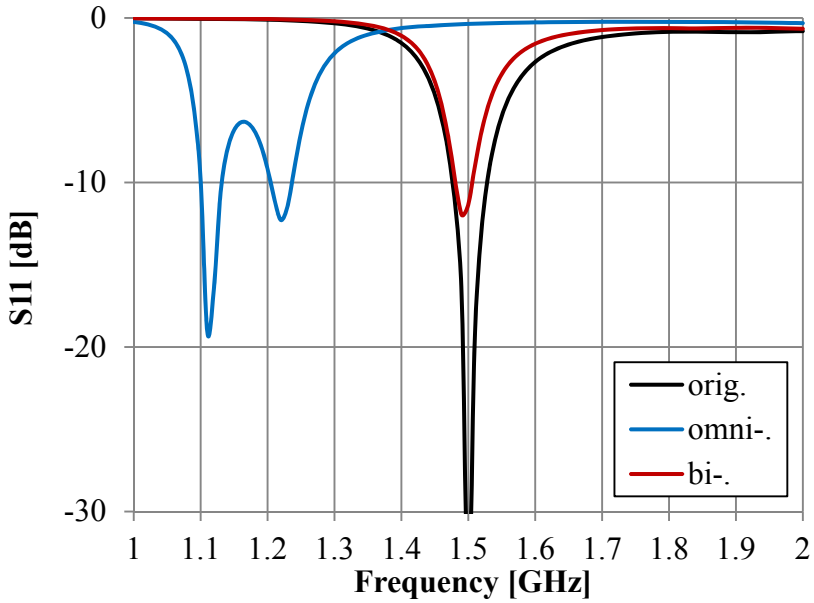

Figure 5. 19 Antenna input responses. Black line denotes the original, blue line denotes the omni-directional and red line denotes the bi-directional type.

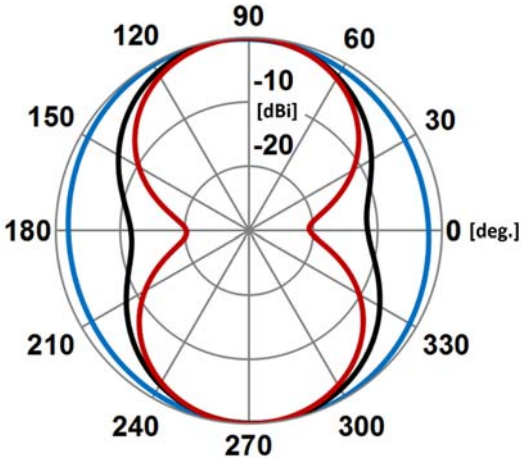

xy-plane (E-plane)

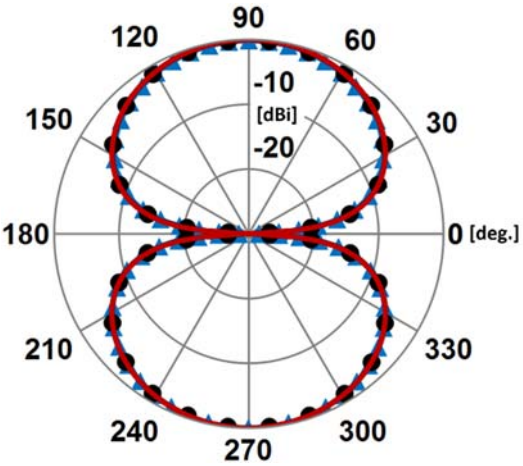

zy-plane (H-plane)

Figure 5. 20 Radiation patterns of $\boldsymbol{E_{\varphi}}$ in *xy*-plane (E-plane) and *zy*-plane (H-plane) of the antenna. Black line (with circular marks in *zy*-plane) denotes the original type, blue line (with triangle marks in *zy*-plane) denotes the omni-directional type (at 1.11GHz), and red line denotes the bi-directional type.

5.3 Four Notched Array with Identical Radiation in Horizontal Plane

As was introduced in Chapter 3, a triple notched array with parasitic elements is used to be horizontal polarization component antenna of the orthogonally dual-polarized antenna in Section 3.2. However, due to the only three notches, ripple coefficient which is an important index to evaluate circular degree of radiation patterns in horizontal plane are ±1 ~ 2.5 dB. The number indicates more than 40 % energy weaken at somewhere in the horizontal plane. As an enhanced model to solve this issue, the four notched array with parasitic elements proposed in Section 3.3 has reduced ripple coefficient of about ±0.65 ~ 0.8 dB due to the increased quantity of notch.

However, we intend to utilize a four notched array without parasitic elements to propose a horizontally polarized reference antenna with ripple coefficient in horizontal plane less than ±0.1 dB. To improve the omni-directional property to such an extraordinarily low level by using some other approaches except adding even more array elements, we need to know more physical insight of the antenna's operating principles. The theory of characteristic modes is one of the best methods to help us penetratingly understand the antenna's mechanism. As an advanced part of the previous Section, this Section is devoted to apply the theory of characteristic modes to provide an in-depth physical insight into the behavior of a four notched array antenna and subsequently get the desired uniform radiation property.

Comparing with the double notched antenna analyzed in the previous Section, there are more related characteristic modes occurring on a four array due to increased antenna size. However, these modes can also be classified to two basic fundamental types; one owns omni-directional radiation pattern in horizontal plane, and the other does not. While in the previous Section directive radiation pattern is obtained by moving the mode with omni-directivity further away from the directive dominant mode, in this Section we do it reversely.

5.3.1 Characteristic Modes Analysis for Four Notched Array

In order to obtain horizontal polarization and omni-directivity in horizontal plane, a notched array antenna with four array-elements is originally proposed at 1.5 GHz. Geometry of the antenna is shown in Figure 5. 21.

As shown in the figure, there are four notches cut out from the bottom conductor layer, and four microstrip lines feed them, respectively, on the upper layer. A power divider is constructed and fed from center. The relative dielectric coefficient of dielectric substrate is 2.6, while the thickness of the substrate is 0.8 mm. Horizontally polarized wave radiated by each notch element form semi-omni-beam in horizontal plane (the plane of antennas' surface). Four such beams compose a dipole-like omni-directional radiation pattern as expected. Figure 5. 22 shows input characteristics of the antenna.

In order to further investigate the operating principle of this antenna, we use the theory of characteristic modes to calculate the antenna. Current distributions of characteristic modes $\boldsymbol{J_1}$ ~ $\boldsymbol{J_4}$ on the antenna are shown in Figure 5. 23. The current of $\boldsymbol{J_1}$ ~ $\boldsymbol{J_3}$ concentrate on the microstrip line but is weak on the ground plane at where the four notches are formed. While to the $\boldsymbol{J_4}$, current flowing on the ground plane is strong, but the current on two sides of the notches are generally in-phase. It should be noticed that $\boldsymbol{J_1}$ ~ $\boldsymbol{J_4}$ are not the all characteristic current modes occurring in concerned frequency spectrum, but are the modes that possible to be excited by the central feeding type. Discussion about other current modes is ignored because it is extraordinarily difficult to excite them by the central feeding.

Figure 5. 24 shows normalized characteristic radiation patterns which are calculated based on the distributions of characteristic currents $\boldsymbol{J_1}$ ~ $\boldsymbol{J_4}$, respectively. By observation of the radiation patterns, it can be found obviously that $\boldsymbol{J_1}$, $\boldsymbol{J_2}$ and $\boldsymbol{J_4}$ contribute to radiating identical radiation patterns in horizontal plane, while different with others, characteristic radiation pattern of $\boldsymbol{J_3}$ acts like two orthogonally arranged "8". Hence $\boldsymbol{J_3}$ is considered contribute to exciting the tail-end of microstrip lines to make them operating as monopoles.

Figure 5. 25 presents frequency responses of the characteristic angles associated with the

characteristic current modes $\boldsymbol{J_1} \sim \boldsymbol{J_4}$ of the originally designed antenna. From Figure 5. 25 it is found that the mode $\boldsymbol{J_1}$, $\boldsymbol{J_2}$, $\boldsymbol{J_3}$ and $\boldsymbol{J_4}$ are in resonant state at 1.02 GHz, 1.4 GHz, 1.55 GHz and 1.8 GHz, respectively. Since the length of each branch of the microstrip lines is 96.8 mm, the value which approximately equals to 1/2 $\lambda_{g[0.96\ GHz]}$, (1/4+1/2)$\lambda_{g[1.44\ GHz]}$ and $\lambda_{g[1.92\ GHz]}$, it is not difficult to comprehend the curves of characteristic angles shown in Figure 5. 25.

Figure 5. 26 shows variation associated with frequencies of antenna's ripple coefficient of radiation patterns in horizontal plane. In the range of bandwidth 1.2 ~ 1.6 GHz, the ripple coefficient varies in ±0.35 ~ 0.8 dB, and increases along with operating frequency.

By observing and comparing the curves of S_{11} and characteristic angles, we may affirm that the double resonances of the antenna are generated by the cooperating of $\boldsymbol{J_1}$, $\boldsymbol{J_2}$ and $\boldsymbol{J_2}$, $\boldsymbol{J_4}$. For one reason, radiation pattern of the practically excited antenna performed similarly with that of the mode $\boldsymbol{J_1}$, $\boldsymbol{J_2}$ and $\boldsymbol{J_4}$. On the other hand, the actual current distribution act as similar with $\boldsymbol{J_1}$ if frequency is below 1.25 GHz, similar with $\boldsymbol{J_2}$ when frequency is between 1.25 GHz ~ 1.5 GHz, and similar with $\boldsymbol{J_4}$ if frequency is above 1.5 GHz. Here we only simulate the antenna in the frequency spectrum 1 ~ 2 GHz. Oppositely, it is considered that $\boldsymbol{J_3}$ is not adequately excited by the actual feeding, since the actual current distribution and radiation pattern do not perform as that of $\boldsymbol{J_3}$. However, we believe the existence of $\boldsymbol{J_3}$ in antenna's operating band does impact on antenna operating so that the ripple coefficient rapidly rises when the frequency is above 1.4 GHz.

From above results, we conjecture $\boldsymbol{J_3}$ greatly impacts on the ripple coefficient of horizontal plane radiation pattern, although this mode is not adequately excited by the feeding. To optimize the antenna that reduce the ripple it is considered effective that remove $\boldsymbol{J_3}$ from the antenna operating band. To adjust the resonant frequency of $\boldsymbol{J_3}$, we should change the length of the last part of microstrip lines. However, since the length of microstrip line not only relate to $\boldsymbol{J_3}$ but also relate to $\boldsymbol{J_1}$ and $\boldsymbol{J_2}$, the optimization should be a comprehensive procedure. In addition, for circularity of the radiation pattern of $\boldsymbol{J_4}$ in horizontal plane is not quite identical, it is maybe efficacious to remove $\boldsymbol{J_4}$ from the antenna operating band, too.

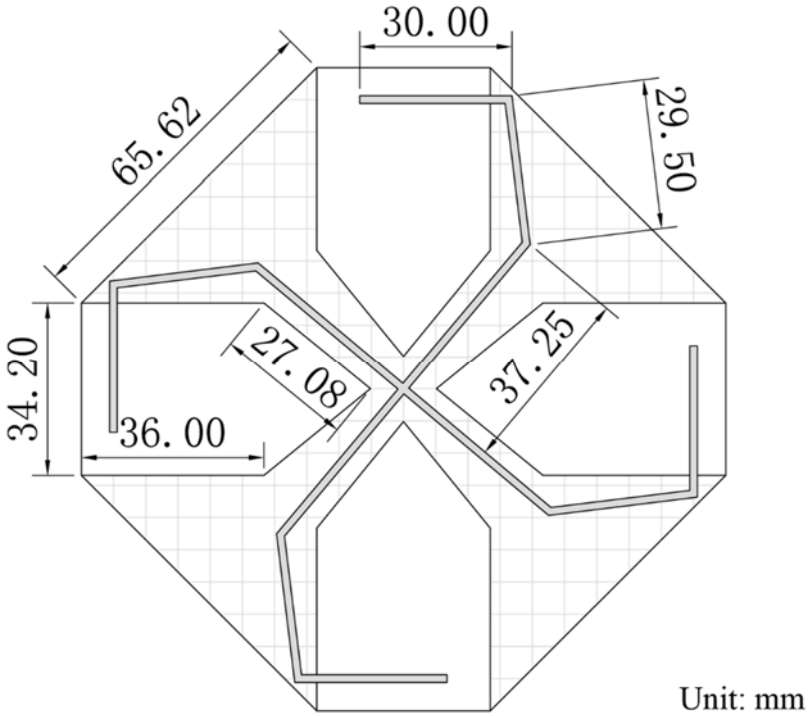

Figure 5. 21 Geometry of the originally proposed notch array antenna. Area in gray denotes microstrip lines arranged on top layer of dielectric-slab, area with gray panes denotes ground conductor arranged on bottom layer.

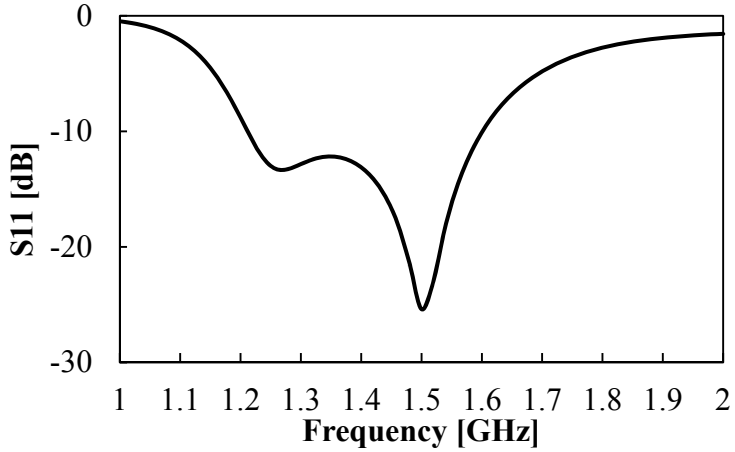

Figure 5. 22 Input response of the originally proposed notch array antenna.

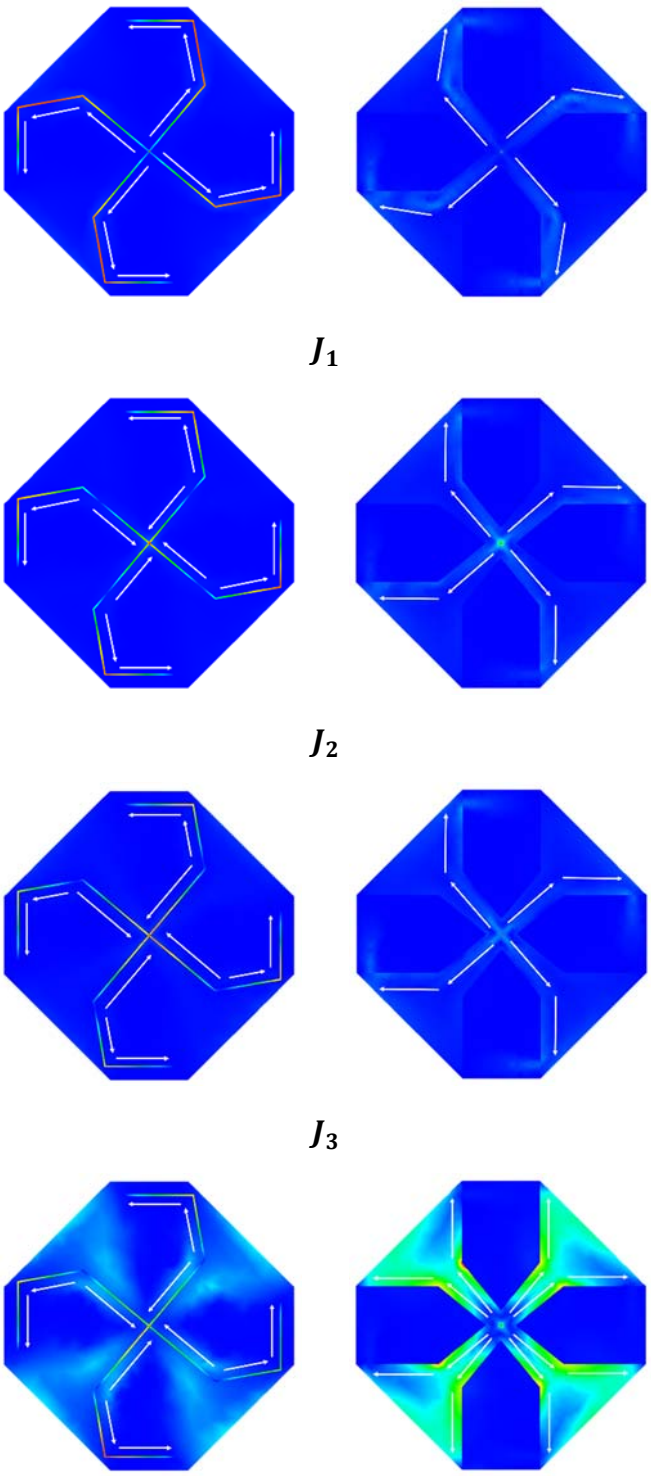

Figure 5. 23 Normalized current distributions of the four characteristic modes.

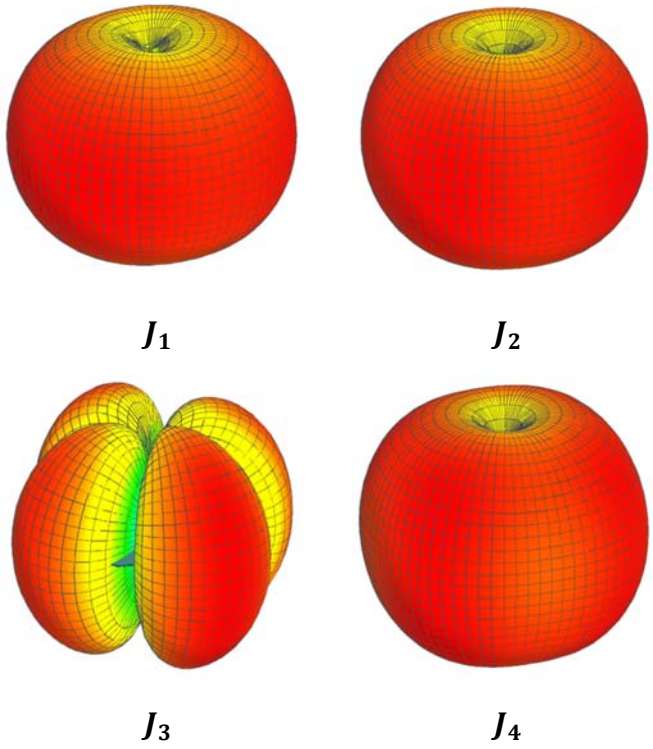

Figure 5. 24 Normalized characteristic radiation patterns of the four characteristic modes.

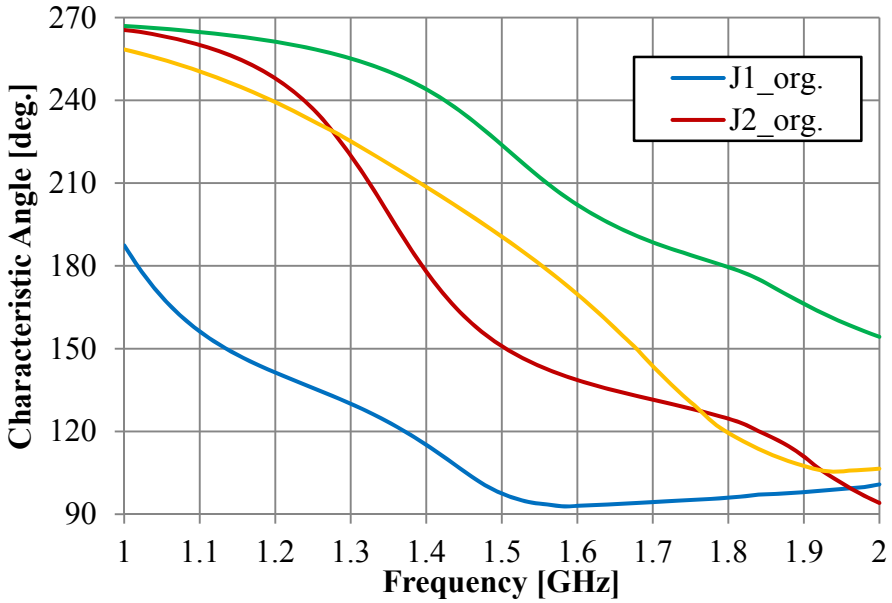

Figure 5. 25 Variation with frequencies of the characteristic angles.

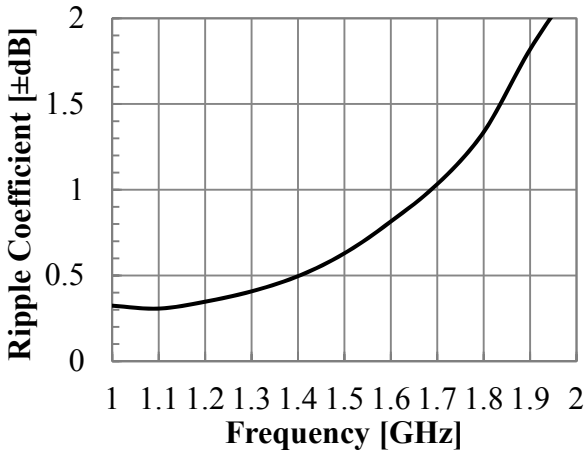

Figure 5. 26 Ripple coefficient characteristics of radiation pattern in horizontal plane of the originally proposed notch array antenna.

5.3.2 Optimized Four Notched Array and Experiment

In order to improve the ripple coefficient characteristic, an optimized notched array antenna is proposed. Figure 5. 27 shows the antenna's geometry. The entire area reduces by 43 % of the original one. The shape of notches becomes a little shorter and wider. Microstrip lines are 26 % shorter, while only the tail-ends parts are longer and designed to circular-arc.

The characteristic angles of the four characteristic modes of the optimized antenna are calculated. Figure 5. 28 shows variation with frequencies of the characteristic angles associated with characteristic modes $\boldsymbol{J_1}$ ~ $\boldsymbol{J_4}$ of the proposed antenna. It can be found that the resonant frequency of $\boldsymbol{J_1}$ and $\boldsymbol{J_2}$ rises to 1.27 GHz and 1.68 GHz, respectively, due to the shortening of microstrip lines.

While due to the smaller ground sheet, resonant frequency of $\boldsymbol{J_4}$ rises over 2 GHz, and is estimated to 2.6 GHz. It merits special attention that the $\boldsymbol{J_3}$ mode resonates at 1.1 GHz this time, which is also outside the range among the resonant frequencies of $\boldsymbol{J_1}$ and $\boldsymbol{J_2}$. This change is considered due to the lengthening of microstrip lines' tail-ends which operate as a

monopoles in the mode 3. Besides, the slopes of these curves near 180˚ become bigger. This change indicates narrower bandwidth of the antenna, which can be confirmed by input response curve shown in Figure 5. 29. The input response illustrates that the optimized antenna resonates at 1.5 GHz and its bandwidth is only 20 % of that of the original one. The resonance is regarded as the cooperating of $\boldsymbol{J_1}$ and $\boldsymbol{J_2}$. However, existence of the $\boldsymbol{J_3}$ mode does not contribute to antenna resonance at 1.1 GHz. But bad influence of $\boldsymbol{J_3}$ to the antenna can be verified clearly by observing ripple coefficient curve shown in Figure 5. 30. In Figure 5. 30, we find the values become very small except that in frequency band around 1.2 ~ 1.3 GHz. The sudden change at this band is considered as a cooperating of $\boldsymbol{J_1}$ and $\boldsymbol{J_3}$. However, the performance in this band is indifferent, while in the concerned antenna operating band of 1.46 GHz ~ 1.54 GHz, ripple coefficients reduce to ±0.1 dB.

This optimized antenna is fabricated and measured in experiment. When a diplopore SMA shown in Figure 5. 31 (a) is utilized for connector, the radiation pattern in horizontal plane distorts; while using a slim coaxial cable shown in Figure 5. 31 (b) can avoid the distortion, but the extra cable is unwanted. To reduce the influence on radiation property, we manually filed a disc SMA, which is shown in Figure 5. 32. Photographs of the sample model with the specially-made disc SMA connector are shown in Figure 5. 33. Measured input response and radiation pattern in horizontal plane are shown in Figure 5. 34 and Figure 5. 35. The measured resonant frequency rises to 1.54 GHz due to the usage of connector which was ignored in the simulation. Measured antenna's radiation pattern of horizontal polarization in horizontal plane at the resonant frequency is illustrated in polar coordinate. Ripple coefficient of the measured pattern is ±0.44 dB. Nevertheless, this value is thought acceptable when precision of the sample is taken into account.

When utilize a circular substrate shown in Figure 5. 36, we find the frequency response of the characteristic modes is almost invariant except that of $\boldsymbol{J_3}$. Figure 5. 37 shows resonant frequency of $\boldsymbol{J_3}$ decreases after utilizing the circular substrate and the peak of ripple curve also decreases, which is shown in Figure 5. 38. As another experiment, we increase a branch of microstrip line on each notch like what in Figure 5. 39 that can provide another resonance shown in Figure 5. 40. Figure 5. 41 shows that ripple in both the resonant bands is very small.

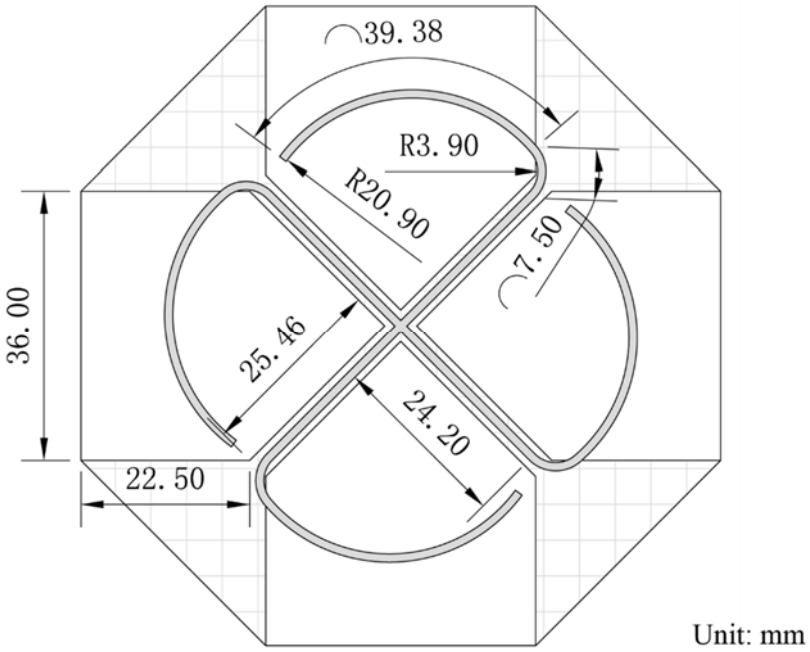

Figure 5. 27 Geometry of the optimized notch array antenna. Area in gray denotes microstrip lines arranged on top layer of die-lectric-slab, area with gray panes denotes ground conduc-tor arranged on bottom layer.

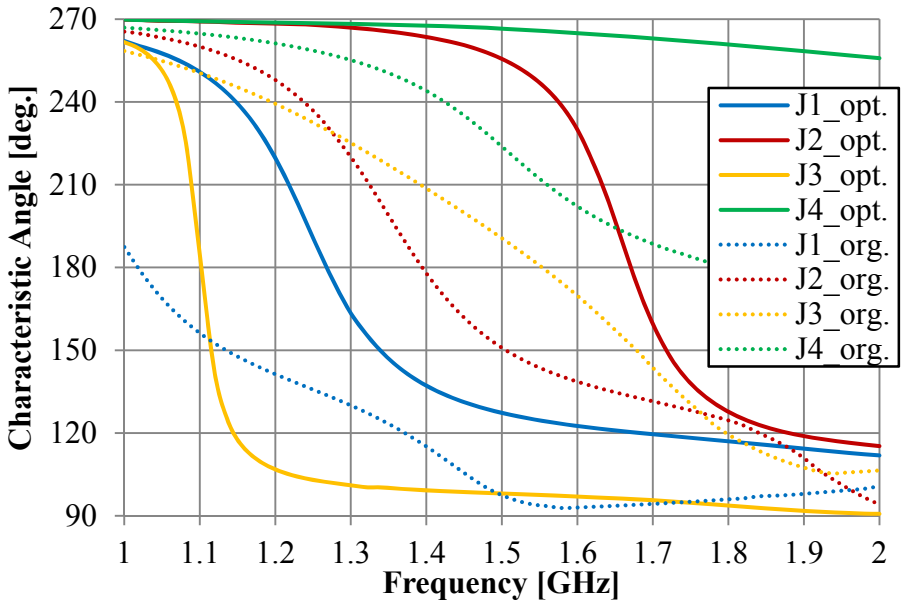

Figure 5. 28 Variation with frequencies of the characteristic angles.

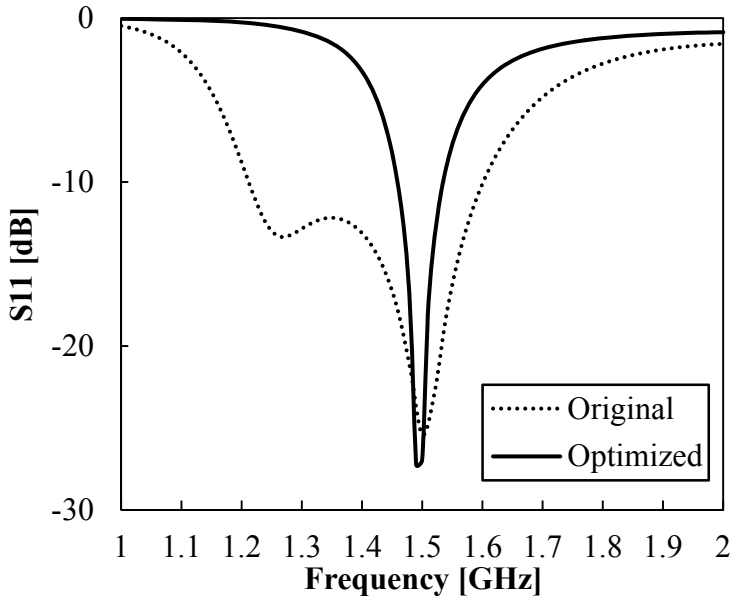

Figure 5. 29 Input response of the originally proposed antenna (dotted line) and the optimized antenna (solid line).

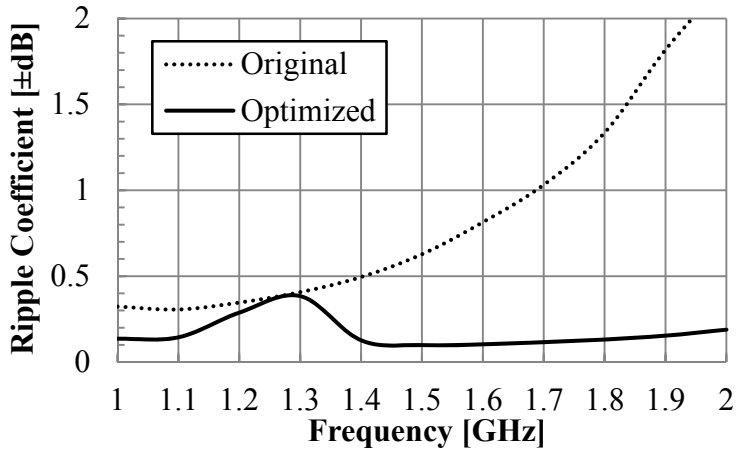

Figure 5. 30 Ripple coefficient characteristics of radiation pattern in horizontal plane of the originally proposed antenna (dotted line) and the optimized antenna (solid line).

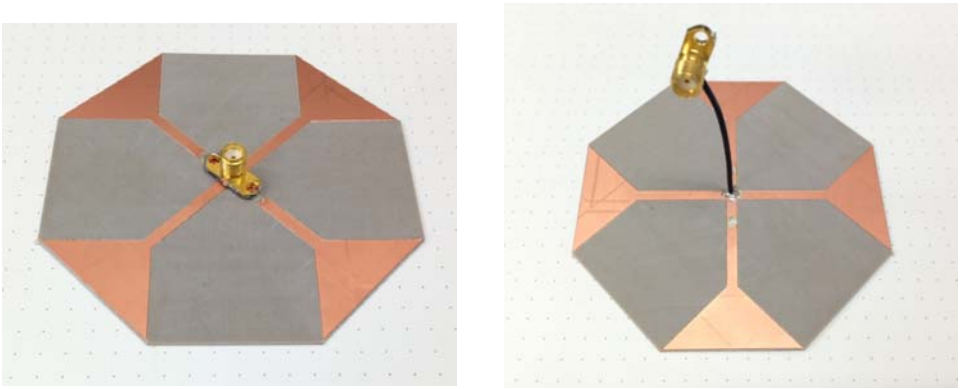

(a) (b)

Figure 5. 31 Fabricated model with diplopore SMA (a) and slim coaxial cable (b).

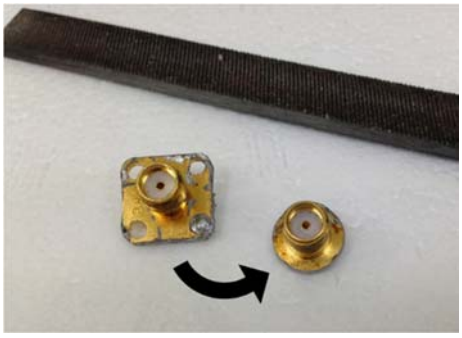

Figure 5. 32 A manually filed disc SMA.

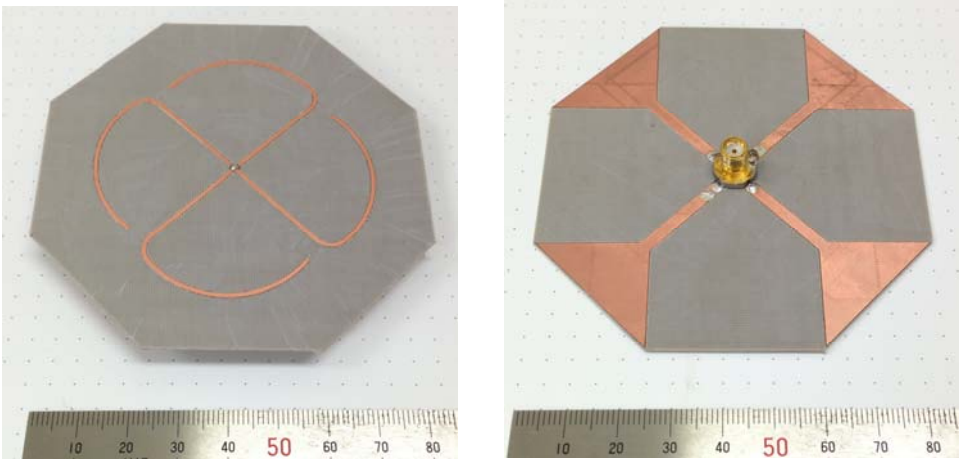

(a) (b)

Figure 5. 33 The fabricated model with disc SMA; (a) top face and (b) bottom face.

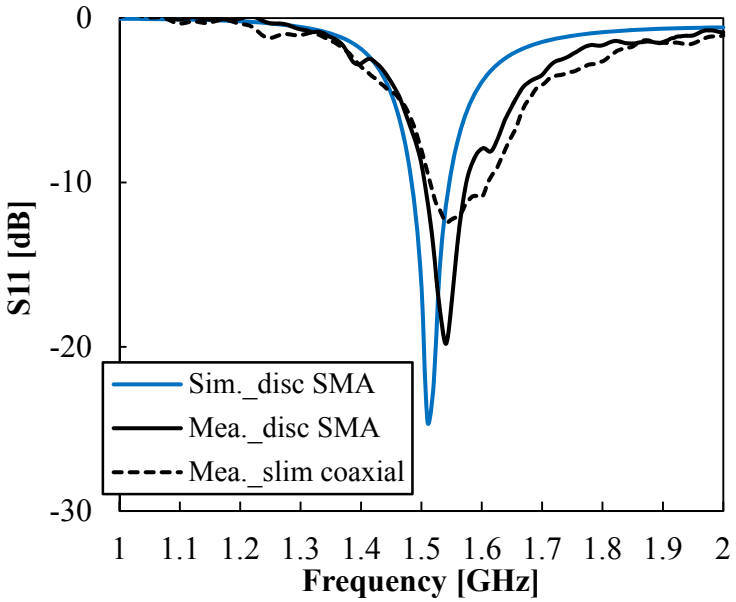

Figure 5. 34 Input response of the fabricated antenna.

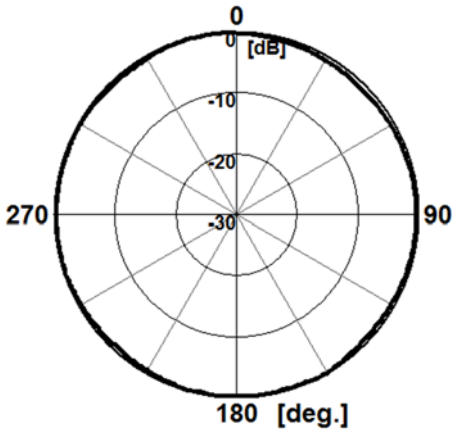

Figure 5. 35 Measured radiation pattern of the fabricated antenna in horizontal plane.

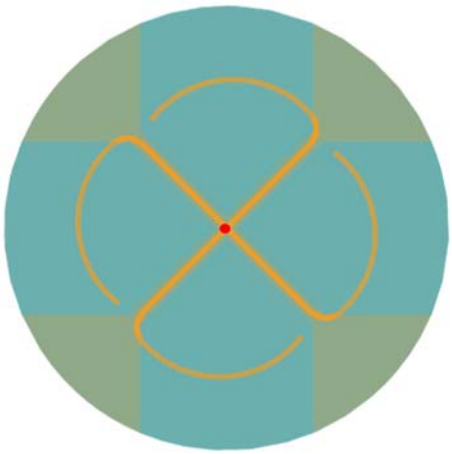

Figure 5. 36 An improved design using circular substrate.

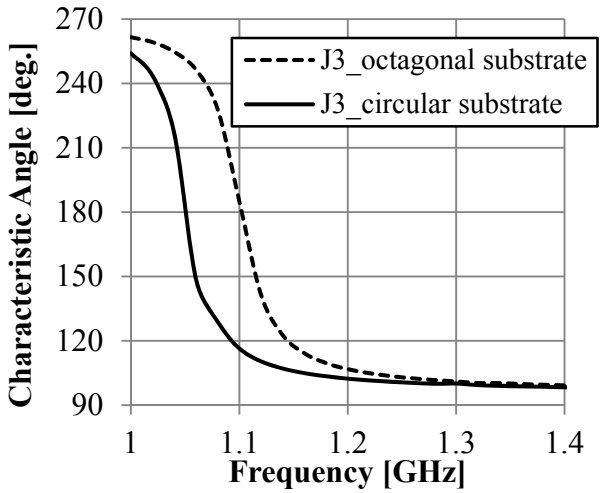

Figure 5. 37 Variation of J3 of using different substrate.

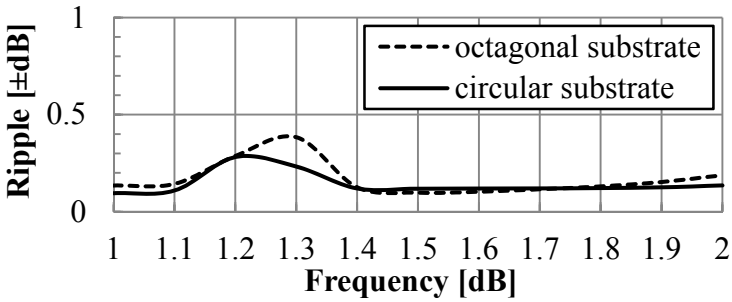

Figure 5. 38 Variation of ripple coefficient of using different substrate.

Figure 5. 39 Double branch of microstrip lines to provide double resonances.

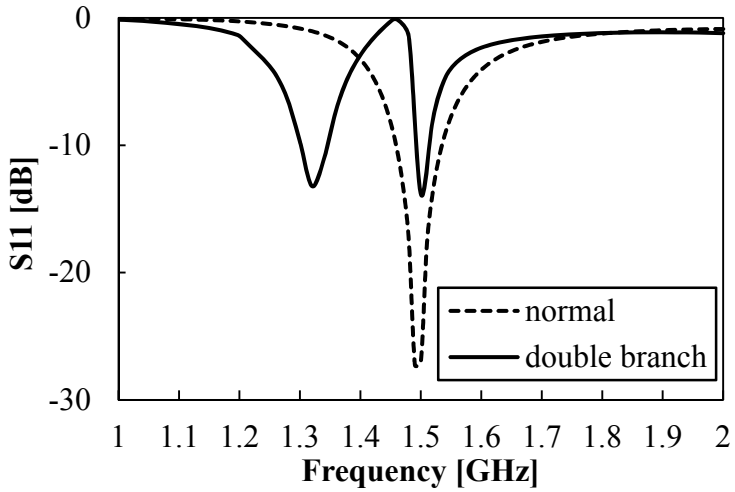

Figure 5. 40 Input responses of the proposed antennas.

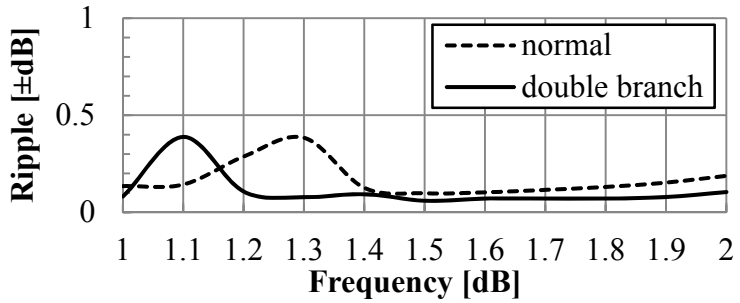

Figure 5. 41 Ripple coefficient of the proposed antennas.

5.4 Summary

In Section 5.2 of this Chapter, we used a double notched antenna as an example to show a way to solve " how to modify an antenna to excite a desired mode which is now inadequately excited? ", and " how to reduce undesired excitation of an undesired mode as far as possible? " this two questions mentioned in the beginning of Chapter 4. To the first question, we excited the $\boldsymbol{J_1}$ mode by moving it close to the dominant $\boldsymbol{J_2}$ mode. Bi-resonance is obtained in lower frequency band and omni-directional pattern is radiated in the operating band, due to the excited $\boldsymbol{J_1}$ mode. Certainly, the antenna gain is very low because of the reduced antenna size and widened bandwidth. However, it is still interesting as an example. In addition, we should notice that although the radiation pattern of $\boldsymbol{J_2}$ mode is not omni-directional in terms of the original type, after the adjustment the new geometry and resonant frequency changed the pattern. In other words, the radiation pattern of a specific characteristic mode is not invariant along with different frequencies.

On the other hand, to the second question, we restrain the $\boldsymbol{J_1}$ mode by moving it further away to the dominant $\boldsymbol{J_2}$ mode. By this adjustment, although the bandwidth becomes narrow, bi-directional radiation pattern is obtained in both E-plane and H-plane. In summary, antenna parameter adjustment is substantially to adjusting the fundamental characteristic modes occurring on the antenna, excite some or restrain some, and the example in this Chapter simply illustrated how to efficiently implement this process.

While in Section 5.3, we used the ripple problem of horizontal plane radiation pattern of a four notched array to illustrate " how to reduce undesired excitation of an undesired mode as far as possible? " The theory of characteristic modes is used to analyze the potential characteristic current modes of the originally designed four notched array to identify the reasons which affect the antenna's radiation property. The existence of $\boldsymbol{J_3}$, in which the tail-end of microstrip lines operate as monopoles, is thought the major factor makes the radiation pattern unsmooth. It should be noticed that $\boldsymbol{J_3}$ is not the only cause of non-uniformity. $\boldsymbol{J_4}$ and some other minor modes existing on the antenna are thought may potentially affect the radiation

of antenna. However, the optimization of antenna's structure especially the microstrip lines makes J_3 resonate at lower frequencies that is outside antenna's operating band. As a result, simulation shows that ripple coefficient reduced to ±0.1 dB in operating band; and, the antenna's performances are confirmed in the experiment.

CHAPTER 6
CONCLUSIONS

As the antenna geometry becomes more complicated, the time required for antenna design can be dramatically reduced by using computers and commercial simulators based on numerical methods. However, even with the support of computers, success of the final design still depends upon the intuition and previous experience of the designers. Actually in most cases, the final optimization is in fact made by “cut and try” methods. As a result, these days antenna design is very much governed by designers’ experience and know-how.

Therefore, we need an analysis method providing thorough physical insight to explain antenna working mechanism. Theory of characteristic modes, which is based on the MoM, is one of the best choices for this issue. Antenna analysis based on the theory provide a set of characteristic modes which have characteristic currents orthogonal to each other at source area and characteristic fields orthogonal to each other at infinity. This set of characteristic modes are current modes numerically obtained for discretionarily shaped conducting bodies, only relate to structure, size and frequency of the antenna, and provide a physical explanation of the radiation phenomena taking place on the antenna. However, it can obtain and control these modes by setting suitable feeding position, amplitude and phase. According to the theory, the excited modes and their synthetic field result as antenna’s resonance and radiation field. This point is the reason why it worth being studied. By calculating and analyzing these characteristic modes in concerned frequency range it may get more information about antenna’s working mechanism, which may be difficult or not that clear by using common analysis. Moreover, by adjusting antenna structure or feeding type may control the modes’ response, therefore these

information can provide guidance for antenna parameters adjustment and optimization.

However, so far, studies and application approaches of the characteristic modes almost concentrated on discussing the question how the characteristic modes impact on the excited antennas resonance characteristics. While, reports about relationship between the characteristic modes and the radiation pattern of antennas with specific excitations are seldom seen. In this thesis, we contributed to solve the two questions of " how to modify an antenna to excite a desired mode which is now inadequately excited? " and " how to reduce excitation for an undesired mode as far as possible? " The two questions have practical meaning for the study of characteristic modes. Hence, it is necessary to find answer from the characteristic mode itself. Concerning the both questions, we demonstrated practical solutions to illustrate how to apply characteristic modes analysis for cross-polarization reduction and for radiation pattern optimizations

First of all, the thesis provides a concise refinement of Integral Equation method based on the MoM and detailed theory review of characteristic modes, in Chapter 2.

In Chapter 3, we proposed a compact composite antenna composed of two orthogonally polarized component antennas for indoor MIMO system that is able to reduce mutual correlation between component antennas and meanwhile, keep compact miniaturization. Besides, a bandwidth and radiation pattern enhanced sample antenna is proposed. In this Chapter, the characteristic modes analysis is utilized to analyze mutual influence between the component antennas when they are combined.

Then, we use the characteristic modes analysis to discuss problem of cross-polarization of a disk loaded monopole antenna which is introduced in Chapter 3. It finds the feeding structure of disk loaded monopole tends to excite those modes have radial current distribution from center area to edge areas of the ground plane; and a ground mode providing absolutely uniform radial current distribution is considered that can reduce the horizontal polarization component radiated by the ground plane. Chapter 4 provides detailed discussion.

In Chapter 5, at first, a double notched antenna is used as an example to show how to make it radiate both omni-directional and bi-directional radiation patterns by adjusting the associated characteristic modes of the antenna. Considering the issue that it was not very clear that how

the unexcited modes of an antenna can impact its radiation pattern, characteristic modes of an omni-directional four notched array antenna are calculated to identify the relationship between an unexcited mode and antenna radiation pattern, also in Chapter 5.

In following Appendix I, the characteristic modes analysis is tried to explain neutralizing phenomenon occurring on two closely adjacent PIFA elements that are connected by a shorted line. While in Appendix II, A 4G cellular antenna designed for eyewear wireless devices is introduced and analyzed by using the theory of characteristic modes to understand the antenna's operational principle and optimized antenna feeding position.

APPENDIX I
CHARACTERISTIC MODES ANALYSIS FOR NEUTRALIZING EFFECT OF SHORTED LINE LINKING TWO ADJACENT PIFA ELEMENTS

Indoor base stations are used to spread conventional cellular mobile communication systems. Antennas such as that proposed in Chapter 3 providing monopole-like radiation pattern are generally useful for the indoor base stations or access points installed on ceiling, while this kind of radiation pattern may cause black area directly under the antenna. Some beam switchable antennas providing both monopole-like radiation pattern and patch-like radiation pattern are proposed to solve the problem [101][102].

In [102], the author proposed two closely arranged Planar Inverted-F Antenna (PIFA) elements as the beam switchable antenna to provide the monopole-like beam and uni-directional patch-like beam, and used a shorted line to reduce mutual coupling between the two elements which was called neutralization in [103].

Nevertheless, in [102], peak value of S_{21} curve barely reduced to -15 dB, and the author has not analyzed and explained more for the neutralizing effect of the shorted line in details. In this Appendix, on one hand, we attempt to make the S_{21} of the antennas in [102] further lower by adjustments and optimizations, on the other hand, we calculate the antenna and numerically

analyze the shorted line's mechanism by using the theory of characteristic modes.

Geometry of the antenna is shown in Figure AI. 1. The two PIFAs are adjacent in centrosymmetry on a ground plate. Deal to the very close arrangement, mutual coupling between the two antennas is very strong. Figure AI. 2 shows S-parameters between the two antenna ports. When a shorted line is inserted to connecting the joint points of feeding pins and plates of the two antennas, peak value of S_{21} reduces to that below -10 dB. Additionally, by observing the changes of S_{21} associated with variation of shorted line's total lengths, it can confirm that the lowest peak value of S_{21}, which approaches -15 dB, appears when $L=0.21\lambda_0$, which is a little longer than the straight distance between the two feed pins. Reason of the reduced S_{21} is thought due to current flowing through the shorted line neutralized the coupling current. Besides, the gap between the antennas is modulated to further learn the characteristics of bandwidth and mutual coupling. We change the gap **g**, and the distance of feeding pin to shorted plate, **d**. Impedance matching can be obtained by adjusting the parameter **d**. 4 patterns of the dimensions A~D, which is shown in Table AI. 1 are calculated. Figure AI. 3 and Figure AI. 4 show S-parameters of the antenna under different dimensions without and with optimized shorted lines, respectively. Although bandwidth behaves unsatisfied, a depression on the S_{21} curves obviously appears when the gap **g** becomes small. This phenomenon can be explained as resonance of the shorted line. The mutual coupling is able to be entirely neutralized in theory when proper dimensions are used. If consider that bandwidth of about 30 MHz is sufficient for normal indoor base stations, the proposed antenna with C dimensions provides adequately low S_{21} to about -18 dB.

Radiation patterns of the antenna with the C dimensions are calculated and shown in Figure AI. 5. The antenna behaves uni-directivity under the out-phase feeding, and monopole-like radiation pattern under the in-phase feeding, respectively. However, the monopole-like radiation pattern can improve if a larger ground is used.

A fabricated antenna with the C dimensions shown in Figure AI. 6 is measured in experiment. Figure AI. 7 and Figure AI. 8 respectively show Calculated and measured S-parameters of the antenna without and with the shorted line. The neutralizing effect can be confirmed by the experiment.

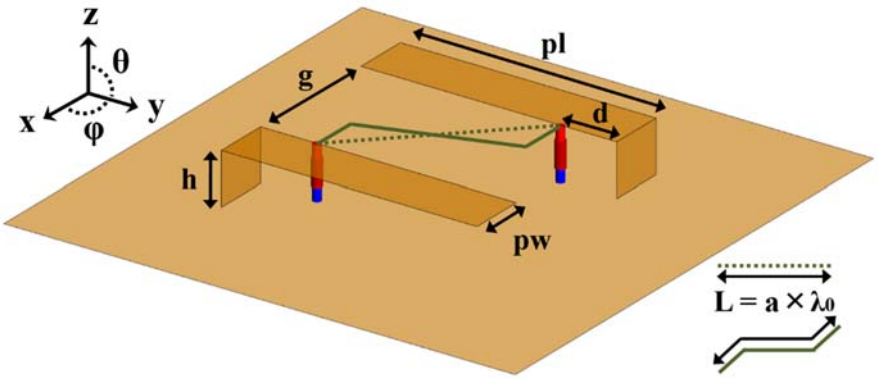

Figure AI. 1 Geometry of the proposed PIFA elements with shorted line. pl=52, pw=9, h=10, d=11, g=32 [mm], L_{min}=0.19λ0, GND:150×150 [mm^2].

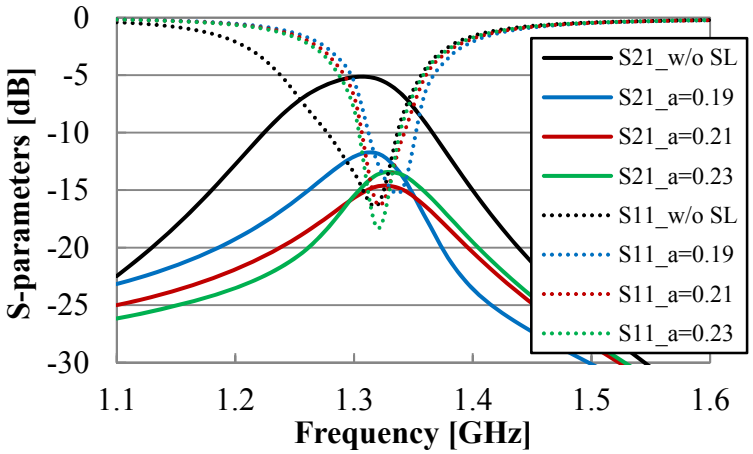

Figure AI. 2 S-parameters with variation in length of the shorted line.

Table AI. 1

Dimensions of the 4 patterns. Other dimensions do not change.

	A type	B type	C type	D type
g [mm]	32	26	22	18
d [mm]	11	12.5	14	16.5
L / λ0	0.21	0.18	0.16	0.13

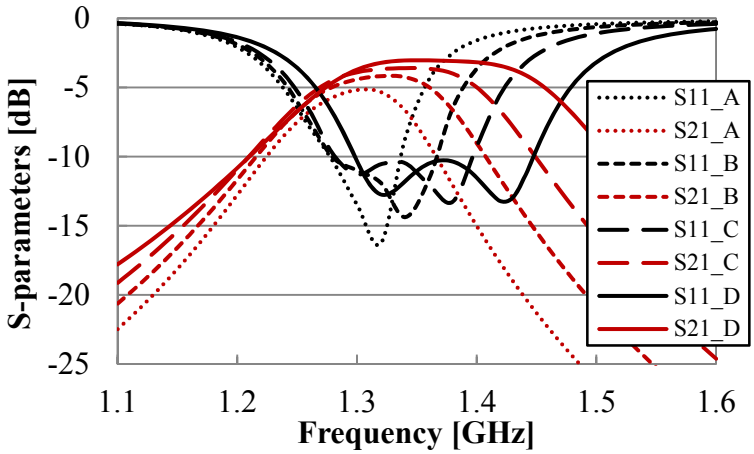

Figure AI. 3 S-parameters of optimized antenna of the 4 patterns without shorted line.

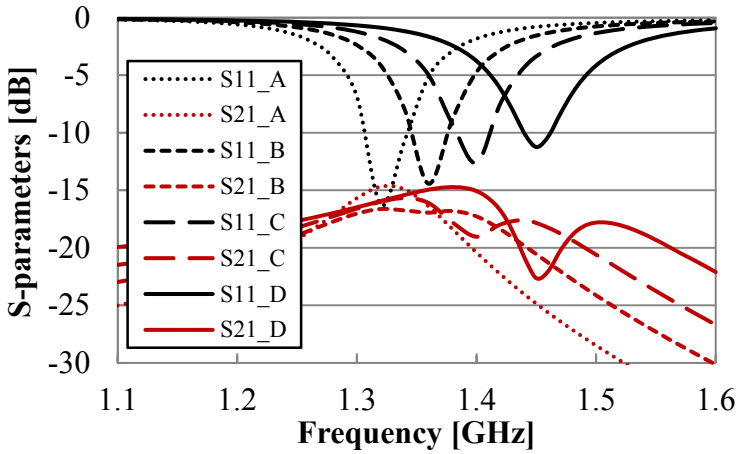

Figure AI. 4 S-parameters of optimized antenna of the 4 patterns with shorted line.

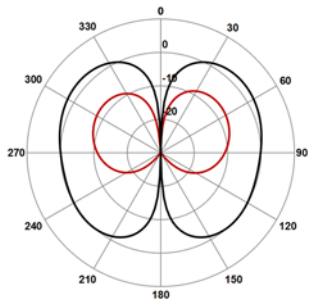

(a) In-phase feeding at zx-plane

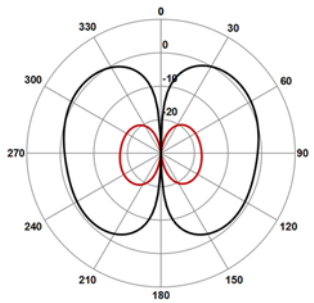

(b) In-phase feeding at zy-plane

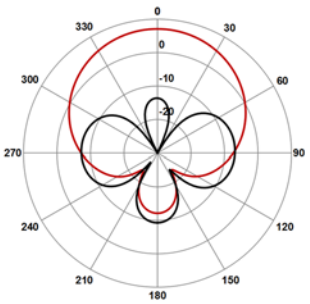

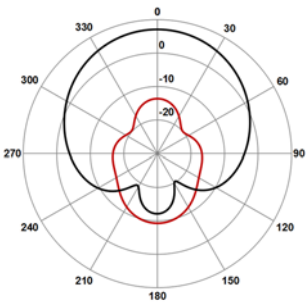

(c) Out-phase feeding at zx-plane (d) Out-phase feeding at zy-plane

Figure AI. 5 Radiation patterns of the antenna with shorted line with C dimensions. Black lines denote $\boldsymbol{E}_{\theta}$ and red lines denote $\boldsymbol{E}_{\varphi}$.

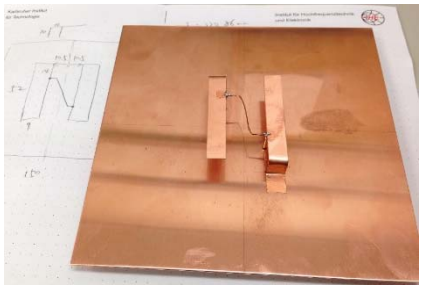

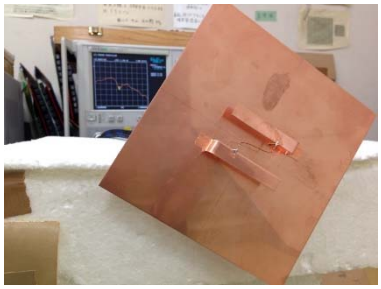

Figure AI. 6 Fabricated antenna with shorted line with the C dimensions.

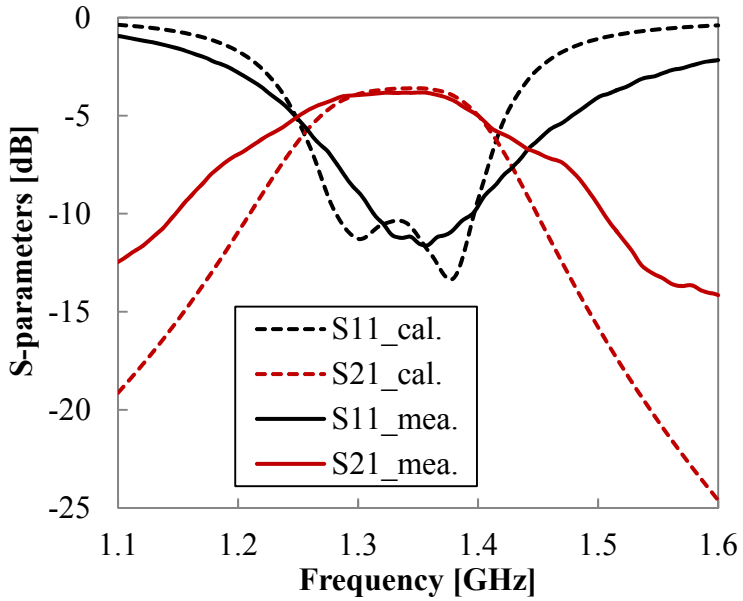

Figure AI. 7 Calculated and measured S-parameters of that without the shorted line.

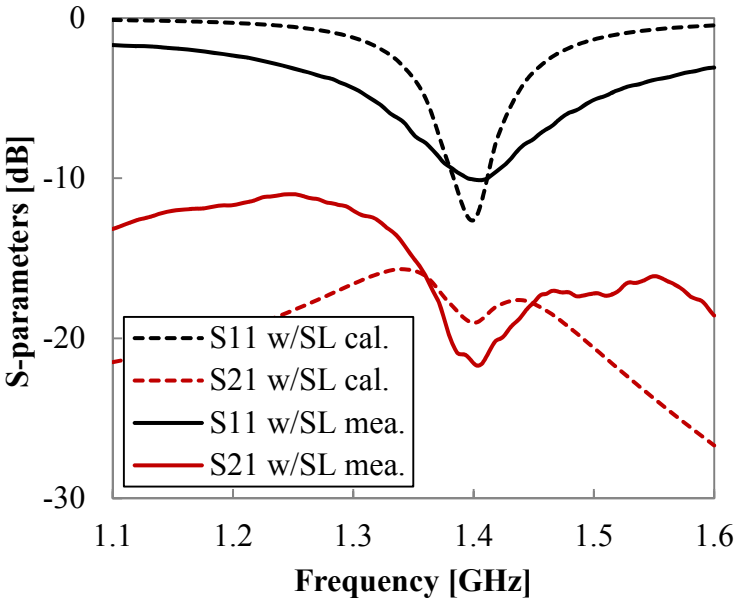

Figure AI. 8 Calculated and measured S-parameters of that with the shorted line.

In order to understand mechanism of the shorted line, we calculate characteristic modes of the antenna. Figure AI. 9 shows first 6 modes of the antenna. It is clearly observed that current concentrate on the two PIFAs only in $\boldsymbol{J_2}$ and $\boldsymbol{J_5}$, hence discussion about the two modes is enough. In Figure AI. 10, current orientation of the two dominant characteristic current modes is shown. By observation we can find that $\boldsymbol{J_2}$ on the two PIFAs is out-phase, and $\boldsymbol{J_5}$ is in-phase. Figure AI. 11 shows characteristic angles of the two modes under the C dimensions. The result shows that no matter is there shorted line inserted or not, no variations appear on the in-phase mode; while, resonant frequency of the out-phase mode increases from 1.25 GHz to 1.35 GHz when the shorted line is inserted. This point indicates that mode $\boldsymbol{J_5}$ does not contain any component about the mutual influences between the two antennas, but mode $\boldsymbol{J_2}$ deeply depends on the mutual relationship between them.

If we observe phase difference between the two modes, we notice large phase difference in antenna operating band exists when there is no shorted line. The large phase difference may be the reason leading to the large S_{21}. While when the shorted line is installed, the two curves close to each other, and the phase difference reduces to 50°~60° in the antenna operating band. The approach indicates approximately same modal excitation V_n^i of the two modes, when the antenna is fed to measure the S-parameters. Additionally, the small phase difference which

close to propagation phase difference associated with the space between the two PIFAs is considered helpful for the mutual offset of the two modes' current that with same modal excitation V_n^i. This is an approximative analysis for the neutralizing effect.

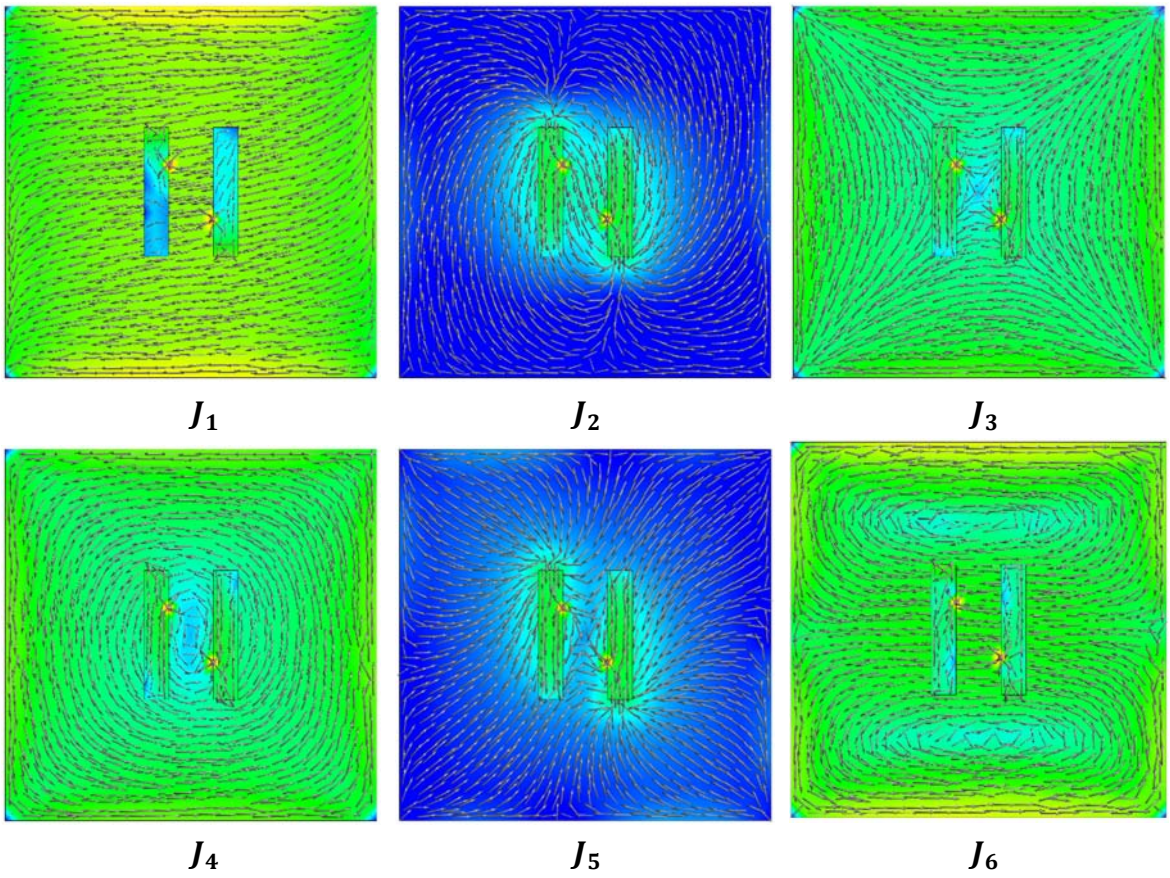

Figure AI. 9 First 6 characteristic modes of the antenna.

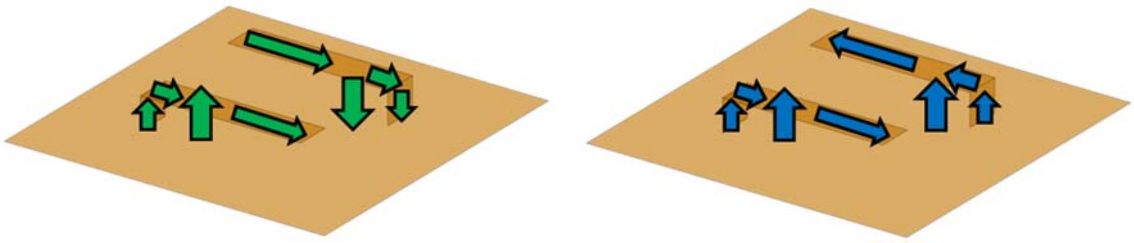

J_2 Out-phase mode J_5 In-phase mode

Figure AI. 10 Current orientation of J_2 and J_5.

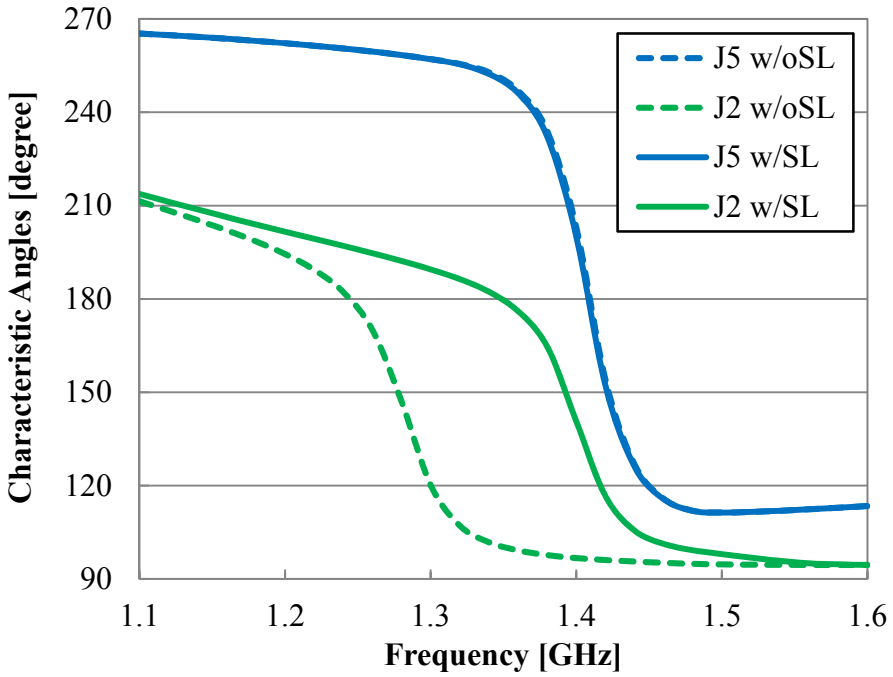

Figure AI. 11 Characteristic angle of the two modes with variation of that without shorted line and that with shorted line in C dimensions.

APPENDIX II
CHARACTERISTIC MODES ANALYSIS FOR A 4G CELLULAR ANTENNA OF EYEWEAR WIRELESS DEVICES

In recent years, wireless devices have quickly developed and earned wide interests and demands all over the world. As a prominent one, Google Glass is currently on development and is planned to be released in 2014[9]. However, the wireless connection of Google Glass version one is currently limited to Bluetooth and WLAN, not operating with cellular mobile networks [104]. Concerning this issue, a feasibility study of 4G cellular antennas for eyewear wireless devices was approached in [105]. In this study, three possible designs with simple printed coupling element antennas, using a printed circuit board (PCB) of FR4 substrate, were proposed to operate within the following frequency bands 700–960 MHz and 1.7–2.7 GHz to support several cellular networks, i.e. LTE, GSM, DCS, PCS and 2.4GHz WLAN standards. Besides, specific absorption rate (SAR) levels in phantom was also taken into account in this feasibility study.

In this Appendix, characteristic modes are calculated and analyzed to further understand how currents flow within the PCB of the eyewear, what is the operational principle and where is the

[9] Currently (11th Dec. 2014) not yet and unknown

best feeding position of the proposed antenna.

As the proposed antenna solutions are described in detail in [105], we just make here a simple summary of its characteristics. First of all, a resonant antenna is evaluated as impractical in a naturally limited space within an eyewear device in normal size to cover both of the target operating bands, especially the 700-960 MHz frequency interval. So, a non-resonant coupling element which excites currents on the ground plane of the PCB is proposed to solve the problem, and the antenna is adjusted to the desired matched impedance in the target frequency band by using a proper matching network. Figure AII. 1 shows the antenna model and specific anthropomorphic mannequin (SAM) phantom model. The coupling element is placed behind the ear to excite the ground plane on the outer side of the PCB. Figure AII. 2 shows the simulated reflection coefficient and the bandwidth potential of the antenna. Also, the target bandwidth potential is included in red in this figure. A dual-band response is confirmed covering target bands of 700–960 MHz and 1.7–2.7 GHz with reflection coefficient below -6 dB by using a 2-element matching network. The radiation patterns are shown in Figure AII. 3 in both bands showing suitable behavior for off-body communications.

The characteristic modes are calculated in order to clearly understand the antenna's operational principle. As the ground plane is the key radiating structure, especially in low frequency, only the PCB substrate with the ground plane is calculated and the coupling element is excluded. Moreover, since it is very hard to find characteristic modes when the phantom is added due to multiple wave reflections inside the phantom, only the antenna is considered. Figure AII. 4 shows our simulation model of the antenna for calculating characteristic modes. Structure and size are the same with the model from [105].

On the ground plane, there are six modes $\boldsymbol{J_0}$ ~ $\boldsymbol{J_5}$ occurring within the frequency range 0.5–2.8 GHz, that are confirmed can resonate. Current distributions of each mode are shown in Figure AII. 5. Then, Figure AII. 6 shows characteristic angles of each mode of the eyewear device from 500MHz to 2.8 GHz. Although it seems that $\boldsymbol{J_0}$ and $\boldsymbol{J_1}$, $\boldsymbol{J_2}$ and $\boldsymbol{J_4}$ have the same distributions, the actual distributions are indeed different. Here we also calculate characteristic angle of the ground plane without substrate and show the results in Figure AII. 6. In this case, there are two modes can be found that are $\boldsymbol{J_0}$ and $\boldsymbol{J_1}$, denoted by dotted lines. We

notice that these two modes are very close to the $\boldsymbol{J_1}$ and $\boldsymbol{J_4}$ of the ground plane with the substrate. Although the frequencies are a little higher, but similar current distribution is confirmed. So, for $\boldsymbol{J_1}$ and $\boldsymbol{J_4}$, currents mainly distribute on the surface of the ground plane which faces free space, as the length of the ground is respectively $\lambda_1'/2$ and two times $\lambda_4'/2$. But for other modes ($\boldsymbol{J_2}$, $\boldsymbol{J_3}$, $\boldsymbol{J_5}$), currents exist in terms of volume distributions [17], and are thought to be sandwiched between the metallic ground plane and the substrate. Moreover, although it is understandable that the characteristic angle and the reflection coefficient or the bandwidth potential shown in Figure AII. 2 cannot perfectly match each other because the coupling element, the matching network and the phantom are ignored in this calculation, we confirm that the resonance in the lower band is caused by $\boldsymbol{J_0}$, $\boldsymbol{J_1}$ and $\boldsymbol{J_2}$, while the resonance at higher band are caused by $\boldsymbol{J_3}$, $\boldsymbol{J_4}$ and $\boldsymbol{J_5}$, respectively. Figure AII. 7 shows the radiation patterns of each individual mode. The combinations and effects of the modes can be better understood by comparing the radiation patterns of modes and that in Figure AII. 3. From this, we confirm the contributions from $\boldsymbol{J_2}$ at 800 MHz and $\boldsymbol{J_3}$ at 2.2 GHz are very limited.

Figure AII. 8 shows characteristic electric near field of the modes. The electric near field is calculated at the position that 10 mm above the ground plane. According to [42], a specific mode can be excited by inductive couplers located at the minima of the electric near field, while capacitive couplers should be placed in the maxima of the electric near field. Because the electric near field and current distribution have a phase difference of 90°; i.e. the electric near field distribution have its minima amplitude at maxima of the current distribution, and vice versa. Since the coupling element which is used to excite the ground plane in [105] is a capacitive coupler, two open ends of the ground plane are appropriate feeding position that can excite almost all the modes. However, if considering eyes more easily absorb electromagnetic wave, the open end which is near eyes maybe not so good. Actually, the results and analysis coincide with measured SAR values reported in [105].

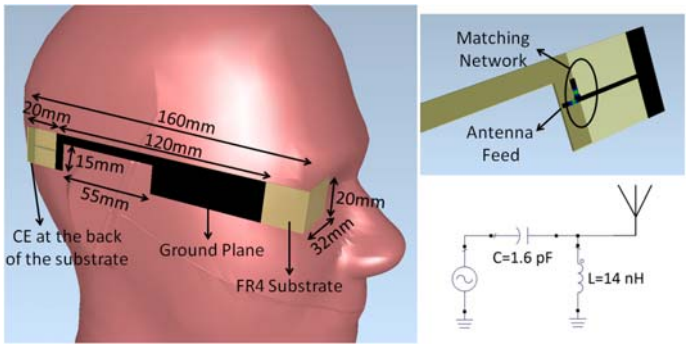

Figure AII. 1 Antenna model with matching network placed on the SAM head phantom [105].

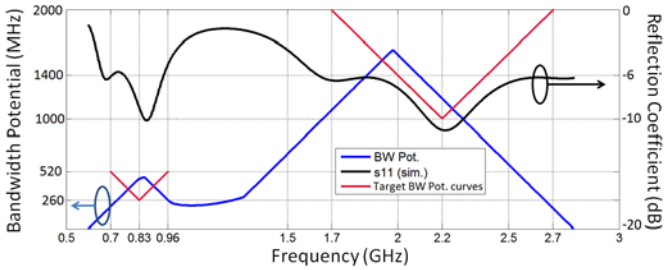

Figure AII. 2 Calculated reflection coefficient and achieved bandwidth potential [105]. Target bandwidth potential is presented in red.

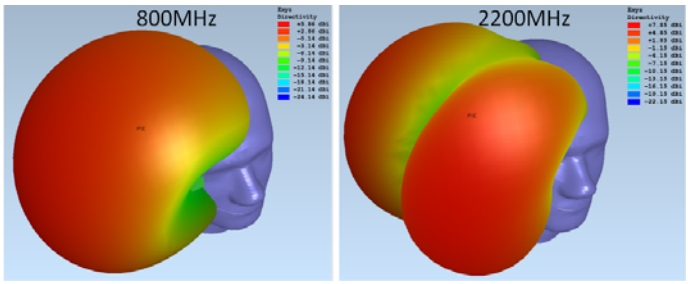

Figure AII. 3 Calculated radiation patterns of the antenna at 800 and 2200 MHz [105].

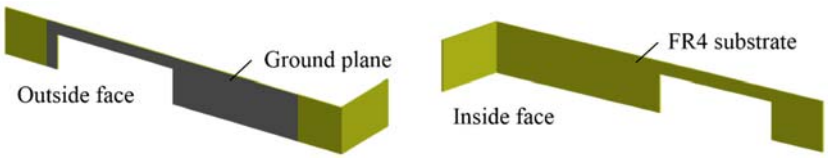

Figure AII. 4 Simulation model of the antenna for calculating characteristic modes.

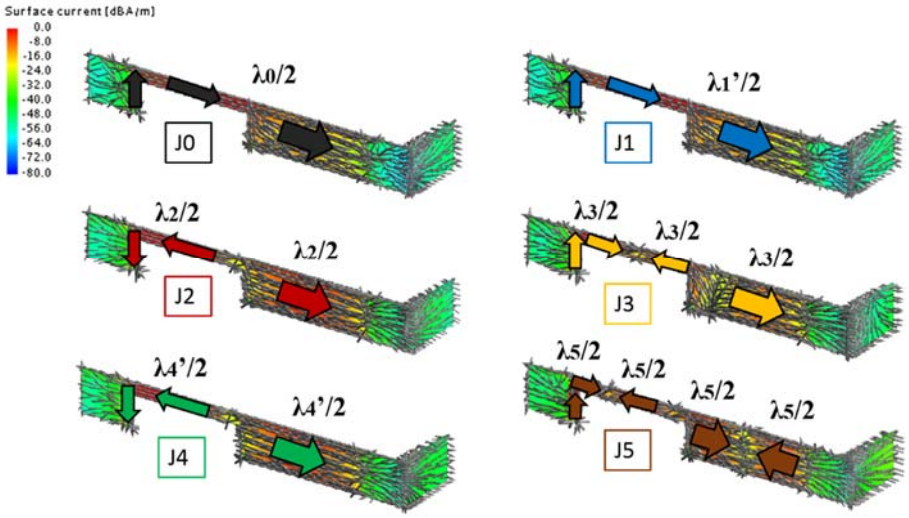

Figure AII. 5 Characteristic current modes occurring on the ground plane of the PCB. λ_n' means the resonant wavelength of $\boldsymbol{J_n}$ distribution on metal surface only, and λ_n for volume distributions (presence of the dielectric of the PCB)

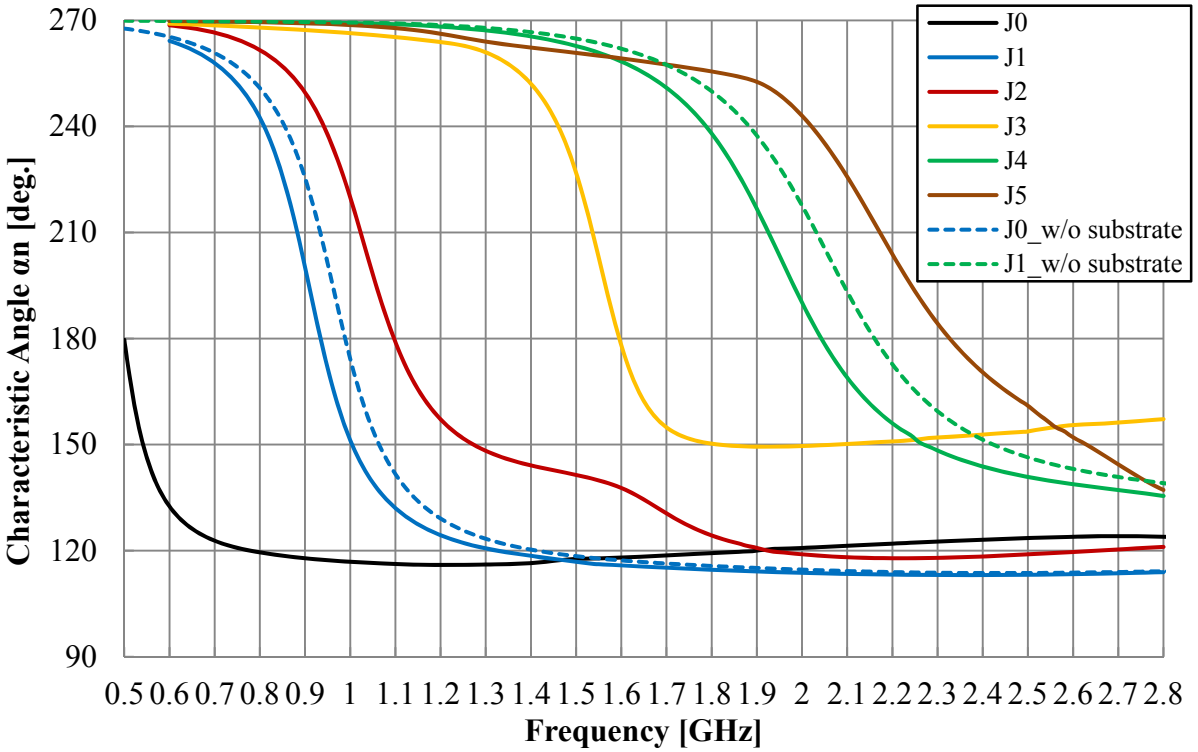

Figure AII. 6 Frequency response of characteristic angles of the modes.

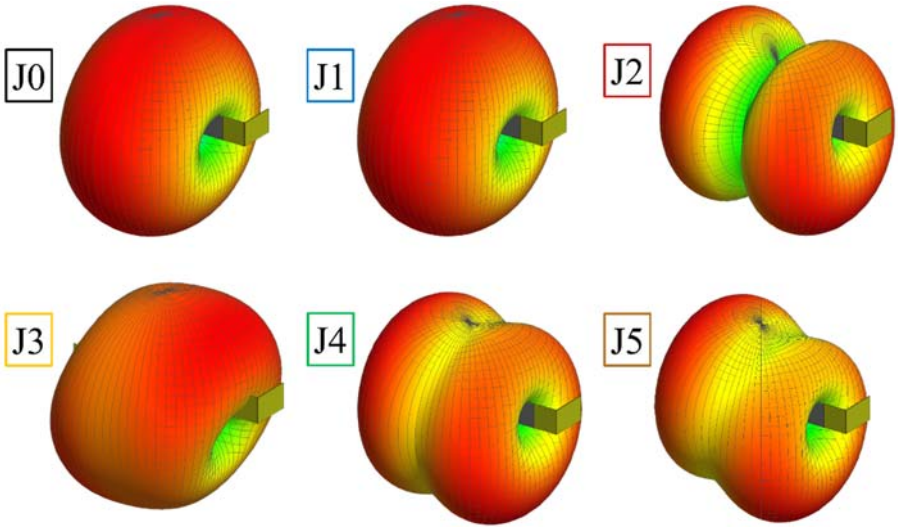

Figure AII. 7 Radiation patterns generated by each of the characteristic modes.

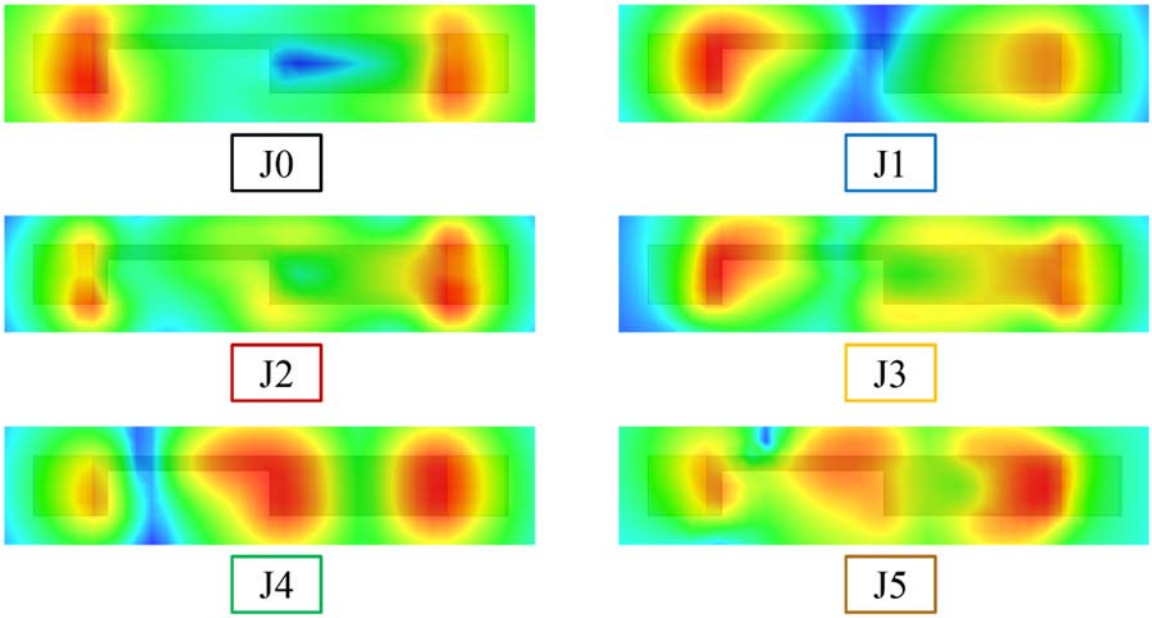

Figure AII. 8 Characteristic electric near field of the modes.

ACKNOWLEDGEMENTS

When I was a child, I was considerably curious to wireless communications. I had too many questions with no answers. For example, how does electromagnetic wave propagate in air; how does receiver antenna catch the electromagnetic wave distribute in air; whether the receiver antenna is able to catch the entire information which has been sent out or not; Is any metal object an antenna, etc. Although I had been reading a lot of popular science books every day, those easy words with cartoon pictures could not thoroughly answer my doubt. When graduated from the high school, I chose wireless communication as my college major. In university, I always remind myself to study as more as possible. Nevertheless, it is difficult to entirely understand the contents of textbooks. People who feel curious will learn more. However, people who learn more will feel the knowledge not sufficient. The reason is that people who have more knowledge will find much more unknown problems. However, knowledge can provide us methods to solve problems. While I was becoming more and more interested in antenna design and desirous to know more about this field, I decided to become a researcher of antenna and wireless communication technologies.

First of all, I am desirous to express my extraordinarily sincere gratitude to my supervisor, Professor Hiroyuki Arai, who directly gave me a chance to study antenna technologies, and has given me a lot of instructions and advices in the past six years. These instructions and advices are very important for me and my study in Japan.

Secondly, I would like to thank my father, Dabin Wang, and my mother, Guiying Du. They

have supported my life and study so far, given many constructive suggestions to me. Their encouragement made me more confident about my future.

I want to express my gratitude to associate Professor Nobuhiro Kuga who helped my study on his course and my work of TA, gave me a lot of advices. I also want to thank Professor Takehiro Adachi and associate Professor Koichi Ichige for their very kindly conversation and encouragement. I would like to thank Professor Toshihiko Baba for his helpful comments to my research.

I would like to profoundly thank Dr. Huiling Jiang and Dr. Yuki Inoue of NTT docomo Corp., Professor Keizo Cho of Chiba Institute of Technology, and Mr. Zhanghuan Li of Nihon Dengyo Kosaku Co., Ltd. who have been directly participating in our joint research of the dual polarization antenna.

I would like to sincerely thank Professor Cyril Luxey and Dr. Aykut Cihangir of EpOC of University Nice-Sophia Antipolis, and associated research team for their great contribution and kind cooperation to our joint research of the eyewear device antenna.

Thanks to all the members of Arai Laboratory, involving OBs and active members.

When I was Master student, Dr. Matsuno showed me how to eat King-size gyudon of Sukiya and occasionally discuss some interesting historical events of Japan or China with me; Dr. Eom made me know many delicious Korean food; Dr. Uchida often kindly spent his forever-not-enough time in my questions and really helped me a lot; Dr. Mikeka shares his happy emotion and bizarre ideas with me in every day; Mr. Kobori taught me a lot of strange Japanese words but I forgot most of them; Mr. Komatsu taught me how to use FEKO and how to be a good listener; Mr. Komatsuzaki was my tutor, but he does not like drink alcohol; Mr. Sagara ate his delicious box lunch every day and always gave us his warm laugh; Mr. Abe and Mr. Mizuno are cool guys and have various unique techniques; Necessarily, I must thank my dear deskmate, Mr. Ota, who always contributed colorful behaviors and happy time to us.

When I was Doctor student, I want to thank Mr. Izumi and Mr. Okura for their help and cooperation; I want to specially thank Miss Rohani, Mr. Gu and Mr. Thomas for our nice chat and our spicy club; I want to thank Mr. Asai, Mr. Yoneyama, Mr. Uesaka, Mr. Hagiwara, Mr. Hori, Mr. Kon, Miss Ohashi, Mr. Kozuki, Mr. Noguchi, Mr. Morimoto and Miss Yamaguchi

for friendly discussion with them about research and job hunting; Other juniors also helped me a lot, they are Mr. Nakamura, Mr. Hasegawa, Mr. Ichinohe, Mr. Hashiguchi, Mr. Ashihara, Mr. Kaneda, Mr. Takahashi, Mr. Matsuda, Mr. Yonezawa, Miss Suzuki, etc. Although I did not spend too much time with them, I sincerely thank these people and I will not forget them.

Thank all the secretaries of Arai Laboratory for their kindly support, they are Ms. Harada, Ms. Terashima and Ms. Takahashi.

Thank Yokohama National University and Global COE Program for financial support; thank JGC-S Scholarship Foundation for financial support in the first year. Thank Mr. Suzuki of Reibundou for giving me a part time job chance in his medical book store.

As far as I know, in Japanese culture, process of one thing is more important than its result. Whatever the result becomes, I obtained knowledge and happiness in the five year's research life without any regret.

Shen Wang

11th Dec. 2014

Yokohama, Japan

REFERENCES

[1] Constantine A. Balanis, “Antenna Theory, Analysis and Design,” 3rd Edition, A John Wiley & Sons, Inc. Publication, 2005.

[2] Constantine A. Balanis, “Advanced Engineering Electromagnetics,” 2nd Edition, vol.E93-B, Wiley, New York, 2012.

[3] E. K. Miller and G. J. Burke, “Low-Frequency Computational Electromagnetics for Antenna Analysis,” Proc. IEEE, Vol. 80, No. 1, pp. 24-43, Jan. 1992.

[4] P. H. Pathak, “High-Frequency Techniques for Antenna Analysis,” Proc. IEEE, Vol. 80, No. 1, pp. 44-65, Jan. 1992.

[5] R. J. Marhefka and W. D. Burnside, “Antennas on Complex Platforms,” Proc. IEEE, Vol. 80, No. 1, pp. 204-208, Jan. 1992.

[6] J. C. Maloney, G. S. Smith, and W. R. Scott Jr., “Accurate Computation of the Radiation from Simple Antennas using the Finite-Difference Time-Domain Method,” IEEE Trans. Antennas Propagat., Vol. 38, No. 7, pp. 1059-1068, Jul. 1990.

[7] D. S. Katz, M. J. Piket-May, A. Taflove, and K. R. Umashankar, “FDTD Analysis of Electromagnetic Wave Radiation from Systems Containing Horn Antennas,” IEEE Trans. Antennas Propagat., Vol. 39, No. 8, pp. 1203-1212, Aug. 1991.

[8] P. A. Tirkas and C. A. Balanis, “Finite-Difference Time-Domain Techniques for Antenna Radiation,” IEEE Trans. Antennas Propagat., Vol. 40, No. 3, pp. 334-340, Mar. 1992.

[9] P. A. Tirkas and C. A. Balanis, “Contour Path FDTD Method for Analysis of Pyramidal Horns With Composite Inner E-Plane Walls,” IEEE Trans. Antennas Propagat., Vol. 42, No. 11, pp. 1476-1483, Nov. 1994.

[10] J. M. Jin, “The Finite Element Method in Electromagnetics,” 3rd Edition, Wiley, New York, 2014.

[11] J. M. Jin and J. L. Volakis, “Scattering and Radiation Analysis of Three-Dimensional Cavity Arrays Via a Hybrid Finite-Element Method,” IEEE Trans. Antennas Propagat., Vol. 41, No. 11, pp. 1580-1586, Nov. 1993.

[12] D. T. McGrath and V. P. Pyati, “Phased Array Antenna Analysis with Hybrid Finite Element Method,” IEEE Trans. Antennas Propagat., Vol. 42, No. 12, pp. 1625-1630, Dec. 1994.

[13] W. Sun and C. A. Balanis, “Vector One-WayWave Absorbing Boundary Condition for FEM Applications,” IEEE Trans. Antennas Propagat., Vol. 42, No. 6, pp. 872-878, Jun. 1994.

[14] R. J. Garbacz and R. H. Turpin, “A generalized expansion for radiated and scattered fields,” IEEE Trans. Antennas Propag., vol. AP-19, no. 3, pp. 348-358, May 1971.

[15] R. F. Harrington and J. R. Mautz, “Theory of characteristic modes for conducting bodies,” IEEE Trans. Antennas Propag., vol. AP-19, no. 5, pp. 622-628, Sep. 1971.

[16] R. F. Harrington and J. R. Mautz, “Computation of characteristic modes for conducting bodies,” IEEE Trans. Antennas Propag., vol. AP-19, no. 5, pp. 629-639, Sep. 1971.

[17] R. F. Harrington and J. R. Mautz, “Characteristic modes for dielectric and magnetic bodies,” IEEE Trans. Antennas Propag., Vol. 20, No. 2, pp. 194-198, Mar 1972.

[18] N. Inagaki and Robert J. Garbacz, “Eigenfunctions of composite Hermitian operators with application to discrete and continuous radiating systems,” IEEE Trans. Antennas Propag., Vol. 30, No. 4, pp. 571-575, Jul. 1982.

[19] N. Inagaki and Robert J. Garbacz, “Correction to "Eigenfunctions of Composite Hermitian Operators with Application to Discrete and Continuous Radiating Systems",” IEEE Trans. Antennas Propag., Vol. 30, No. 6, pp. 1268, Jul. 1982.

[20] David M. Pozar, “Antenna synthesis and optimization using weighted Inagaki modes,” IEEE Trans. Antennas Propag., Vol. 32, No. 2, pp. 159-165, Feb. 1984.

[21] David M. Pozar, “Correction to "Antenna synthesis and optimization using weighted Inagaki modes",” IEEE Trans. Antennas Propag., Vol. 35, No. 6, pp. 742, Jun. 1987.

[22] D. Liu, Robert J. Garbacz and David M. Pozar, “Antenna synthesis and optimization using generalized characteristic modes,” IEEE Trans. Antennas Propag., Vol. 38, No. 6, pp. 862-868, Jun. 1990.

[23] R. F. Harrington and J. R. Mautz, “Control of radar scattering by reactive loading,” IEEE Trans. Antennas Propag., Vol. 20, No. 4, pp. 446-454, Jul. 1972.

[24] J. R. Mautz and R. F. Harrington, “Modal analysis of loaded N-port scatterers,” IEEE Trans. Antennas Propag., Vol. 21, No. 2, pp. 188-199, Mar. 1973.

[25] R. F. Harrington and J. R. Mautz, “Pattern synthesis for loaded N-port scatterers,” IEEE Trans. Antennas Propag., Vol. 22, No. 2, pp. 184-190, Mar. 1974.

[26] E. H. Newman, “Small antenna location synthesis using characteristic modes,” IEEE Trans. Antennas Propag., Vol. 27, No. 4, pp. 530-531, Jul. 1979.

[27] Robert J. Garbacz and David M. Pozar, “Antenna shape synthesis using characteristic modes,” IEEE Trans. Antennas Propag., Vol. 30, No. 3, pp. 340-350, May 1982.

[28] B. A. Austin and K. P. Murray, “The application of characteristic-mode techniques to vehicle-mounted NVIS antennas,” IEEE Antennas and Propagation Magazine, Vol. 40, No. 1, pp. 7-21, 30, Feb. 1998.

[29] M. Cabedo-Fabres, E. Antonino-Daviu, A. Valero-Nogueira, and M. Ferrando-Bataller, “The theory of characteristic modes revisited: A contribution to the design of antennas for modern applications,” IEEE Antennas Propag. Mag., vol. 49, no. 5, pp. 52–68, Oct. 2007.

[30] H. Kawakami and G. Sato, “Broad-band characteristics of rotationally symmetric antennas and thin wire constructs,” IEEE Antennas Propag. Mag., Vol. 35, No. 1, pp. 26-32, Jan. 1987.

[31] K. A. Obeidat, B. D. Raines and R. G. Rojas, “Antenna design and analysis using characteristic modes,” IEEE Antennas and Propagation Society International Symposium 2007, pp. 5993-5996, Jun. 2007.

[32] K. A. Obeidat, B. D. Raines and R. G. Rojas, “Design and analysis of a helical spherical antenna using the theory of characteristic modes,” IEEE Antennas and Propagation Society International Symposium 2008, pp. 1-4, Jul. 2008.

[33] E. Antonino-Daviu, M. Cabedo-Fabres, M. Gallo, M. Ferrando-Bataller and M. Bozzetti, “Design of a Multimode MIMO Antenna Using Characteristic Modes,” 3rd European Conference on Antennas and Propagation, EuCAP 2009, pp. 1840-1844, Mar. 2009.

[34] A. Araghi and G. Dadashzadeh, “Oriented Design of an Antenna for MIMO Applications Using Theory of Characteristic Modes,” IEEE Antennas and Wireless Propagation Letters, Vol. 11, pp. 1040-1043, Aug. 2012.

[35] A.r Krewski, Werner L. Schroeder and K. Solbach, “Multi-band 2-port MIMO LTE Antenna Design for Laptops Using Characteristic Modes,” 2012 Loughborough Antennas & Propagation Conference, pp. 1-4, Nov. 2012.

[36] H. Li, Z. T. Miers and B. K. Lau, “Design of Orthogonal MIMO Handset Antennas Based on Characteristic Mode Manipulation at Frequency Bands Below 1 GHz,” IEEE Trans. on Antennas and Propagation, Vol. 62, No. 5, pp. 2756-2766, May 2014.

[37] P. Miskovsky and A. Arbin, “Evaluation of MIMO Handset Antennas with Decorative Metal Elements, Using Characteristic Modes,” Antennas and Propagation Society International Symposium (APSURSI), 2014 IEEE, pp. 1423-1424, Jul. 2014.

[38] I. Szini, A. Tatomirescu and G. Pedersen “On Small Terminal MIMO Antenna Correlation Optimization Adopting Characteristic Mode Theory,” Antennas and Propagation Society International Symposium (APSURSI), 2014 IEEE, pp. 1425-1426, Jul. 2014.

[39] M. Bataller, E. Daviu, M. Fabres and A. Nogueira, “UWB Antenna Design Based on

Modal Analysis," European Conference on Antennas and Propagation (EuCAP) 2009, pp. 3530-3534, Mar. 2009.

[40] E. Daviu, M. Fabrés, M. Bataller and V. Peñarrocha, "Modal Analysis and Design of Band-Notched UWB Planar Monopole Antennas," IEEE trans. on antennas and propagation, Vol. 58, No. 5, pp. 1457-1467, May 2010.

[41] Y. Chen and C. Wang, "Characteristic-Mode-Based Improvement of Circularly Polarized U-Slot and E-Shaped Patch Antennas," IEEE antennas and wireless propagation letters, Vol. 11, pp. 1474-1477, 2012.

[42] R. Martens, E. Safin and D. Manteuffel, "Inductive and capacitive excitation of the characteristic modes of small terminals," Proc. Loughborough Antennas Propag. Conf. 2011, pp. 1-4, Nov. 2011.

[43] S. K. Chaudhury, W. L. Schröder and H. J. Chaloupka, "Multiple antenna Concept based on Characteristic Modes of Mobile Phone Chassis," EUCAP 2007, Barcelona, Nov. 2007.

[44] S. K. Chaudhury, H. J. Chaloupka and A. Ziroff, "Multiport antenna Systems for MIMO and Diversity," EUCAP 2010, Barcelona, Apr. 2010.

[45] D. Manteuffel and R. Martens, "A Concept for MIMO Antennas on Small Terminals based on Characteristic Modes," IWAT 2011, Hong Kong, Mar. 2011.

[46] R. Martens, E. Safin and D. Manteuffel, "Selective Excitation of Characteristic Modes on Small Terminals," EUCAP 2011, Roma, Apr. 2011.

[47] S. N. Makarov, "Antenna and EM Modeling With Matlab," Wiley, New York, 2002.

[48] S. M. Rao, D. R. Wilton and A. W. Glisson, “Electromagnetic Scattering by Surfaces of Arbitrary Shape,” IEEE trans. on antennas and propagation, Vol. 30, No. 3, pp. 409-418, May 1982.

[49] https://www.feko.info/about-us/News/release-of-feko-suite-6.2-feature-overview

[50] https://www.feko.info/about-us/News/release-of-feko-suite-6.3-feature-overview

[51] https://www.feko.info/product-detail/productivity_features/characteristic-mode-analysis/characteristic-mode-analysis_6_3

[52] R. E. Burgess, “Aerial Characteristics,” Wireless Engr., Vol. 21, pp. 154-160, Apr. 1944.

[53] J. D. Kraus, “Antennas,” pp. 359-434, Chapters 9-10, McGraw-Hill, New York, 1988.

[54] S. A. Schelkunoff and H. T. Friis, “Antennas: Theory and Practice,” pp. 213-242, Wiley, New York, 1952.

[55] A. A. Pistolkors, “The Radiation Resistance of Beam Antennas,” Proc. IRE, Vol. 17, pp. 562-579, Mar. 1929.

[56] R. Bechmann, “On the Calculation of Radiation Resistance of Antennas and Antenna Combinations,” Proc. IRE, Vol. 19. pp. 461-466, Mar. 1931.

[57] P. S. Carter, “Circuit Relations in Radiation Systems and Applications to Antenna Problems,” Proc. IRE, Vol. 20, pp. 1004-1041, Jun. 1932.

[58] R. F. Harrington, “Matrix Methods for Field Problems,” Proc. IEEE, Vol. 55, No. 2, pp. 136-149, Feb. 1967.

[59] R. F. Harrington, “Field Computation by Moment Methods,” Macmillan, New York, 1968.

[60] J. H. Richmond, “Digital Computer Solutions of the Rigorous Equations for Scattering Problems,” Proc. IEEE, Vol. 53, pp. 796-804, Aug. 1965.

[61] L. L. Tsai, “Moment Methods in Electromagnetics for Undergraduates,” IEEE Trans. Educ., Vol. E-21, No. 1, pp. 14-22, Feb. 1978.

[62] R. Mittra, “Computer Techniques for Electromagnetics,” Pergamon, New York, 1973.

[63] J. Moore and R. Pizer, “Moment Methods in Electromagnetics,” John Wiley and Sons, New York, 1984.

[64] J. J. H. Wang, “Generalized Moment Methods in Electromagnetics,” John Wiley and Sons, New York, 1991.

[65] C. A. Balanis, “Advanced Engineering Electromagnetics,” John Wiley and Sons, New York, 1989.

[66] R. E. Collin and F. J. Zucker, “Antenna Theory Part 2,” Chapters 23-24, McGraw-Hill, New York, 1969.

[67] T. R. Srkap and E. Arras, “Electromagnetic scattering from dielectric bodies,” IEEE Trans. Antennas Propagat., Vol. 37, No. 5, pp. 673-676, Mar. 1989.

[68] T. R. Srkap and E. Arras, “An integral equation approach to the analysis of finite microstrip antennas: volume/surface formulation,” IEEE Trans. Antennas Propagat., Vol. 38, No. 3, pp. 305-312, Mar. 1990.

[69] C. C. Lu and C. Yu, “Analysis of microstrip structures of finite ground plane using the

hybrid volume-surface integral equation approach," IEEE Antennas and Propagation Society International Symposium 2002, Vol. 4, pp. 162-165, 2002.

[70] T. F. Eibert and V. Hansen, "On the calculation of potential integrals for linear source distributions on triangular domains," IEEE Trans. Antennas Propagat., Vol. 43, No. 12, pp. 1499-1502, Dec. 1995.

[71] P. Zwamborn and P. M. Van den Berg, "The three dimensional weak form of the conjugate gradient FFT method for solving scattering problems," IEEE Transactions on Microwave Theory and Techniques, Vol. 40, No. 9, pp. 1757-1766, Sep. 1992.

[72] R. Mittra and C. A. Klein, "Stability and Convergence of Moment Method Solutions," in Numerical and Asymptotic Techniques in Electromagnetics, Chapter 5, R. Mittra (Ed.), Springer-Verlag, New York, pp. 129-163, 1975.

[73] T. K. Sarkar, "A Note on the Choice Weighting Functions in the Method of Moments," IEEE Trans. Antennas Propagat., Vol. 33, No. 4, pp. 436-441, Apr. 1985.

[74] T. K. Sarkar, A. R. Djordjevi´c and E. Arvas, "On the Choice of Expansion and Weighting Functions in the Numerical Solution of Operator Equations," IEEE Trans. Antennas Propagat., Vol. 33, No. 9, pp. 988-996, Sep. 1985.

[75] S. M. Rao, D. R. Wilton and A. W. Glisson, "Electromagnetic scattering by surfaces of arbitrary shape," IEEE Trans. Antennas Propagat., Vol. 30, no. 3, pp. 409-418, May 1982.

[76] D. H. Schaubert, D. R. Wilton and A. W. Glisson, "A tetrahedral modeling method for electromagnetic scattering by arbitrarily shaped inhomogeneous dielectric bodies," IEEE Trans. Antennas Propagat., Vol. 32, no. 1, pp. 77-85, Jan. 1984.

[77] S. Makarov, "MoM antenna simulations, with Matlab: RWG basis functions," IEEE

Antennas and Propagation Magazine, Vol. 43, no. 5, pp. 100-107, Oct. 2001.

[78] http://en.wikipedia.org/wiki/Hermitian_adjoint

[79] http://en.wikipedia.org/wiki/Kronecker_delta

[80] V. Anreddy and M. Ingram, "Antenna selection for compact dual-polarized MIMO systems with linear receivers," in Global Telecommunications Conference, IEEE GLOBECOM '06, pp. 1-6, Nov. 2006.

[81] H. R. Chuang, L. C. Kuo, "3-D FDTD design analysis of a 2.4GHz polariza-tion-diversity printed dipole antenna with integrated balun and polarization-switching circuit for WLAN and wireless communication applications" IEEE Trans. Microwave Theory and Techniques, Vol.51, no. 2, pp.374-381, Feb. 2003.

[82] N. Kuga, H. Arai, and N. Goto, "A notch-wire composite antenna for polarization diversity reception," IEEE Trans. Antennas Propag., vol 46, no.6, pp.902-906, Jun. 1998.

[83] N. Kuga, K. Kowaita, "A horizontal polarized omnidirectional pattern antenna composed of two notched-plate panel elements," Proc. of ISAP' 04, Aug. 2004.

[84] S. Hosono, H. Arai, N. Goto, "A flat diversity antenna by disk loaded monopole and three notches", Proc. of ISAP' 92, vol. 3, pp. 697-640, Sept. 1992.

[85] S. Wang, H. Arai, Y. Inoue, K. Cho, "A compact flat omni-directional diversity antenna with three notches," 2010 IEICE Society Conference, B-1-91, Sept. 2010.

[86] S. Wang, H. Arai, Y. Inoue, K. Cho, "A Small Low Profile Dual-Polarization Antenna for Indoor MIMO Systems," Proc. of ISAP' 2011, WeB1-3, Lotte Hotel Jeju, Jeju, Korea, Oct. 2011

[87] T. Hori, “Broadband / multiband printed antennas,” IEICE, Trans. Commun., vol. E88-B, no.5, pp.1809-1817, May 2005.

[88] D.H. Schaubert and F.G. Farrar, “Some conformal, printed circuit antenna designs,” Proc. Workshop Printed Circuit Antenna Tech., pp. 5-1, Oct. 1979.

[89] C. Wood, “Improved bandwidth of microstrip antennas using parasitic elements,” Proc. IEE, Pt. H, vol. 127, pp.231-234, 1980.

[90] K. Wong, L. Chou and C. Su, “Dual-band flat-plate antenna with a shorted parasitic element for laptop applications,” IEEE Trans. Antennas and Propag., vol 53, no.1, pp.539-544, Jan. 2005.

[91] W. R. Deal, N. Kaneda, J. Sor, Y. Qian and T. Itoh, “A new quasi-Yagi antenna for planar active antenna arrays,” IEEE Trans. Microw. Theory Tech., vol. 48, no. 6, pp. 910-918, Jun. 2000.

[92] T. Ma and S. Jeng, "A printed dipole antenna with tapered slot feed for ultrawide-band applications," IEEE Trans. Antennas and Propag., vol. 53, no. 11, pp. 3833-3836, Nov. 2005.

[93] K. Chang, H. Kim, K. Hwang, I. Yoon, and Y. Yoon, "A triple-band printed dipole antenna using parasitic elements," Microwave and Optical Technology Letters, Vol. 47, pp. 221-223, 2005.

[94] S. Blanch, S., J. Romeu and I. Corbella, “Exact representation of antenna system diversity performance from input parameter description,” IEE Electronics Letters, Vol. 39, pp. 705-707, May 2003.

[95] N. Ishii and H. Arai, “Research Trend of Measurement Methods for Total Radiated Power from an Antenna in Japan,” IEICE Transactions on Communications (Japanese Edition), Vol. J95-B, No. 5, pp. 607-617, May 2012. (in Japanese)

[96] W. A. Johnson, “The notch aerial and some applications to aircraft radio installations,” Proceedings of the IEE - Part B: Radio and Electronic Engineering, Vol. 102, No. 2, pp. 211-218, Mar. 1995.

[97] H. Arai and N. Goto, “Flat antennas for indoor cellular system,” IEEE Antennas and Propagation Society International Symposium (APS) 1994, pp. 344-347, Jun. 1994.

[98] H. Arai and K. Kohzu, “A bidirectional notch antenna,” IEEE Antennas and Propagation Society International Symposium (APS) 1996, pp. 42-45, Jul. 1996.

[99] H. Arai and K. Cho, “Cellular and PHS Base Station Antenna Systems,” IEICE Trans. on Commun. Vol.E86-B, No.3, pp.980-992, Mar. 2003.

[100] H. Arai, K. Kohzu, T. Mukaiyama and Y. Ebine, “Bi-directional Notch Antenna with Parasitic Elements for Tunnel Booster System,” Antennas and Propagation Society International Symposium (APS), 1997 IEEE, pp. 2218-2221, Jul. 1997.

[101] K. Abe, H. Arai, N. Takemura and T. Mitsui, “Switched Beam Antenna Using Parasitic Elements,” 2011 International Symposium on Antennas and Propagation (ISAP), Oct. 2011.

[102] K. Abe, H. Arai, N. Takemura and T. Mitsui, “Beam Switched Antenna by Phase Difference Feed,” 2010 International Symposium on Antennas and Propagation (ISAP), Oct. 2010.

[103] A. Diallo, C. Luxey, P. Le Thuc, R. Staraj and G. Kossiavas,“ Study and Reduction of the Mutual Coupling Between Two Mobile Phone PIFAs Operating in the DCS1800 and UMTS Bands, ”IEEE. Trans. Antennas Propag., Vol.54, No.11, Nov. 2006.

[104] http://www.google.com/glass/start/

[105] A. Cihangir, W. G. Whittow， C. J. Panagamuwa, F. Ferrero, G. Jacquemod, F. Gianesello and C. Luxey “Feasibility Study of 4G Cellular Antennas for Eyewear Communicating Devices” IEEE Antennas and wireless Propag. Letters, Vol. 12, pp.1704-1707, Oct. 2013.

PUBLICATIONS AND AWARDS

Journal Publications (with review)

1. Shen Wang, Hiroyuki Arai, Huiling Jiang and Keizo Cho, "A Low-Profile Orthogonally Polarized MIMO Antenna for Indoor Base Station," IEICE Transactions on Communications, Vol. E96-B, no. 6, pp. 641-647, Jun. 2013.

2. Shen Wang and Hiroyuki Arai, "Analysis of an Optimized Notch Array Antenna by Using the Theory of Characteristic Modes," IEEE Antennas and Wireless Propagation Letters, Vol. 13, pp. 253-256, Jan. 2014.

International Conference Publications (with review)

3. Shen Wang, Hiroyuki Arai, Yuki Inoue and Keizo Cho, "A Small Low Profile Dual-Polarization Antenna for Indoor MIMO Systems," ISAP 2011, Jeju, Korea, Oct. 2011.

4. Shen Wang, Hiroyuki Arai, Huiling Jiang and Keizo Cho, "A Compact Orthogonal Dual-Polarization Combined Antenna for Indoor MIMO Base Station," ANTEM 2012, Toulouse, France, Jun. 2012.

5. Shen Wang, Kenta Abe, Hiroyuki Arai, Nobuyasu Takemura and Tsutomu Mitsui, “A Low-Profile Switched Beam Antenna Using Parasitic Elements for Indoor Base Station,” IWEM 2012, Chengdu, China, Aug. 2012. **(Awarded)**

6. Shen Wang, Hiroyuki Arai, Huiling Jiang, Keizo Cho and Zhanghuan Li, “Bandwidth Enhancement of a Compact Dual-Polarized Indoor Base Station Antenna,” IWAT 2013, Karlsruhe, Germany, Mar. 2013.

7. Shen Wang and Hiroyuki Arai, “Analysis of a Horizontally Polarized Antenna with Omni-Directivity in Horizontal Plane Using the Theory of Characteristic Modes,” ISAP 2013, Nanjing, China, Oct. 2013.

8. Shen Wang and Hiroyuki Arai, “Characteristic Modes Analysis on Neutralizing Effect of Shorted Line for Two Adjacent PIFA Elements,” IWAT 2014, Sydney, Australia, Mar. 2014.

9. Shen Wang and Hiroyuki Arai, “A Horizontally Polarized Notch Array Antenna with Good Radiation Identity in Horizontal Plane and Its Characteristic Modes Analysis,” AP-S 2014, Memphis, USA, Jul. 2014.

10. Shen Wang, Hiroyuki Arai, Aykut Cihangir and Cyril Luxey, “Characteristic Modes Analysis of A 4G Cellular Antenna for Eyewear Wireless Devices,” IWEM 2014, Sapporo, Japan, Aug. 2014. **(Awarded)**

IEICE Technical Reports (without review)

11. 王珅，新井宏之，蒋恵玲，長敬三，“室内基地局用低姿勢偏波共用 MIMO アンテナ” 電子情報通信学会アンテナ・伝播研究会，AP2011-101，pp.69-72, 2011 年 11 月.

12. 王珅，新井宏之，蒋恵玲，長敬三，李章煥，“小型広帯域偏波共用基地局アンテナ” 電子情報通信学会アンテナ・伝播研究会，AP2012-148，pp.139-142, 2013年 1 月.

IEICE General/Society Conferences (without review)

13. Shen Wang, Hiroyuki Arai, Yuki Inoue and Keizo Cho, “A Compact Flat Omni-directional Diversity Antenna with Three Notches,” 2010 年電子情報通信学会ソサイエティ大会.

14. Shen Wang, Hiroyuki Arai, Huiling Jiang and Keizo Cho, “Compact Dual-Polarization Composite Antenna for Indoor MIMO Base Station,” 2011 年電子情報通信学会ソサイエティ大会.

15. 王珅，新井宏之，“水平面内一様指向性を有する水平偏波アンテナ” 2013 年電子情報通信学会総合大会.

16. 王珅，新井宏之，“Characteristic Modes 法による水平面内一様指向性を有する水平偏波アンテナの解析” 2013 年電子情報通信学会ソサイエティ大会.

17. 王珅，新井宏之，“近接配置した PIFA 素子間の短絡線を用いた結合抑制の Characteristic Modes 法解析” 2014 年電子情報通信学会総合大会.

Patent

18. 蒋恵玲，長敬三，新井宏之，王珅，“アンテナ，” P2013-46331A，日本国特許庁，平成 25 年 3 月 4 日